MINERAL PROCESSING TECHNOLOGY II

STUDENTS MANUAL

O.K. ILUNGA

JUNE 20121

Introduction

Mineral processing equipment performance depends on the behaviour of each particle that is processed. It is however impossible, though necessary, to design equipment (base Computational procedures) that considers each of the particles due to their bigger number and their difference. Useful models cannot be based on average properties of particles either.

Individual particles differ from each other by:

- Properties that influence their behaviours in equipment, the two most important of these properties are the size and mineralogical composition.
- Other properties such as shape, specific gravity, fracture energy, surface area, surface energy.

In addition to the particle size and mineral composition, comminution, classification and concentration are dependent also on specific gravity, brittleness which influences the behaviour of particles. Examples: Gravity concentration makes use of differences in specific gravity between particles to separate them.

Particles properties are not totally independent of each other. For example the specific gravity is related to the mineralogical composition. Surface energy of a particle is related to mineral composition on the surface of the particle.

Some aspects of the particle's properties in a population are needed with more details for models to be sufficiently sensitive to individual particle properties although these properties cannot be defined for each individual particle. Such aspects or scheme are provided by a description using distribution functions.

CHAPTER I

DISTRIBUTION FUNCTIONS

The distribution function for a particular property defines quantitatively how the values of that property are distributed among the particles in the entire population.

Best known and most widely used distribution function is the particle size distribution function$P(d_p)$.

1.1 Particle size distribution function

The particle size distribution function $P(d_p)$ is the mass fraction of particles in the population having a size less than or equal to d_p.

1.2 Properties of particle size distribution function

a) $P(0)$ = 0

This means that there no particle which is less than 0

b) $P(\infty)$ =1

This means all particles have size less than ∞

c) $P(d_p)$ increases from 0 to 1 as dp increases from 1 to ∞, meaning that the fraction of particles having size d_{p1} are included in the fraction of particle having size d_{p2} ($d_{p2} \geq d_{p1}$)

1.3 Meaning of particle size

The concept of particle size is not quite clear because particles have irregular shape. The meaning depends on applications: It is:

a) The smallest hole opening in a square-mesh screen through which the particle will fall.

b) the terminal falling velocity in a fluid of specified viscosity and density, the particle has then the size the sphere that falls at the same rate

c) The size of the sphere that has the same cross section when the particle sets on its more stable surface.

d) the size of the sphere that has similar volume or surface area

Statistical dimensions of particles are determined using optical microscope or electrons microscope. These optical methods is limited to sizes greater than 100 microns

It is therefore important to mention the method used to determine a particle size when given.

In practical applications the particle population is divided into groups identified by the smallest and largest size in the group.

1.4 Determination of the particle size distribution function

1.4.1 Numerical determination of the particle size distribution function

The value of P can be measured experimentally at different mesh sizes of the set of sieves in the laboratory. This data is usually presented in tabular form showing mesh size against fraction smaller than that mesh.

1.4.2 Graphical representation of the particle size distribution

A variety of different graphical coordinate systems represent the distribution function as a straight line.

The particle size axis is usually plotted on a logarithmic coordinate scale.

The mesh sizes in the standard sieve series vary in geometric progression because experience has shown that the classification leaves almost same of solids on each sieve. Thus each mesh size is a constant factor larger than the previous one. The constant factor is usually $\sqrt[4]{2}$ or $\sqrt{2}$ as shows Table 1.1 The mesh sizes in such a series are plotted as equidistant points on a logarithmic scale.

Table 1.1: Standards sieve sizes and corresponding Tyler scale

Standard size (um)	38	45	53	63	75	90	106	125	150
Tyler Scale (mesh)	400	325	270	250	200	170	150	115	100
Multiplied factor		38x $\sqrt[4]{2}$	45x $\sqrt[4]{2}$	53x $\sqrt[4]{2}$	63x $\sqrt[4]{2}$	75x $\sqrt[4]{2}$	90x $\sqrt[4]{2}$	106x $\sqrt[4]{2}$	125x $\sqrt[4]{2}$

Particle size distribution function is not directly useful for modelling unit operations in mineral processing therefore the density function which is discrete density function pi(dp) is used.

1.5 Discrete Density function

The discrete density function $p_i(d_p)$ is the mass fraction of the particle population that has size between D_{i-1} and D_i and is presented in equation (1.1)

It is also called fractional discrete density function

$$p_i(d_p) = \int_{D_i}^{D_{i-1}} dP(d_p) = P(D_{i-1}) - P(D_i) = \Delta P_i \quad (1.1)$$

$D_{i-1} - D_i = \Delta d_p$ is a finite width of the size class which varies from size to size.

1.6 Class size and class boundaries

The concept of the particle classes allows building models for metallurgical processes from the description of class behaviours instead individual particles behaviours. The size class is includes all particles of the population that have size falling within the class lower and upper boundaries $\mathrm{d_p}$ and $\mathrm{d_p} + \Delta \mathrm{d_p}$. Class boundaries are specified by means of a subscript. Example Di indicates the lower boundary of size class I, thus Di ≥ Di+1. The top size class has only one boundary D1 and it includes all particles which have size greater than D1.

Each class has a representative size, and all particles in the class are assumed to behave as if they had the same size as the representative. This assumption is correct only if the size class is narrow and a ratio of $\sqrt{2}$ series for the class boundaries is the largest geometric ratio that can be safely used. Narrow size intervals lead to a large number of particle classes therefore more computation will be needed.

1.7 Empirical Distribution Functions

There are many empirical distribution functions which accurately represent the size distribution of particle populations:

1.7.1 Types of empirical distribution functions

a) Rosin-Rammler distribution function

The Rosin-Rammler distribution function is represented by equation (1.2)

$$\mathrm{P(D)} = 1 - \exp\left[-\left(\frac{\mathrm{D}}{\mathrm{D_{63.2}}}\right)^{\alpha}\right] \tag{1.2}$$

Where $\mathrm{D_{63.2}}$ is the size at which the distribution function has the value 0.632.

b) Log-normal distribution

The Log-normal distribution function is represented by equation (1.3)

Where D_{50} is the size at which the function is 50

$$\mathrm{P(DP)} = \mathrm{G}\frac{\ln\left(\frac{\mathrm{D}}{\mathrm{D_{50}}}\right)}{\sigma} \tag{1.3}$$

G(x): is called Gaussian or Normal distribution function and is represented by equation (1.4)

$$\mathrm{G(x)} = \frac{1}{\sqrt{2\pi}}\int_{-\infty}^{\mathrm{x}} \mathrm{e}^{-\mathrm{t}^2/2}\mathrm{dt} \tag{1.4}$$

It is tabulated in literature. D_{50} is the median size, the particle size at which P(D50) = 0.5 and σ is determined through equation (1.5)

$$\sigma = 1/2(\ln\mathrm{D_{84}} - \ln\mathrm{D_{16}}) \tag{1.5}$$

Many distributions of particle sizes in crushing tend to the log-normal distribution after many successive fracture events.

Plotting the cumulative percent passing on (y axis) against the sieve sizes on a log scale (x-axis) should produce a straight line (See Graph Appendix A1)

c) Logistic distribution

Logistic distribution is represented through equation (1.6)

$$P(D) = \frac{1}{1+\left(\frac{D}{D_{50}}\right)^{-\lambda}} \qquad (1.6)$$

1.7.2 Transformation of empirical distribution function

a) Transformation of the Rosin-Rammler distribution function

This function be transformed to:

Considering equation (1.2), equation (1.7) which is the transformed Rosin Rammler equation can be obtained as follow:

$$P(D) = 1 - \exp\left[-\left(\frac{D}{D_{63.2}}\right)^{\alpha}\right] \rightarrow 1 - P(D) = \exp\left[-\left(\frac{D}{D_{63.2}}\right)^{\alpha}\right]$$

$$\rightarrow \frac{1}{1-P(D)} = exp\left(\frac{D}{D_{63.2}}\right)^{\alpha} \rightarrow ln\frac{1}{1-P(D)} = \left(\frac{D}{D_{63.2}}\right)^{\alpha}$$

$$lnln\frac{1}{1-P(D)} = \alpha lnD - \alpha \ln D_{63.2} \qquad (1.7)$$

The plot of the lnln of reciprocal of 1-P(D) against the ln of D will then produce data points that lie on a straight line whenever the data follow the Rosin-Rammler distribution. This defines the Rosin-Rammler coordinate system.

b) Transformation of the log normal distribution function

The log-normal distribution equation (1.3) can be transformed using the inverse function H(G) (equation (1.9) of the function G. This inverse function is defined in such a way that if

G(x) = g, (1.8)

Then x = H(g) (1.9)

From (1.3), $H\big(P(D)\big) = \frac{\ln(\frac{D}{D_{50}})}{\sigma}$ (1.10)

The plot of *H(P(D))* against log *D* will be linear whenever the data follow the log-normal distribution. This is the lognormal coordinate system.

c) Transformation of Logistic distribution

The logistic distribution equation (1.6) can be transformed to equation (1.11) as follow:

$$P(D) = \frac{1}{1+\left(\frac{D}{D_{50}}\right)^{-\lambda}} \rightarrow \frac{1}{P(D)} = 1 + \left(\frac{D}{D_{50}}\right)^{-\lambda} \rightarrow \frac{1}{P(D)} - 1 = \left(\frac{D}{D_{50}}\right)^{-\lambda} \rightarrow ln\left(\frac{1}{P(D)} - 1\right) = -\lambda ln\frac{D}{D_{50}}$$

$$-ln\left(\frac{1}{P(D)} - 1\right) = \lambda lnD + \lambda lnD_{50} \qquad (1.11)$$

This transformed distribution function shows that the plot of $-ln\left(\frac{1}{P(D)} - 1\right)$ against lnD will be a straight line in the logistic coordinate system whenever the data follow the logistic distribution. Plotting the data in these coordinate systems is a convenient method to establish which distribution function most closely describes the data.

1.8 Truncated size distributions

1.8.1 Definition

Let's consider D_1 as a parent particle, when this particle is broken, no resulting progenity particle will have size larger than D_1. The distribution of the progenities population is said to be truncated at the parent size D_1 and its value will 1 as shows equation (1.12).

$$P(D) = 1 \qquad (1.12)$$

1.8.2 Types of Truncated distribution

a) logarithmic distribution function

The logarithmic function as shows equation (1.13) is a truncated distribution

$$P(D) = \left(\frac{D}{D'}\right)^{\alpha} \text{ for } D \leq D' \qquad (1.13)$$

which satisfies equation (1.12).

D' is the largest particle in the population and α is a measure of the spread in particle sizes.

Other truncated distributions are the Gaudin-Meloy and Harris distributions.

b) Gaudin – Meloy Distribution function

The Gaudin – Meloy function represented by equation (1.14) is a truncated distribution at D'

It is given by: $P(D) = 1 - \left(1 - \frac{D}{D'}\right)^{n}$ for D≤D' (1.14)

d) Harris distribution

The Harris distribution as presented in equation (1.15) is truncated at D'

$$P(D) = 1 - \left(1 - \left(\frac{D}{D\prime}\right)^{s}\right)^{n} \text{ for } D \le D' \tag{1.15}$$

Truncated versions of the Rosin-Rammler, log-normal and logistic distributions can be generated by using a transformed size scale. The size is first normalized to the truncation size E = D/D' and the transformed size is defined by

$$\eta = \frac{\varepsilon}{1-\varepsilon}$$

The truncated Rosin-Rammler distribution is then represented as shows equation (1.16)

$$P(D) = 1 - exp\left(-\left(\frac{\eta}{\eta_{63.2}}\right)^{\alpha}\right) \text{ for } D \le D' \tag{1.16}$$

The The truncated log-normal distribution is then represented by equation (1.17)

$$P(D) = G\left(\frac{\ln(\frac{\eta}{\eta_{50}})}{\sigma}\right) \tag{1.17}$$

With $\sigma = 1/2(\ln(\eta_{84}) - \ln(\eta_{16}))$

Example 1.1

Test the following particle size distribution if it follows:

a) Rosin Rammler, determine graphically α and $D_{63.2}$ using the normal graph paper or special Rosin Rammler logarithmic paper

b) Logistic distribution and determine λ and D_{50}

Mesh size mm	Mass % Passing
6.80	99.5
4.75	97.5
3.40	93.3
2.36	86.4
1.70	76.8
1.18	65.8
0.850	55.0
0.600	45.1
0.425	36.7
0.300	29.6
0.212	23.5
0.150	18.3
0.106	13.9
0.075	10.0
0.053	7.1
0.038	5

Answers

a)

Determination of α, First Complete the table with informations as follows

Mesh size mm	Cumulative mass passing	P(D)	Mech size in microns	1/(1-P(D)	LNLN(1/(1-P(D))	LND
6.800	99.500	0.995	6800.000	200.000	1.667	8.825
4.750	97.500	0.975	4750.000	40.000	1.305	8.466
3.400	93.300	0.933	3400.000	14.925	0.994	8.132
2.360	86.400	0.864	2360.000	7.353	0.691	7.766
1.700	76.800	0.768	1700.000	4.310	0.379	7.438
1.180	65.800	0.658	1180.000	2.924	0.070	7.073
0.850	55.000	0.550	850.000	2.222	-0.225	6.745
0.600	45.100	0.451	600.000	1.821	-0.511	6.397
0.425	36.700	0.367	425.000	1.580	-0.782	6.052
0.300	29.600	0.296	300.000	1.420	-1.047	5.704
0.212	23.500	0.235	212.000	1.307	-1.317	5.357
0.150	18.300	0.183	150.000	1.224	-1.599	5.011
0.106	13.900	0.139	106.000	1.161	-1.899	4.663
0.075	10.000	0.100	75.000	1.111	-2.250	4.317
0.054	7.100	0.071	54.000	1.076	-2.608	3.989
0.038	5.000	0.050	38.000	1.053	-2.970	3.638

Secondly, considering equation (1.7), Plot LNLN(1/(1-P(D)) against LN(D). Note that the resulting plot is a straight line and conclude that the distribution follows the Rosin Rammler empirical distribution function. Thirdly measure the angle between the line and the horizontal axis which is about 52^{o} and α . Determine the tangent of the angle, TAN (52^{O}) = α = 1.3

Consider the transformed Rosin Rammler function $lnln\left(\frac{1}{1-P(D)}\right) = \alpha \ln(D) - \alpha \ln(D^*)$

The plotted line crosses the y axis at y = - 6

Meaning $-6 = -1.3\ LN\ (D_{63.2}) \rightarrow D_{63.2} = e^{\frac{6}{1.3}} = 101$

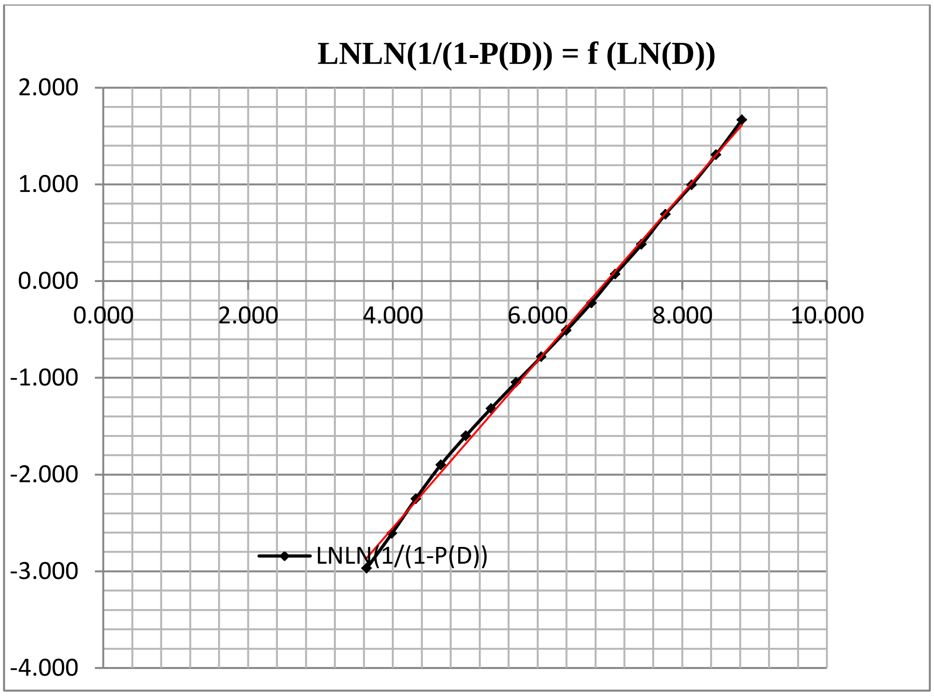

b)

Proceed in a similar way like in a.

Example 1.2

The table represented below shows the lab results of a grinding research project. Show that the particle size distribution follows the Rosin Rammler empirical distribution function and determine the mass fraction passing 200 microns.

Aperture(mm)	Mass (%)
13300	0
4750	20.9
2360	21.1
1180	20.9
600	10.3
300	15.7
150	4.3
75	2.3
-75	4.5

1.9 The Distribution Density Function

1.9.1 Definition

If x represent any particle characteristic of interest, P(x) is the mass fraction of the particle population where particles have the value of that characteristic less than or equal to x .

The distribution density function p(x) is defined by equation (1.18)

$$p(x) = \frac{dP(x)}{dx} \quad (1.18)$$

1.9.2 Relationship between discrete density function and distribution density function

The discrete density function is related to the density function through equation (1.19):

$$p_i = \int_{D_i}^{D_{i-1}} p(x)dx = P(D_{i-1}) - P(D_i) \quad (1.19)$$

p(x)dx can be regarded as the mass fraction of the particle population that consists of particles having the value of the characteristic in the range (x, x+dx).

Applied to the two boundaries, the property presented in equation (1.19) shows that the sum of all fractions is unity as shows equation (1.20).

$$\int_0^\infty p(x)dx = P(\infty) - P(0) = 1 \quad (1.20)$$

1.10 The Distribution by Number, the Representative Size and Population Averages

1.10.1 Definition

The distribution by number $\Psi(x)$ is the fraction by number of particles in the population having size equal to x or less. It is possible to link the particle characteristics to the number fraction

1.10.2 Number density function

The number density function is defined by equation of the type presented in (1.21)

$$\Psi = \frac{d\Psi(x)}{dx} \quad (1.21)$$

1.10.3 Discrete number density function

The discrete number density is instead represented by equation of type (1.22):

$$\Psi_i = \Psi(N_{i-1}) - \Psi(N_i) = \Delta\Psi_i \quad (1.22)$$

Where N_{i-1} and N_i represent the class boundaries

1.10.4 Representative size and Average

a) Average by number

In most case, the average is considered to represent all members of the population.

The average value of any characteristic is determined through equation (1.23):

$$\overline{x_N} = \frac{1}{N_T}\sum_{j=1}^{N_T} x^{(j)} \tag{1.23}$$

In equation (1.23), $x^{(j)}$ is value of the characteristic property for particle j, N_T is the total number of particles in the population. The number of terms in the summation is greatly reduced by collecting particles that have equal values of *x* into distinct groups. If the number of particles in group i is represented by $\mathbf{x^{(i)}}$ and the value of x for particles in this group is represented by xi, then the average value of the property x in the whole population is given by equation (1.24)

$$\overline{x_N} = \frac{1}{N_T}\sum_{i=1}^{N} n^{(i)} x_i \tag{1.24}$$

Where N: the total number of groups that are formed and the ratio $\frac{n^{(i)}}{N_T}$ is the fraction by number of the particle population having size x_i

a more convenient way of evaluating the average is presented in equation (1.25):

$$\overline{x_N} = \sum_{i=1}^{N} x_i \Psi_i \tag{1.25}$$

b) Average by particle mass

Weighted by particle mass, the average can be used rather than by number as shows equation (1.26)

$$\bar{x} = \frac{1}{M_T}\sum_{i=1}^{N} m^{(i)} x_i \tag{1.26}$$

Where, M_T represents the total mass of material in the population, $m^{(i)}$ the mass of particles in the group i having representative value xi and the ratio $\frac{m^{(i)}}{M_T}$ is the fraction by mass of particles in the group i

This ratio is related to the distribution function by:

$$\frac{m^{(i)}}{M_T} = P(x_{i+1}) - P(x_i) = \Delta P_i \ ; \ \bar{x} = \sum_{i=1}^{N} x_i \, \Delta P_i \ ; \ \bar{x} = \sum_{i=1}^{N} x_i \, p_i(x)$$

as the group widths decrease to zero this equation is transformed to equation (1.27)

$$\bar{x} = \int_0^1 x dP(x)$$

$$\bar{x} = \int_0^\infty xp(x)dx \tag{1.27}$$

1.10.5 Variance of the Distribution

The variance is a statistic measure and is represented by equation (1.28).

$$\sigma^2 = \int_0^\infty (x - \bar{x})^2 p(x) dx \tag{1.28}$$

The distribution density function is useful for the evaluation of the average of any function of the particle property x as represented in equation (1.29)

$$\overline{f(x)} = \int_0^\infty f(x) p(x) dx \tag{1.29}$$

In the same way, the average value of the property, x, weighted by number is obtained through equation (1.30) and in general through equation (1.31)

$$\overline{x_N} = \int_0^\infty x \Psi(x) dx \tag{1.30}$$

In general

$$\overline{f(x)_N} = \int_0^\infty f(x) \Psi(x) dx \tag{1.31}$$

Example 1.3

if all particles in the population are spherical, the average particle volume is the average value of $\frac{\pi {d_p}^3}{6}$, then the average particle volume is obtained by integration through equation (1.32):

$$= \int_0^\infty \frac{\pi {d_p}^3}{6} \Psi(d_p) dd_p \text{ `} \tag{1.32}$$

The description of the particle behaviour is well achieved by using the concept of representative size for each size class. A representative size for size class i is defined by equation (1.33):

$${d_{p_i}}^3 = \frac{1}{\Psi_i(d_p)} \int_{D_i}^{D_{i-1}} {d_p}^3 \Psi(d_p) dd_p \tag{1.33}$$

Where $\Psi(d_p)$ is the number distribution density function and $\Psi_i(d_p)$ is the number fraction of the population in size class i. The representative size can also be determined using equation (1.34):

$$d_{p_i} = \frac{1}{p_i} \int_{D_i}^{D_{i-1}} d_p p(d_p) dd_p = \frac{1}{p_i} \int_{D_i}^{D_{i-1}} d_p p(d_p) dd_p \tag{1.34}$$

The definitions of representative size require the knowledge of distribution function. It is however the size classes and their representative should be defined independently of the size distribution. For this reason, the geometric mean presented in equation (1.35) of the upper and lower boundaries can be used as representative size as shows

figure 1.1

$$d_{pi} = (D_i D_{i-1})^{1/2} \tag{1.35}$$

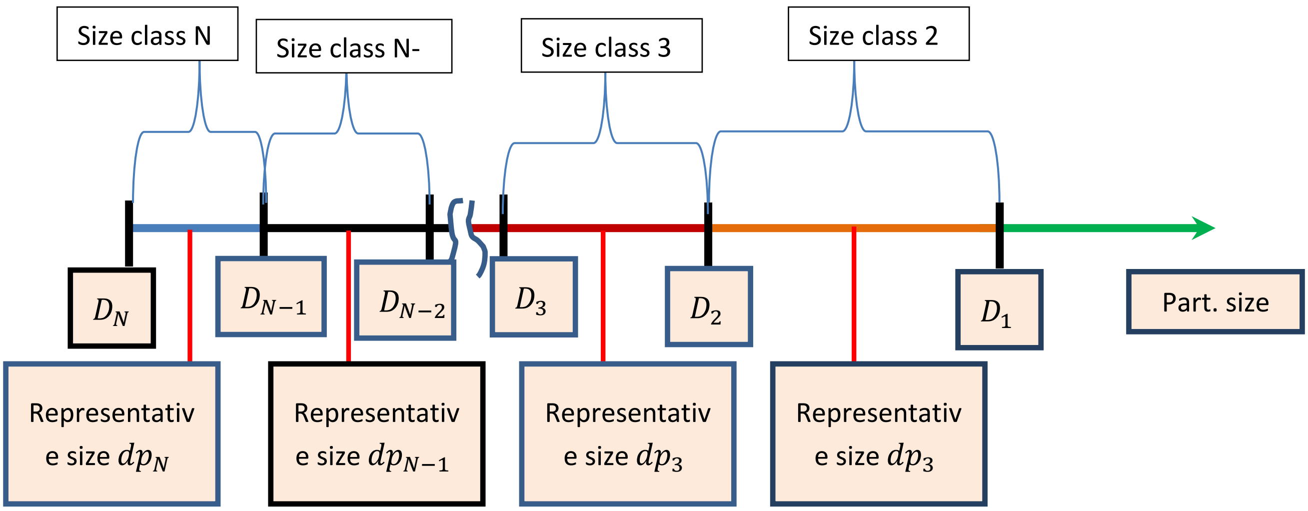

Figure 1.1: Arrangement of size classes and representative sizes along the particle size axis.

Since $D_N = 0$ and D_0 is undefined, equation (1.35) cannot be used to calculate the representative sizes in extreme size classes. These sizes are calculated using equation (1.36) and (1.37):

$$d_{p1} = \frac{{d_{p2}}^2}{d_{p3}} \tag{1.36}$$

$$d_{pN} = \frac{{d_{pN-1}}^2}{d_{pN-2}} \tag{1.37}$$

These formulas show that dpi vary in a geometric progression between the two extreme size classes. The primary objective of mineral processing is the separation of materials based on mineralogical composition to produce concentrates. The objective of comminution operations is the separation of minerals by fragmentation. Unfortunately, separation is not perfect and many particles, no matter how finely ground, will contain a mixture of two or more mineral species. Particles with single mineral are said to be perfectly liberated.

The amount of liberated minerals is a complex function:

- crystalline structure
- mineralogical texture of the ore
- the comminution fracture pattern.

Particles consist of more than one mineral; therefore the mineralogical composition is described by a vector ***g*** of different mineral fractions. Each element of vector g represent a specific mineral fraction in the particle. The number of elements in the vector is equal to the number of minerals including gangue minerals.

Example 1.4

A particle consisting of 25% by mass of chalcopyrite, 35% of sphalerite and 40% of gangue will be described by a mineral fraction vector *g* = (0,25 0,35 0,40) as shows figure 1.2. A number of discrete classes of mineral fractions can be defined. The range of each component of the vector ***g***, must be specified for each class of particles. The fractional discrete distribution function can be defined as before.

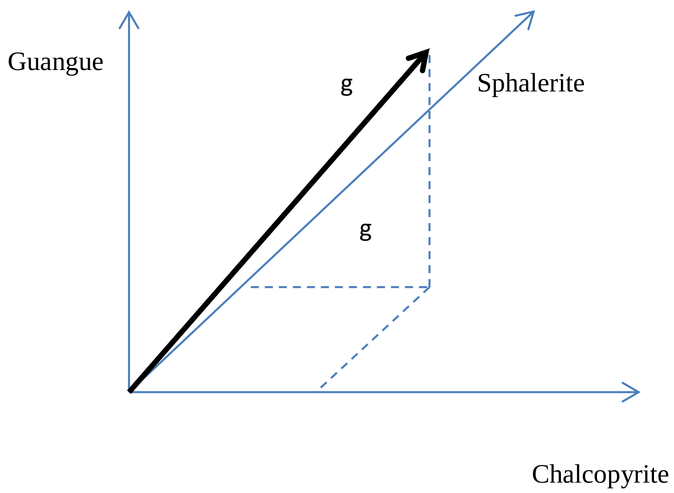

Figure 1.2 Multicomponent mineral vector

If a single valuable mineral only is considered to be important, *g* is a scalar and the distribution function *P(g)* will have the form shown in figure 1.3.

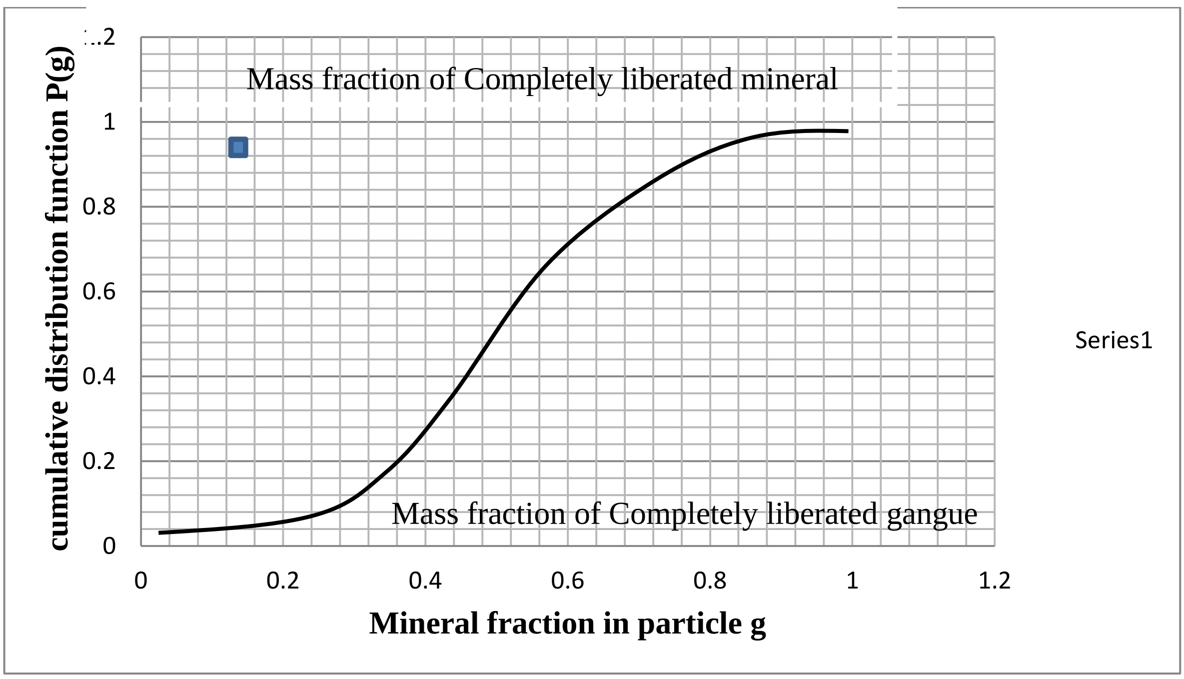

Figure 1.3: Cumulative distribution function against mineral composition

The concentration of particles in the two extreme classes representing completely liberated gangue and mineral respectively is represented by the step discontinuities in the distribution functions.

1.11 Joint Distribution Functions

1.11.1 Definition

The joint distribution function P(dp,g) is defined as the mass fraction of the total particle population that has size dp and mineral fraction g. The population can also be divided into a finite number of discrete classes, each identified by the variables g and dp. Thus the space of variable g and dp can be sectioned on a rectangular grid.

1.11.2 Discrete fractional distribution density function

The discrete fractional distribution density function is defined by: $p_{ij}(d_p, g)$ which is the fraction of material with size in the range$(D_i D_{i-1})$, and composition $(G_{j-1} G_j)$.

It is the mass of material in area (b) figure 1.5

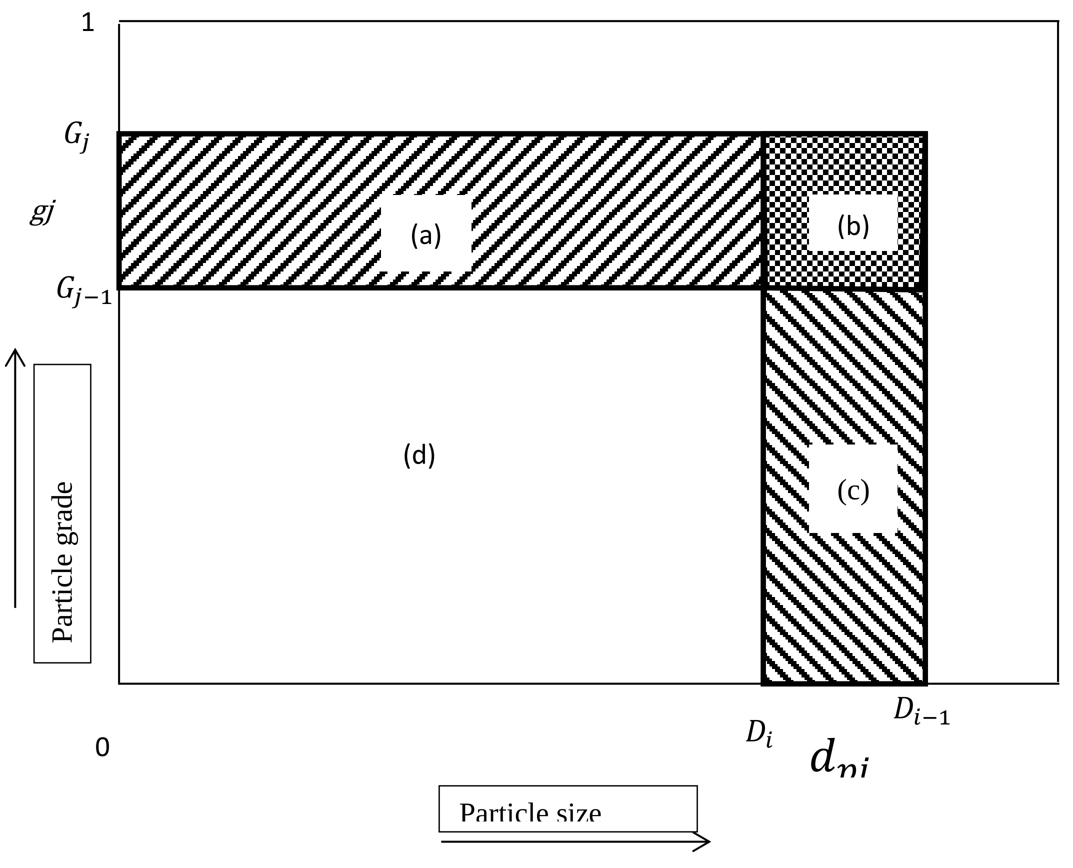

Figure: 1.5 discrete fractional distribution density function in two-dimensional

The cumulative distribution function is illustrated by reference to figure 1.5 and represented by equation 1.38.

$P(D_{i-1}, G_j)$ = fraction of material in areas a+b+c+d

$P(D_i, G_{j-1})$ = fraction of material in area d

$P(D_i, G_j)$ = fraction of material in area a+d

$P(D_{i-1}, G_{j-1})$ = fraction of material in area c+d (1.38)

Therefore in general equation (1.39) can be developped

$$p_{ij}(d_p, g) = P(D_{i-1}, G_j) - P(D_i, G_j) - P(D_{i-1}, G_{j-1}) + P(D_i, G_{j-1}) \quad (1.39)$$

and this is the mass fraction of particle population that has $D_i \leq d_p \leq D_{i-1}$ and $G_{j-1} \leq g \leq G_j$. For higher dimensional distributions the idea will be similar to two dimensions. This is the case when several mineral species are present. The value of $p_{ij}(d_p, g)$ does not change if the order of its arguments dp and g are reversed as shows equation (1.40).

$$p_{ij}(d_p, g) = p_{ji}(g, d_p,) \quad (1.40)$$

1.12 Conditional Distribution Functions

1.12 1 Definition

The conditional discrete density function $p_{ji}(g \backslash d_p,)$ is defined as the mass fraction of the particles in size class i (i.e. have size between Di and Di-1), that are in composition class j.

In size classification, particles with different mineralogical composition will be trapped on the same test sieve. For example, particles in the finest size class will be relatively rich in completely liberated ones.

The screening is called a conditioning operation and the distribution function for each size class is called a conditional fractional distribution function.

These conditional distribution functions can be related to the distribution functions as shows figures 1.6 and 1.7

In Figure 1.6, the particle population is separated into required size classes by screening.

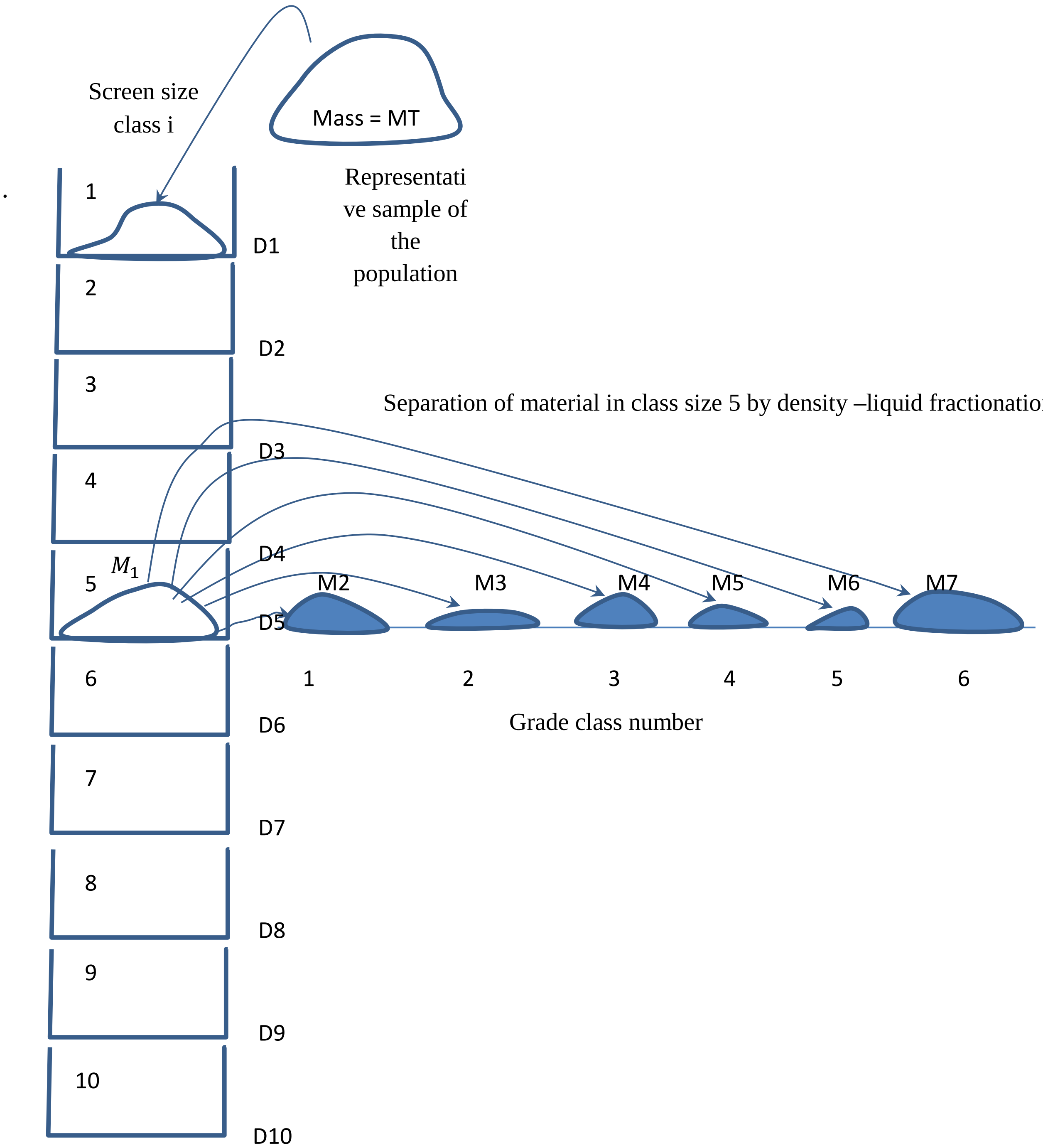

Figure 1.6 Distribution of particle grade conditioned by particle size.

The material on each screen is then separated on the basis of particle mineral content by dense-liquid fractionation for example. The two discrete distribution functions are defined in terms of the masses of material produced by these two sequential operations. From definitions, equations (1.410) , (1.42) and (1.43) can be established

$$p_{35}(g, d_p) = \frac{M_4}{M_T} \qquad (1.41)$$

$$p_{35}(g\backslash d_p) = \frac{M_4}{M_1} \qquad (1.42)$$

$$p_5(d_p) = \frac{M_1}{M_T} \qquad (1.43)$$

Combining these equations, the generation formulation is deduced as shows equation (1.44)

$$p_{35}(g\backslash d_p) = \frac{M_4}{M_1} = \frac{\frac{M_4}{M_T}}{\frac{M_1}{M_T}} = \frac{p_{35}(g,d_p)}{p_5(d_p)} \qquad (1.44)$$

$p_{j5}(g\backslash d_p)$ shows how the material on screen 5 is distributed with respect to the particle composition. In Figure 1.7 the separation is done on the basis of mineral content first, and then each particle grade class is classified by screening. This produces the size distribution conditioned by particle grade and represented mathematically by equation (1.45)

$$p_{53}(d_p\backslash g) = \frac{M\prime_6}{M\prime_1} = \frac{M\prime_6/M_T}{M\prime_1/M_T} = \frac{p_{53}(d_p,g)}{p_3(g)} \qquad (1.45)$$

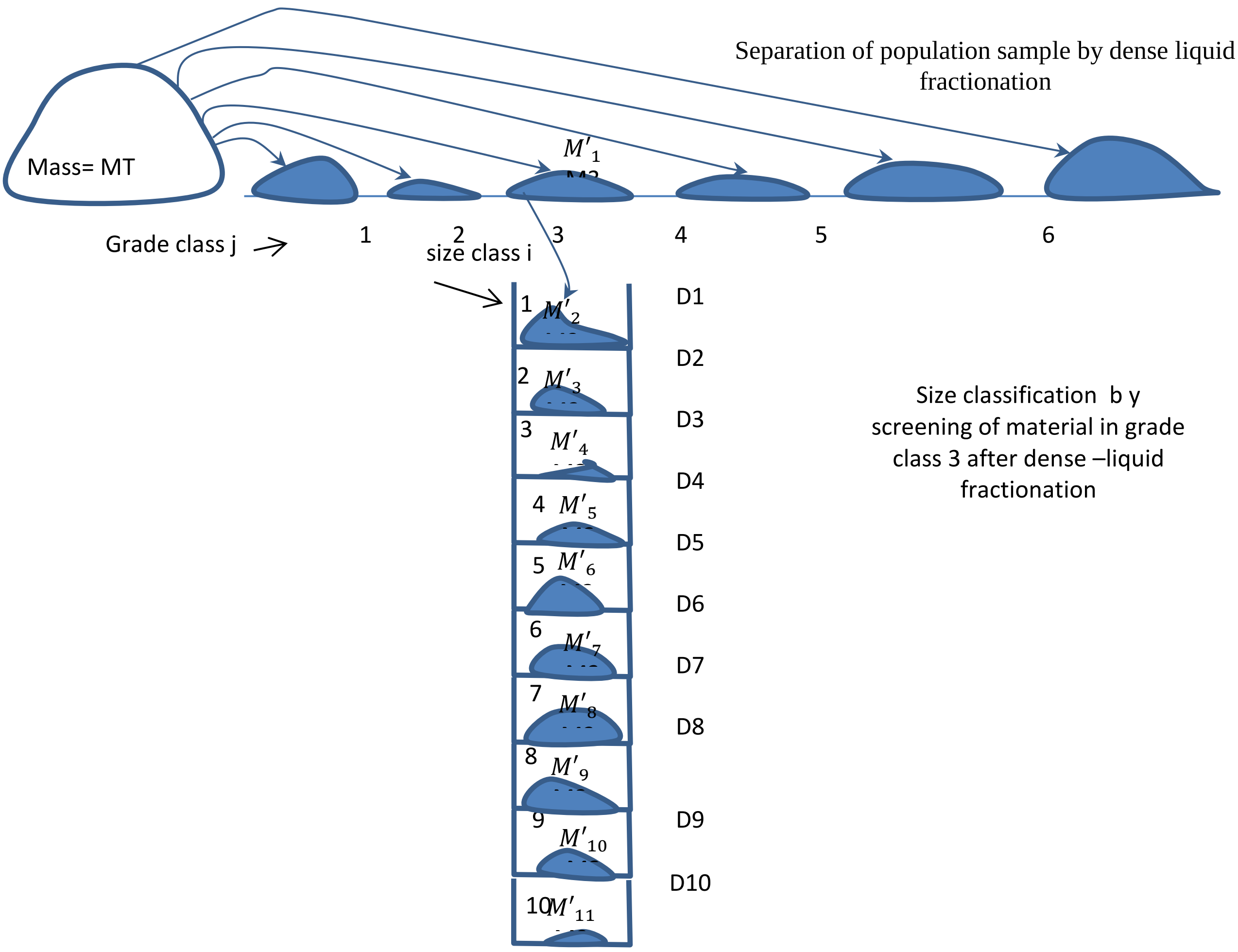

Figure 1.7: Distribution of particle size conditioned by particle grade.

This is the fraction of particle of the population in size class 5 having the composition class 3

Knowing: $M_2 + M_3 + M_4 + M_5 + M_6 + M_7 = M_1$ and $\sum_{j=1}^{6} p_{ji}(g\backslash d_p) = 1$

Then equation (1.47) can generated in more general terms

$$\sum_{j=1}^{6} \mathrm{p_{j5}}(\mathrm{g}, \mathrm{d_p}) = \mathrm{p_5}\,(\mathrm{d_p}) \qquad (1.46)$$

In general if M is the mass of the total population, the mass of particles that fall in the two classes j and i simultaneously is $\mathrm{Mp_{ji}}(\mathrm{g}, \mathrm{d_p})$. If only particle in dp class are considered, meaning $\mathrm{Mp_i}(\mathrm{d_p})$, the conditional distribution is represented by equation (1.47):

$$\mathrm{p_{ji}}(\mathrm{g}\backslash\mathrm{d_p}) = \frac{\mathrm{Mp_{ji}}(\mathrm{g},\mathrm{d_p})}{\mathrm{Mp_i}(\mathrm{d_p})} = \frac{\mathrm{p_{ji}}(\mathrm{g},\mathrm{d_p})}{\mathrm{p_i}(\mathrm{d_p})} \qquad (1.47)$$

The importance of equation (1.47) is that it helps to determine joint discrete distribution function $p_{ji}(g, d_p)$ from conditional distribution function $p_{ji}(g\backslash d_p)$ which can be measured through equations (1.48) – (1.51)

$$p_{ji}(g, d_p) = p_{ji}(g\backslash d_p)p_i(d_p) \qquad (1.48)$$

$$p_{ji}(g, d_p) = p_{ij}(d_p, g) \qquad (1.49)$$

$$p_{ji}(g, d_p) = p_{ij}(d_p/g)p_j(g) \qquad (1.50)$$

$$p_{ji}(g\backslash d_p)p_i(d_p) = p_{ij}(d_p/g)p_j(g) \qquad (1.51)$$

Equation (1.48) corresponds to experiment where population is first screened and each fraction is separated into composition classes.

Equation (1.51) corresponds to a separation on the basis of composition (e.g magnetic, electrostatic, or dense liquid techniques) first, and each composition class is screened latter..

In any case, the joint distribution function can be generated. But the first procedure is less convenient than the second because of the experimental difficulties associated with separation by composition. It is usually more efficient to combine one composition separation with many size separations done in the laboratory than the other way. The density functions satisfy the following rules presented in series of equations (1.52)-(1.55):

$$\sum_i \sum_j p_{ij}(x, y) = 1 \qquad (1.52)$$

$$\sum_j p_{ij}(x, y) = \sum_j p_{ij}(x\backslash y)p_j(y) = p_i(x) \qquad (1.53)$$

$$\sum_i p_{ij}(x, y) = \sum_i p_{ij}(x\backslash y)p_i(y) = p_j(x) \qquad (1.54)$$

$$\sum_i p_{ij}(x\backslash y) = 1 \qquad (1.55)$$

The conditional distribution functions $P(g\backslash d_p)$ and the associated density functions are $\mathrm{p}(\mathrm{g}/\mathrm{d_p})$ are related by equation (1.56) and (1.57)

$$\mathrm{p}(\mathrm{x}/\mathrm{y}) = \frac{\mathrm{dP}(\mathrm{x}\backslash\mathrm{y})}{\mathrm{dx}} \tag{1.56}$$

$$\mathrm{p}(\mathrm{x}/\mathrm{y}) = \frac{\mathrm{P}(\mathrm{x}\backslash\mathrm{y})}{\mathrm{dx}} \tag{1.57}$$

and satisfy the rules similar represented through equations (1.58) to (1.61)

$$\int\int \mathrm{p}(\mathrm{x},\mathrm{y})\mathrm{dxdy} = 1 \tag{1.58}$$

$$\int \mathrm{p}(\mathrm{x},\mathrm{y})\mathrm{dxdy} = \mathrm{p}(\mathrm{x}) \tag{1.59}$$

$$\int \mathrm{p}(\mathrm{x},\mathrm{y})\mathrm{dx} = \int \mathrm{p}(\mathrm{y}/\mathrm{x})\mathrm{p}(\mathrm{x})\mathrm{dx} = \mathrm{p}(\mathrm{y}) \tag{1.60}$$

$$\int \mathrm{p}(\mathrm{y}/\mathrm{x})\mathrm{dx} = 1 \tag{1.61}$$

1.12.2 Practical representations of conditional grade distributions

1.12.2.1 The washability curve method

This method is based on the dense liquid fractionation laboratory method Figure 1.8 and 1.9). Floating and sinking particles are separated in an organic liquid of density between 1200 Kg/m3 to 3200 Kg/m3. The fraction of the particle population that has density less than the density of the liquid will float while the others will sink. By linking the particles composition to the density of the particle, the measured fraction is equal to the cumulative distribution P(g). Dense-liquid fraction testing is often done on specific size fractions; it helps to determine the conditional cumulative grade distribution$P(g\backslash d_p)$.

1.12.2.2 The parallel method

The method of analysis is called parallel method because identical samples of the population are analysed in parallel.

The parallel method generates the cumulative distribution P(g). The value of the cumulative distribution function can be measured at different values of g by using different liquids that have densities adjusted to correspond to specific particle mineral composition.

If a particular size fraction is separated on composition basis, it generates the conditional distribution P(gdp).

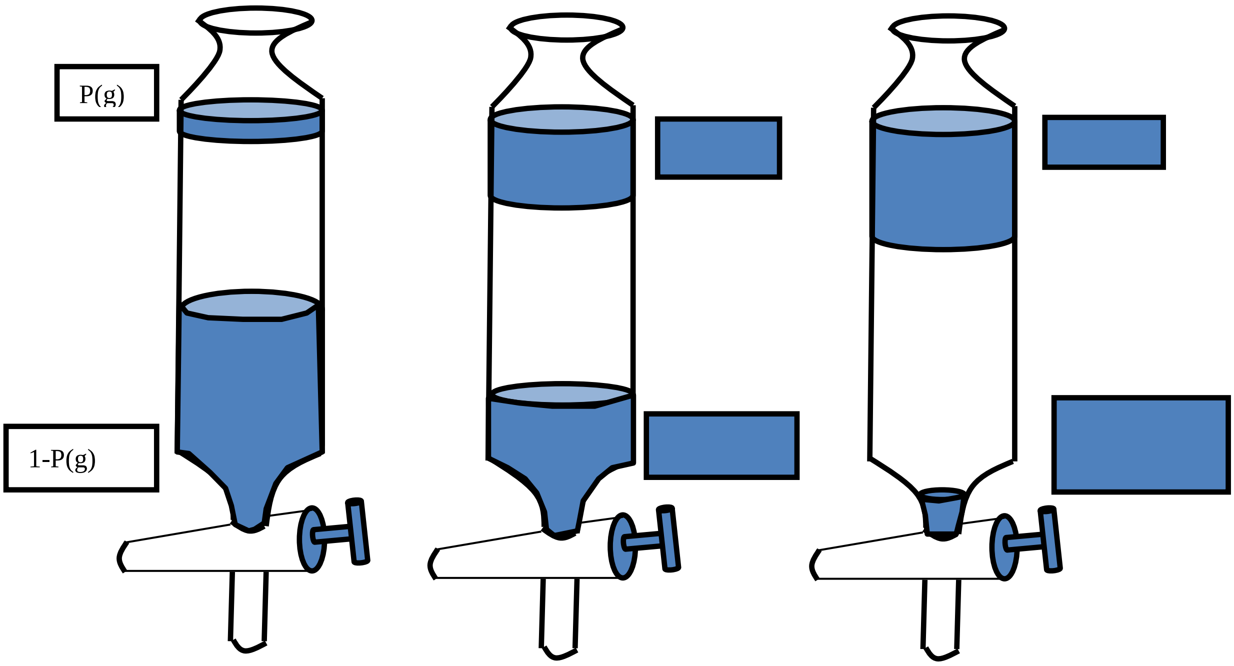

Figure 1.8 Representation of the dense-liquid fractionation experiments.

1.12.2.3 The sequential method

Instead of analysing N identical samples at N different densities, a single sample is separated sequentially at N different densities. The sink fraction from the first test is tested at the next higher density after which the sink from the second test passes to the third liquid and so on until separations at all N densities as shows figure 1.9

1.12.2.4 Advantages of sequential method

This method uses smaller quantities of sample and yields additional information that is particularly useful and valuable in the analysis and simulation of mineral processing operations. The sequential method generates the discrete distribution$p_j(g)$.

If a particular size fraction is used, this test generates the conditional discrete distribution $p_j(g_j, d_p)$

Each float fraction is collected, dried and sent for further analysis such us particle density by pycnometry, elemental analysis by X-ray fluorescence analysis or atomic adsorption spectrometry and particle size analysis if a size-composite sample is used. Some typical test results are shown in table 1.2.

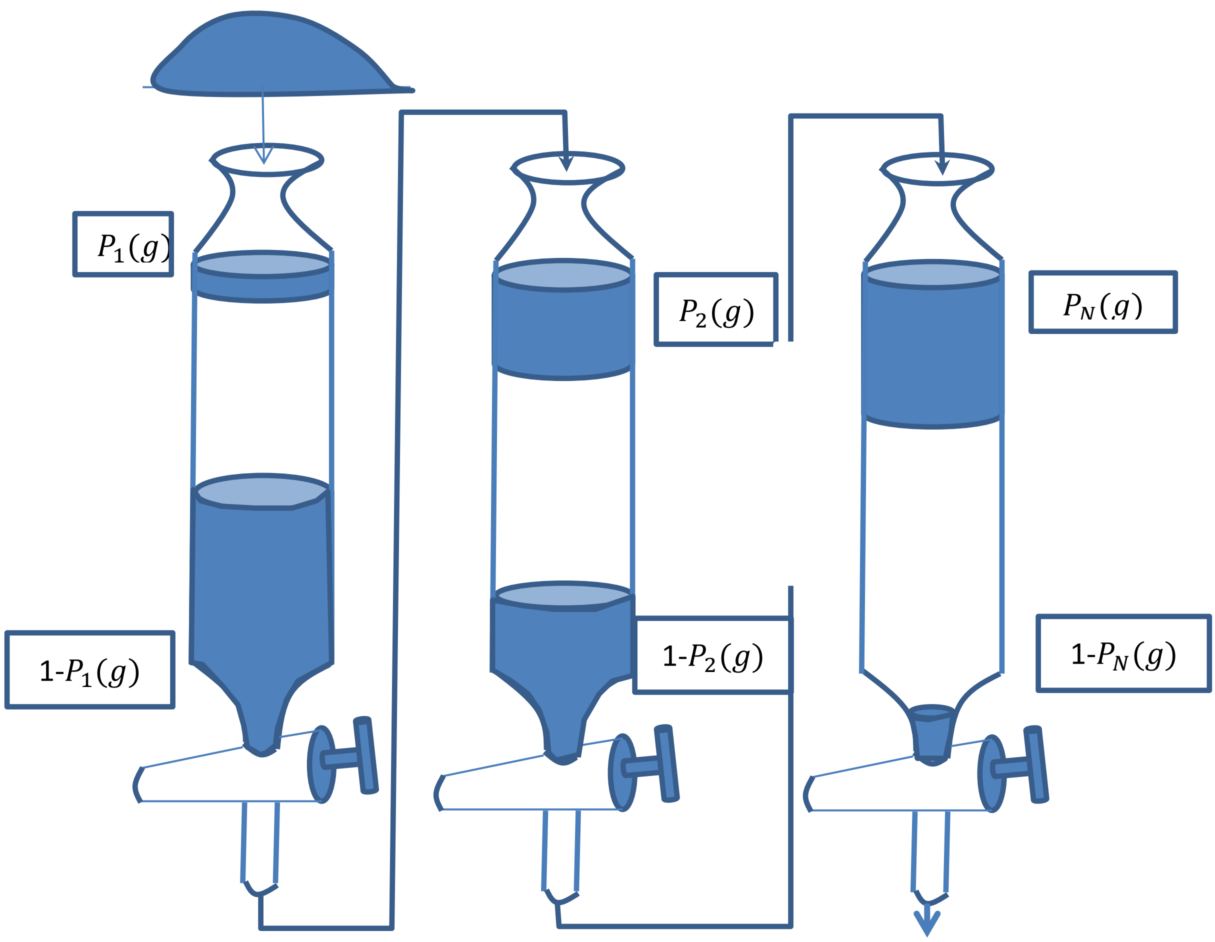

Figure 1.9 Representation of the dense-liquid fractionation experiment.

1.12.2.4 Relationship between mineral composition and density

In these two experiments, the density of a particle can be related to its mineralogical composition. If the material has only two minerals, the relationship is represented as in equation (1.62):

$$\frac{1}{\rho} = \frac{g}{\rho_M} + \frac{1-g}{\rho_G} \tag{1.62}$$

Where ρ = density of a particle; ρ_M = density of the mineral phase; ρ_G = density of the gangue phase; g = mass fraction of mineral in the particle

The inverse of equation (1.62) is shown in equation (1.63), and indicates that the mineral grade is a linear function of the reciprocal of the particle density.

$$g = \left(\frac{\rho_G - \rho}{\rho_G - \rho_M}\right)\frac{\rho_M}{\rho} \tag{1.63}$$

For samples with more minerals, additional information is required from the dense-medium test to relate the composition to the separating density; this requires analysis of each floating fraction.

Table 1.2 Typical dense liquid test results for two minerals sample

Liquid specific gravity	Total mass yield in this fraction %	% CaO	% SiO_2
Float at 2.85	21.6	19.30	18.2
2.85-2.88	5.7	21.76	2.49
2.88-2.91	3.20	10.15	1.52
2.91-2.94	0.90	9.67	2.92
2.94-2.96	6.70	2.95	3.89
2.96-3.03	61.0	0.96	2.55
Sink at 3.03	0.00		

Typical data are shown in Table 1.2 from which, the average mineralogical composition of particles in each fraction can be estimated. In this case the calcite content is estimated from the CaO assay and the magnesite content is estimated by difference assuming that only the three minerals magnesite, calcite and silica are present. The relationship between the particle density and its mineralogical is represented by equation (1.64):

$$\rho^{-1} = \sum_{m=1}^{M} g_m {\rho_m}^{-1} \quad (1.64)$$

If the density intervals used in the dense-liquid test are narrow, the average density of the particles in each density fraction can be assumed to be midpoint. The densities calculated from the mineralogical compositions and the known densities of the minerals should correspond quite closely with the midpoint densities as shown in table 1.2.

Table 1.2 Typical dense liquid test results for more than two minerals sample

Liquid specific gravity	% Magnesite	% Calcite	% SiO2	Calculated density kg/m3
Float at 2.85	21.6	19.30	18.2	2828
2.85-2.88	5.7	21.76	2.49	2867
2.88-2.91	3.20	10.15	1.52	2935
2.91-2.94	0.90	9.67	2.92	2933
2.94-2.96	6.70	2.95	3.89	2968
2.96-3.03	61.0	0.96	2.55	2985
Sink at 3.03	0.00			

1.13 Measurement of grade distributions by image analysis

Automatic image analysis helps to determine the distribution of particle grades in a sample from a narrow size fraction.

1.13.1 Procedure for the grade determination by image

Particles are mounted in random orientation and sectioned, and their microscopic image is generated by optical or scanning electron microscopy which reveals each mineral phase that is to be measured. A typical image of a binary mineral system for different minerals is shown in figure 1.10 (a-c). The apparent grade of each particle section in the image can be readily determined when the image is stored in digital form. The apparent areal grad of a particle section is the ratio of mineral phase pixels to total pixels in the section.

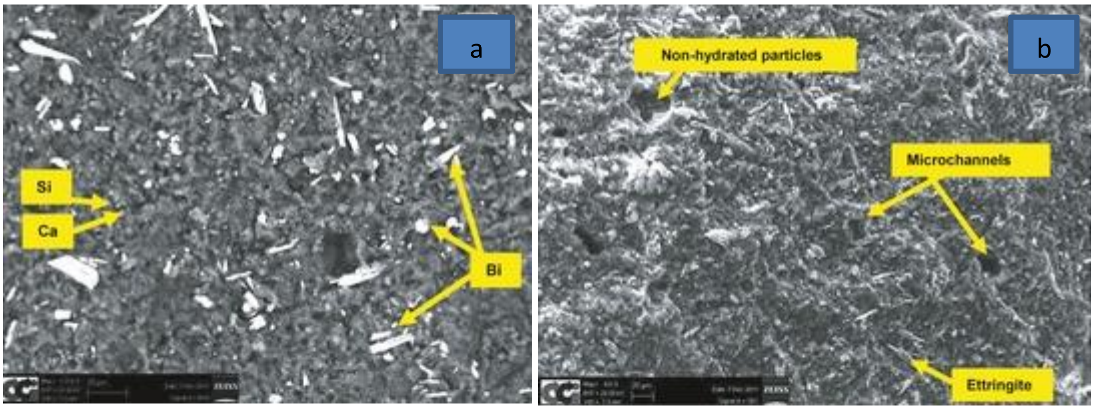

Ettringite: $Ca_6Al_2(SO_4)_3(OH)_{12}\cdot 26H_2O$

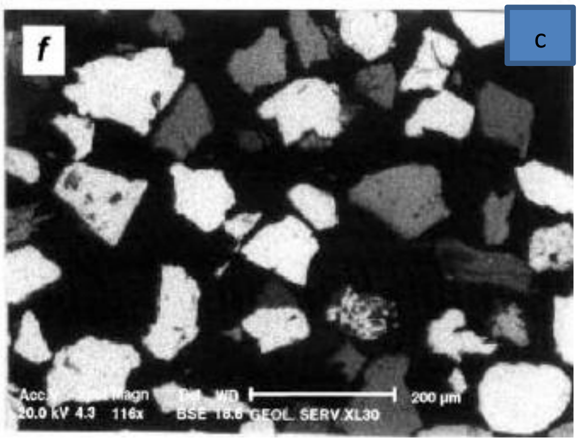

(f) Bright monazite grains. $(Ce,La)PO_4$

Figure 1. 10: binary mineral system

Alternatively the apparent grade can be determined by linear or areal measurement. Typical histograms of measured linear grade distributions are shown in Figure 1.11. These histograms are based on 12 grade classes which describe pure gangue in class 1, pure mineral in class 12 and 10 equally spaced grade classes in the grade fraction range from 0.0 to 1.0. Note that 11 separate size fractions were analysed.

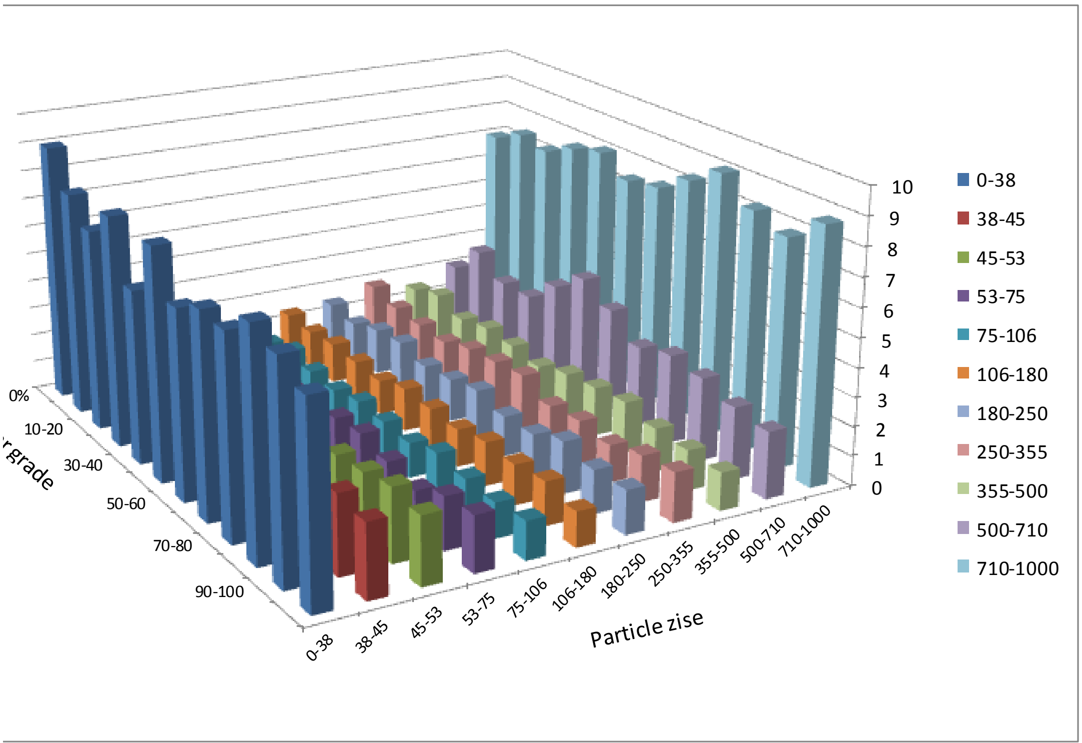

Figure 1.11 Distribution of linear grades measured by image analysis of many images

The measured apparent grade distributions must be stereologically corrected to convert them to the desired grade distribution. The stereological correction is a typical inverse problem and requires the solution of the integral equation

$$P(g_m \backslash d_p) = \int_0^1 P(g_m \backslash g, d_p) p(g \backslash d_p) d_g$$

gm represents the measured apparent grade, either linear or areal,

g represents the true grade of a particle.

$P(g_m \backslash d_{pi})$ is the cumulative distribution of apparent grades that is measured in the image. Solution of the integral equation requires care for accurate answers using effective methods which are available. A histogram of the true volumetric distribution of particle grades is shown in Figure 1.12 after stereological correction of the data in figure 1.12.

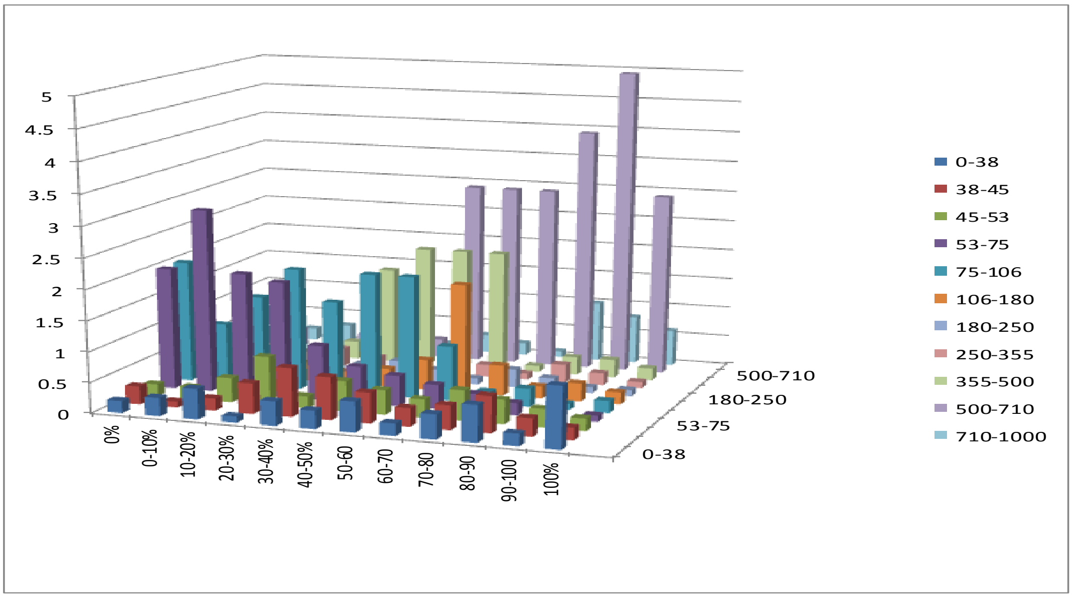

Figure 1.12: A histogram of the true volumetric distribution of particle grades

1.13.2 Independence

It might happen that two properties are distributed independently of each other. If the two properties are k and dp, then the relationship in equation (1.65) can be established.

$$p_{ji}\left({}^{k}/_{d_p}\right) = p_j(k) \qquad (1.65)$$

which means that the distribution of k values (these could be flotation rate constants for example) is the same within any size class as it is across the entire population which h leads to equation (1.66), this leads to

$$p_{ji}(k, d_p) = p_j({}^{k}/_{d_p})p_i(d_p) = p_j(k)p_i(d_p) \qquad (1.66)$$

which shows that the joint distribution for two properties that are independent can be generated as the product of the two separate distribution functions

1.13.3 Distributions by Number

In some situations it is useful to use number fractions rather than mass fractions when dealing with particle populations. The relationship between the mass distribution functions and the number distribution function can be deduced as follow:

The number distribution function $\Psi(d_p)$ is defined as the number fraction of particles in the entire population having size $\leq d_p$. Number distribution functions and number distribution density functions can be defined in a similar way for each of the distribution types already defined for mass fractions.

In particular the discrete number fractional distribution function is defined by equation (1.67)

$$\Psi_i(d_p) = \frac{\text{number of particles in size class i}}{\text{Total number of particles in the population}} = \frac{n_i d_p}{N} \tag{1.67}$$

The number distributions can be related to the mass distributions as follows: Ψ(m)dm: number fraction of particles having mass in the range (m, m + dm), $\Psi\left({}^{m}/_{d_p}\right) dm =$ Number fraction of particles of size dp that have mass in range (m, m + dm) which is the distribution density for particle mass conditioned by particle size. Knowing that $p_i(d_p)$ is the mass fraction of particles in size class I, m = Mass of a particle of size d_p, M = total mass of particles in the population, N = total number of particles in the population then equation (1.69) can developed as

$$.Mp(d_p) = N\int_0^\infty m\Psi(m, d_p)\,dm$$

$$= N\int_0^\infty m\Psi(m\backslash d_p)\Psi(d_p)\,dm \tag{1.69}$$

$$= N\varphi(d_p)\int_0^\infty m\Psi(m\backslash d_p)\,dm$$

$$= N\Psi(d_p)\overline{m}(d_p)$$

Using previous relationship in relation to mass fractions, equation (1.70) can be deducted

$$Mp_i(d_p) = M\int_{D_i}^{D_{i-1}} p(d_p)dd_p$$

$$Mp_i(d_p) = N\int_{D_i}^{D_{i-1}} \Psi(d_p)\overline{m}(d_p)dd_p \tag{1.70}$$

If the shape of a particle is statistically independent of size (a good approximation for single particle populations) can be represented by equation (1.71)

$$\beta = \frac{\overline{m}\ (d_p)}{{d_p}^3} = \frac{\overline{m}(d_p)}{{d_{pi}}^3} \tag{1.71}$$

Equation (1.70) can be simplified by using equation (1.71) combined with equation (1.43) gives equation (1.72)

$$Mp_i(d_p) = N\frac{\overline{m}\ d_{pi}}{{d_{pi}}^3}\int_{D_i}^{D_{i-1}} {d_p}^3\ \Psi(d_p)dd_p \tag{1.72}$$

$$Mp_i(d_p) = N\overline{m}d_{pi}\Psi_i(d_p)$$

The relationship between N and M is obtained from equation (1.73), and can be developed into equation (1.74) as follow:

$$M = M\sum_i p_i(d_p) = N\sum_i \overline{m}\ (d_{pi})\Psi_i(d_p)$$

$$\frac{M}{N} = \sum_i \bar{m}\,(d_{pi})\Psi_i(d_p) \qquad (1.73)$$

$$= \beta \sum_i d_{pi}{}^3\, \Psi_i(d_p) \quad \text{or}$$

$$\frac{M}{N} = \beta \int_0^\infty d_p{}^3 \Psi(d_p) dd_p \qquad (1.84)$$

where equation (1.71) has been used. Substituting equation (1.74) into equation (1.72) the exact relationship between the discrete distribution by mass $p_i(d_p)$ and the discrete distribution by number $\Psi_i(d_p)$ is obtained in equation (1.75) and equation (1.76) is deduced in similar way.

$$p_i(d_p) = \frac{d_{pi}{}^3 \Psi_i(d_p)}{\sum_i d_{pi}{}^3 \Psi_i(d_p)} \qquad (1.75)$$

$$\Psi_i(d_p) = \frac{p_i(d_p) / d_{pi}{}^3}{\sum_i p_i(d_i)/d_{pi}{}^3} \qquad (1.76)$$

1.14 Internal and External Particle Coordinate and Distribution Densities

So far particles have been classified based on particle size and the mineralogical composition. They are the most important properties in mineral processing and hydrometallurgical processes.

For effective models development of the unit operations, it is necessary to ensure a detailed description of particles. However it is impossible to describe a particle completely, because concepts such as shapes, surface topography, surface energy etc. cannot be clearly quantified. Therefore only finite and small number of variables can be chosen to describe the particle properties for modelling reasons.

The nature of particles is described by properties called the **internal coordinates of the particle phase space**. The choice of these coordinates depends on the model need and the primary objective of modelling the unit operations is to link them together for a plant flowsheet for the plant to be simulated.

Some examples of internal coordinates are Particles size; this is perhaps the most important of all; mineralogical composition; chemical composition; particle shape; surface specific energy

It might happen that internal coordinates that are required to model one of the unit operations is not appropriate for the other models therefore, internals coordinates of each model must be identified. This means that some of the internal coordinates will be redundant in some of the unit models.

1.14.1 External coordinates

External coordinates are parameters that physically locate or track the particles in unit operations. The particle location might have a significant effect on the particle behaviour and can help to describe the operation of the unit. The distribution functions that were described in the previous section can be related to corresponding distribution density functions. It is convenient to formulate a generalized model in terms of the joint distribution density function for all the internal and external particle coordinates.

The generalized particulate distribution density function $\Psi(x)$ is an ordinary function of the vector argument *x. This vector* comprises all of the external and internal coordinates that are relevant to the problem on hand. All possible vectors *x* make up the particle phase space.

$\Psi(x)$ is defined as the number fraction density i.e. the number fraction of the entire particle population that occupies unit volume of the particle phase space. The finite particle distribution functions defined previously can be constructed from the distribution density as follows. In the case where the phase space consists only of the particle size (dp) and the particle grade (g), the number fraction is determined through equation (1.77)

$$\Psi_{ij}(d_p, g_i) = \int_{D_i}^{D_{i-1}} \int_{G_i}^{G_{i-1}} \Psi\,(d_{p,} g) dd_p d_g \tag{1.77}$$

The mathematical description of Ψ is sometimes difficult. For example it may not be possible to obtain it in terms of any known transcendental functions and it may have to include Dirac delta functions. Particular examples are the two extreme ends of the liberation spectrum. Thus we tend to avoid Ψ for practical modelling work and use it only to develop some important model structures.

1.14.2 Particle Properties Derived from Internal Coordinates

Some examples are: Metal content percentage comes from the mineralogical composition,

The magnetic susceptibility of the particle from the magnetic susceptibilities of the each mineral…

The density is related to mineralogical composition by equation (1.78)

$$\frac{1}{\rho} = \sum_{m=1}^{M} \frac{g_m}{\rho_m} \tag{1.78}$$

Where $\rho_m \rho_m$: density of mineral phase; ρ: density of particle; g_m: mass fraction of mineral phase *m* in the particle (particle grade).

1.15 The Population Balance Modelling Method

As particles move through different unit operations, internal and external coordinates change due to their physical location change and alteration of their original characteristics. External and internal coordinates of a particle defines the coordinate location of the particle in the phase space. There must be enough internal coordinates in order to characterize the particle with details and some internal coordinates may be multidimensional.

If a particle has more than two minerals, the mineralogical composition vector must include one coordinate for each mineral. The number of these coordinates can be infinite, for example, during leaching processes when the concentration of the species that is being leached varies continuously within the particle and the chemical composition must be known at every point within the particle.

In general the concentration profile of the leached component will be low near the surface of the particle and higher further inside where lixiviate has not attained high concentrations. This is due to diffusional resistance within the particle; therefore the concentration profile depends on the processing history of the particle. In practice it is more convenient to use finite than therefore approximations must be made.

A case of one-dimensional internal characterisation is the topochemical processes where the radial position of the topochemical interface inside the particle gives information on the concentration profile and its effect on the rate of the chemical process. There is a large class of particulate rate processes that can be modeled topochemically. This makes topochemical models very powerful models for the descriptions of particulate rate processes.

Furthermore topochemical models allow the calculation of the rate at which the topochemical boundary moves and this rate is very important in the formulation of population balance models for the particle population as a whole.

1.16 The Fundamental Population Balance Equation

1.16.1 Some definitions

$\Psi(x)dx$: the number fraction of particles per unit volume of phase space. i.e. the number fraction of the particle population that occupies a small volume around the phase coordinate $\boldsymbol{x}$.

x: is the coordinate point in phase space $x \epsilon R^N$; u: is a vector of "velocities" at which particles change their phase coordinates.

For example this could be the rate of change of particle size by attrition when particle size is an internal coordinate, the rate of movement of the topochemical interface when the position of the interface is the internal coordinate or the rate of change of particle composition when the particle undergoes chemical change. The corresponding elements for the external coordinate are the physical velocities in three-dimensional space.

R(x): is the rate at which particles at coordinate position $\boldsymbol{x}$ are destroyed. This rate is specified as mass per unit volume of phase space per unit time.

Win: is the mass rate at which solid material is fed to the system

Wout: is the mass rate at which solid material is withdrawn from the system.

The material in the feed and product is distributed in the phase space according to $\Psi_{in}$and Ψ_{out} respectively.

m(x): is the average mass of a particle at point $\boldsymbol{x}$ in the phase space.

N: is the total number of particles in the system.

A: is the rate of addition of material in the feed stream.

Q: is the rate of removal material through product removal streams

B(**x;x**') is a distribution function that describes the way material can move suddenly over discrete distances in phase space following physical destruction or breakage.

B(**x;x**') is the mass fraction of solid material that has a phase coordinate less then **x** after destruction of a particle at phase coordinate **x**'.

The statement " the phase coordinate of a particle is less than **x "** must be interpreted to mean that every phase coordinate of the particle is less than the corresponding element of **x.**

b(**x;x**') is the corresponding density function.

a(**x;x**') is the distribution density for particles produced by attrition and other surface wear processes at **x**'.

In general a(**x;x**') and b(**x;x**') are very different from each other and in practical applications each needs to be determined separately.

Consider a region Rc of the particle phase space and include in Rc all processes that change the coordinates of particles. The region Rc is completely enclosed by a surface Sc.

These processes are

1. Movement across the boundaries of Rc (convective motion in phase space).
2. Arrivals by finite steps from other regions in the phase space.
3. Destruction of particles in region Rc.
4. Physical additions and withdrawals in feed and product streams.

An accounting of individual particles in the reference region Rc is determine through equation (1.79)

$$\frac{\partial}{\partial t}\int_{Bc} N\Psi(x)dx = -\int_{Sc} N\Psi(x)u.n.d\sigma - D + B - Q + A \quad (1.79)$$

Where n is the outward pointing normal vector to the surface Sc at point x.

In mineral processing systems solid mass is conserved, this brings important constraints on the formulation of model equations.

The destruction processes can be described by destroyed mass rate per unit volume of phase space which is determined by equation (1.80)

$$D = \int_{Rc} \frac{R(\Psi(x),x,F[\Psi(x)])}{\overline{m}(x)} dx \quad (1.80)$$

and is specified as number of particles broken per unit time in the control volume *Rc*.

The notation *F1*[Ψ*(**x**)*] indicates that the destruction function process *D* is a function of the entire distribution function Ψ*(**x**)* and not only of the value of Ψ *(**x**)* at **x**. This is the cause for example of dependence of breakage rates in a mill on the amount of fine and coarse particles present. The birth processes results from the products of the destruction processes since mass must be conserved, it is described by equation (1.81)

$$B = \int_{Rc} \frac{1}{\overline{m}(x)} \int_{R'(x)} R(\Psi(x'), x', F[\Psi(x)])\, b(x,x')dx'dx$$

$$- \int_{Rc} \frac{N}{\overline{m}(x)} \int_{R''(x)} \Psi(x')u(x')\nabla\overline{m}(x')a(x,x')dx'dx \quad (1.81)$$

Where $R'(x)$ and $R''(x)$ are the regions of space from which progeny particles can enter the small phase volume *d**x*** around the point ***x*** by breakage and attrition processes respectively. These are called the feeder regions for point ***x***.

The conservation of mass constraint distinguishes mineral processing systems from other particulate processes such as crystallization and leaching in which mass transfers between the solid phase and the liquid phase and solid phase mass is not conserved.

Mass enters and leaves the processing volume by physical addition and removal through feed and product streams. The addition rate is determined through equation (1.82).

$$A = \text{Win} \int_{Rc} \left(\frac{N}{M}\right)_{in} \Psi_{in}(x)dx \quad (1.82)$$

and the removal rate equation (1.83)

$$Q = \sum_j W_{out\,j} \int_{Rc} \left(\frac{N}{M}\right)_j \Psi_{out\,j}(x)dx \quad (1.83)$$

where j is the different physical output streams. The integral over the surface of the reference region is inconvenient and this can be converted to an integral over the volume by application of the divergence theorem by using equation (1.84).

$\int_{Sc} N\Psi(x)u.n\, d\sigma = \int_{Rc} N\nabla.u\Psi(x)dx$ (1.84)

The final working equation for steady-state operation is developed and presented in equation (1.85):

$$N\int_{Rc}\nabla.u(x)dx + \int_{Rc}\frac{R\Psi(x),x,F[\Psi(x)]}{\bar{m}(x)}dx - \int_{Rc}\frac{1}{\bar{m}(x)}\int_{R'(x)}R(\Psi(x'),x',F[\Psi(x)])b(x,x')dx'dx +$$

$$\int_{Rc}\frac{N}{\bar{m}(x)}\int_{R'(x)}R(\Psi(x')u(x').\nabla\bar{m}(x')a(x,x')dx'dx = -\sum_j W_{out\,j}\left(\frac{N}{M}\right)_j\int_{Rc}\Psi_{out\,j}(x)dx +$$

$$W_{in}\left(\frac{N}{M}\right)_{in}\int_{Rc}\Psi_{in}(x)dx \qquad (1.85)$$

This equation can be modified in a number of ways to suit the requirements of any particular application. It can be written in terms of mass density functions by substituting for Ψ (**x**) in terms of p(**x**) using equations such as (1.79).

Since the region Rc is random, equation (1.85) can be written as a functional integro-differential equation as shows equation (1.86)

$$N\nabla.u\Psi(x) + \frac{R\Psi(x),x,F[\Psi(x)]}{\bar{m}(x)} - \frac{1}{\bar{m}(x)}\int_{Rx}R(\Psi(x'),(x'),F[\Psi(x')])b(x,x')dx' +$$

$$\int_{R'(x)}R(\Psi(x')u(x').\nabla\bar{m}(x')a(x,x')dx'dx -$$

$$\sum_j W_{out\,j}\left(\frac{N}{M}\right)_j\int_{Rc}\Psi_{out\,j}(x)dx + W_{in}\left(\frac{N}{M}\right)_{in}\Psi_{in}(x) \qquad (1.86)$$

This form of the population balance equation is usually the most convenient for analytical solution. The population balance equation can be solve only $\int \Psi(x)dx = 1$ where the integral is taken over the entire phase space. The two breakage functions b(**x;x**') and a(**x;x**') must satisfy two important conditions

$\int_{R_{A\prime}} b(x,x')dx = 1$ and $\int_{R_{A\prime\prime}} a(x,x')dx = 1$ where RA' and RA'' are the regions of the phase space that can be reached by progeny particles that are formed by breakage (for b) or attrition (for a) at point **x**'. They are called the accessible regions of phase space and they are complementary to the feeder regions R' and R'' The determination of the feeder regions R' and R'' and the accessible regions RA' and RA'' can be quite difficult. It is usually easier to define the accessible regions than the feeder regions and this fact can have a significant effect on the choice of computational algorithms that can be used successfully.

In most applications the fundamental population balance equation will be reduced to an appropriate discrete form with the region *Rc* corresponding to the appropriate particle class

1.16.2 The General Population Balance Equation for Comminution Machines

The population balance equation provides a powerful model for the description of industrial comminution machines. It help to develop uniform model that describes the operating behaviour of rod, ball, semi-autogenous, and autogenous mills. Considering only one internal coordinate, the particle size, and assuming that the breakage and wear processes are not dependent on the position of the particle in the mill, the external coordinates become irrelevant. The general equation (1.86) is therefore written in the form of equation (1.87)

$$N\frac{d}{dx}\left(u(x)\Psi(x)+\frac{R\Psi(x),x,F[\Psi(x)]}{\beta x^3}-\frac{1}{\beta x^3}\int_{Rx}R(\Psi(x'),(x'),F[\Psi(x')]\right)b(x,x')dx'+$$
$$\frac{N}{\beta x^3}\int_{R'(x)}\Psi(x')u(x').\frac{d\beta x'^3}{dx}a(x,x')dx'=-W\left(\frac{N}{M}\right)_{in}\Psi_{out}(x)+W\left(\frac{N}{M}\right)_{in}\Psi_{in}(x) \quad (1.87)$$

In equation (1.87) the scalar x represents the particle size dp and the average mass of a particle is related to the size by equation (1.88)

$$\bar{m}\,(x)=\beta x^3 \quad (1.88)$$

A commonly-used model for the rate of attrition and other wear processes such as chipping is: “this rate is proportional to the surface area of the particle”.

Using a spherical particle as a reference, it can be written as represented by equation (1.89)

$$\frac{\pi dx^3}{6\,dt}=\frac{K'\pi x^2}{2} \quad (1.89)$$

which indicates that the velocity at which a wearing particle moves in phase space is constant and is given by equation (1.90)

$$u(x)=\frac{dx}{dt}=-K' \quad (1.90)$$

A more general model for surface wear processes is represented in equation (1.91)

$$\frac{dx}{dt}=-K(x)=-Kx^{\Delta} \quad (1.91)$$

where Δ is a constant between 0 and 1. This can be developed into equation (1.92)

$$\frac{dm}{dt}=-K\frac{\pi\rho_s x^{2+\Delta}}{2} \quad (1.92)$$

If $\Delta = 0$ the specific surface wear rate is constant while $\Delta > 0$ means that the specific surface wear rate increases as the size of the particle increases. As shown above $\Delta = 0$ corresponds to the assumption that surface wear rate is proportional to the surface area of the particle while $\Delta = 1$ means that the surface wear rate is proportional to the mass of the particle. It is usual to develop the population balance equation in terms of the distribution by mass and equation (1.67) is converted using equation (1.74) into equation (1.93)

$$\Psi(x)=\frac{Mp(x)}{N\beta x^3} \quad (1.93)$$

Equation (1.87) becomes

$$-\frac{M}{\beta}\frac{d\left(K(x)p(x)/x^3\right)}{dx}+\frac{R\Psi(x),x,F[\Psi(x)]}{\beta x^3}--\frac{1}{\beta x^3}\int_{Rx}R(\,p(x'),x',F[p(x')]b(x,x')dx'-$$

$$\frac{M}{\beta x^3}\int_{R'(x)}\frac{p(x')}{x'^3}3K(x')x'^2a(x,x')dx' = -W\frac{p_{out}(x)}{\beta x^3}+W\frac{p_{in}(x)}{\beta x^3} \quad (1.94)$$

The rate of destruction is intensive with respect to the average mass density over phase space. Consider two systems having the identical phase space but containing different total masses. In particularΨ (**x**) is identical for both systems.

Then, $\frac{R_1(p(x),x,F[p(x)])}{R_2((px),x,F[p(x)])}=\frac{M_1}{M_2}$

$$R\big((px),x,F[p(x)]\big) = MR'(p(x),x,F[p(x)]) \quad (1.95)$$

Furthermore a logical assumption relating to the physical breakage process would suggest that equation (1.95) can be written in the form of equation (1.96)

$$R\big((px),x,F[p(x)]\big) = Mp(x)k(x,F[p(x)]) \quad (1.96)$$

Where $k(x,F[p(x)])$ is the specific rate of breakage of material of size x and it represents the breakage rate when 1kg of material of size x is in the mill. The average residence time in the mill is given by equation (1.97)

$$\tau = \frac{M}{W} \quad (1.97)$$

where W is the flowrate through the mill.

Equation (1.94) becomes

$$-\tau\frac{dK(x)p(x)}{dx}+3\tau K(x)\frac{p(x)}{x}+\tau R(p(x),x,F[p(x)]$$
$$-\tau\int_{R\prime(x)}R'(p(x),x'F[p(x)])b(;x')dx'$$
$$-\tau\int_{R\prime\prime(x)}3K(x')\frac{p(x')}{x'}a(x;x')dx = p_{in}(x)-p_{out}(x)$$

(1.98)

This is the fundamental population balance equation for any comminution process and it incorporates both autogenous and media-induced breakage. It is difficult to solve this integro-differential equation mainly because the functions R, b and a are strongly nonlinear. Under conditions that apply to practically useful situations, only numerical solutions are possible

CHAPTER II

FORCES ON PARTICLES

2.1 Forces on particles

Force/moments determine the kinetics of motion.

2.1.1 External forces

External force are those acting external to the body.

external force can be classified in two types:

2.1.2 Body forces

Body forces are those forces which act based on mass or volume of the particle: gravitational force, Magnetic force

2.1.3 Surface force

Surface force is the **force** that acts across an internal or external **surface** element in a particle.

2.1.4 **Surface force** can be decomposed into two perpendicular components

Pressure force acts normally over an area

stress forces acts tangentially over an area.

2.1.5 Internal Forces

Internal forces acting between two parts of the same particle.

2.1.6 Drag Force

When a solid particle moves through a fluid it experiences a drag force that resists its motion.

Drag force has its origin in two phenomena:

The frictional drag on the surface

The frictional drag is caused by the viscosity of the fluid as it flows over the surface of the particle. This component is called viscous drag and is illustrated in figure 2.1. The increase in pressure that is generated in front of the particle as it moves through the fluid.

There are two pressure regions:

A region of high pressure $P1$ is formed immediately in front of the particle as it forces its way through the fluid.

a region of relatively low pressure is formed immediately behind the particle. The pressure drop *P*1 – *P*2 gives rise to a force on the particle given by (*P*1 – *P*2)*Ac*

Ac is the cross-sectional area of the particle measured perpendicular to the direction of motion. This is called the form drag. The total force on the particle is the sum of the viscous drag and the form drag.

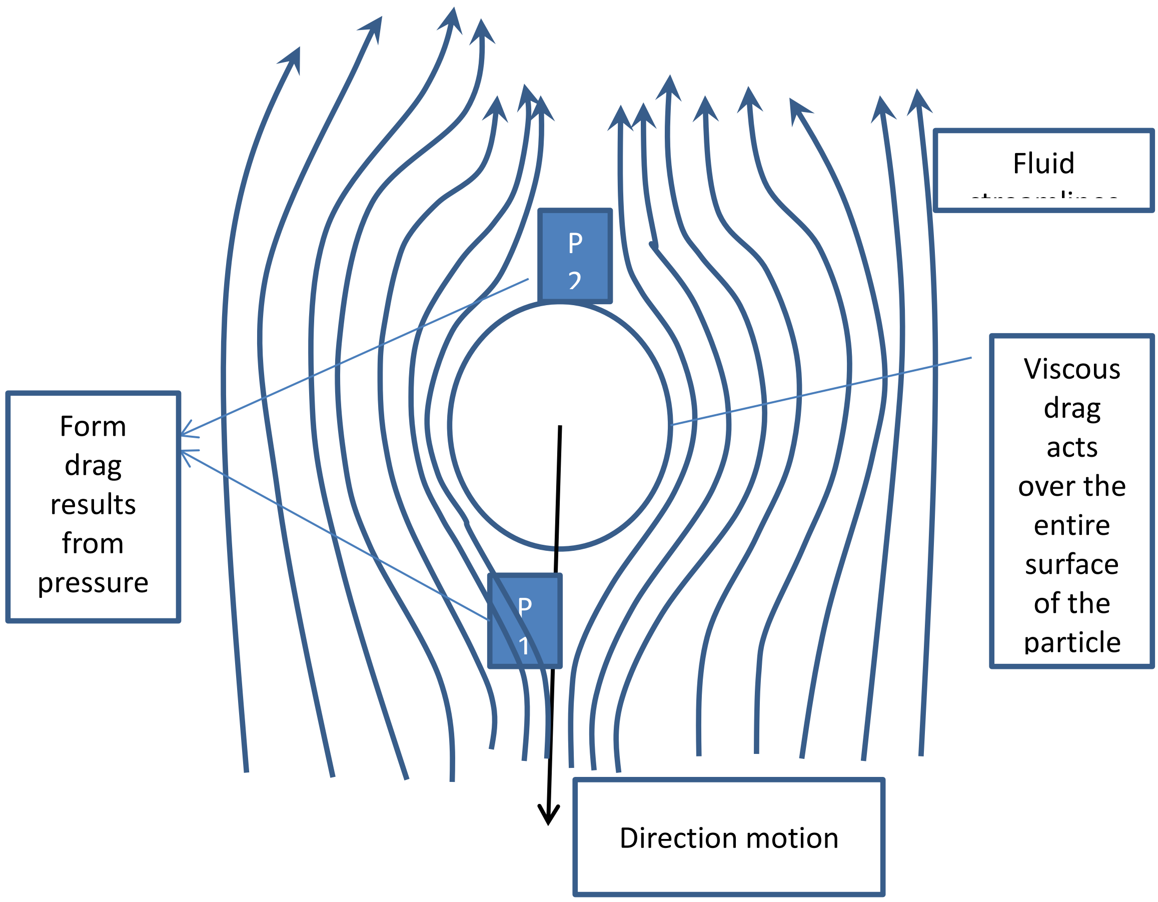

Figure : 2.1: Configuration of the drag force on particle

The drag force is determined through equation 2.1

$$\text{Drag force} = 0.5C_D(v_r - v_r)^2\rho_f A_C \quad (2.1)$$

Where ρ_f is the fluid density; Ac: the cross-sectional area of the particle; CD: the drag coefficient.

Centrifugal force

The apparent force that is felt by an object moving in a curved path that acts outwardly away from the center of rotation and is calculated through the equation (2.2)

$$\text{Centrifugal force} = \frac{{v_0}^2}{r} v_p(\rho_s - \rho_f) \quad (2.2)$$

where v_0 is the tangential component of the particle velocity vector, r: the radius of the tangential motion; v_p the volume of the particle; $\boldsymbol{\rho_s}$: the density of the solid.

2.1.7 Gravitational Force

The gravitational force is determined through equation 2.3

$$\text{Gravitational force} = hR^2\Delta\rho g \qquad (2.3)$$

Where h is the close separation distance between surfaces (0.2 mm at physical contact); Δρ: density dofference between the particle and water; Gg: acceleration due to gravity

2.1.8 Electrical force

The electric force is determined through equation (2.4)

$$\text{Electrical forfe} = \varepsilon\varepsilon_0\xi^2 \qquad (2.4)$$

Where ε_0 is the permittivity of free space; ε: dielectric constant; ξ: zeta potential

2.1.9 Inertial force

Inertial force is a force that resists a change in velocity of an particle and is calculated through equation (2.5)

$$\text{Inertial force} = h^2R^5(\Delta\rho)^3g^2 \qquad (2.5)$$

2.1.10 Van der waals force

The relatively weak attractive forces between neutral atoms and molecules that collide or pass close to each other and is calculated using equation (2.6). They are short range forces and decay rapidly to zero away from a surface. Van der Waals forces arise because of the electric polarization induced in each of the particles by the fluctuation of electron cloud surrounding the nucleus of electrically neutral atoms

$$\text{Van der Waals force} = A_H\mu^2 \qquad (2.6)$$

Where A_H is the Hamaker constant; μ: viscosity of water

Example 6.6.1:

Compute the force ratios given in Table 6.6.2 for an aqueous flotation system for which, R = 1 μm , Δρ= 3000 kg/m3, ξ = 100 mV and $A_H = 1x10^{-20}.J$ $\mu = 1.10^3$Pa s $\varepsilon = 80$, Take h = 1 nm. Comment on your results.

Solution

The permittivity of free space $\varepsilon_0 = 8.854.10^{-12}\mathrm{C}^2\mathrm{J}^{-1}\mathrm{m}^{-1}$

$$\frac{\text{Gravitational force}}{\text{Electric force}} = \frac{(1.10^{-9})(1.10^{-6})^2(3000(9.8)}{(80)(8.854.10^{-12})(0.1)^2} = 4.2.10^{-6}$$

$$\frac{\text{Gravitational force}}{\text{Van der waals force}} = \frac{(1.10^{-9})^2(1.10^{-6})^2(3000)(9.8)}{1.10^{-20}} = 2.9.10^{-6}$$

$$\frac{\text{Inertial force}}{\text{Electrical force}} = \frac{(1.10^{-9})(1.10^{-6})^5(3000)^3(9.8)^2}{(80)(8.854.10^{-12})(0.1)^2(1.10^{-3})^2} = 3.7.10^{-10}$$

$$\frac{\text{Inertial force}}{\text{Van der waals force}} = \frac{(1.10^{-9})^2(1.10^{-6})^5(3000)^3(9.8)^2}{(1.10^{-20})1.10^{-3})^2} = 2.6.10^{-10}$$

These values show that the gravitational and inertial forces are much smaller than the electrical and van der Waals forces for this system.

2.2 Interactions between Particles at a Fluid Interface (Colloid theory)

2.2.1 Meniscus

Meniscus is interfacial deformation near the particle caused by the attachment of a particle to the boundary between two fluid phases. The overlap of such two deformations gives rise to lateral capillary interaction or force between the particles. A lateral capillary force between similar particles is attractive and brings causes particle aggregation and ordering, and plays an important role in the production of various two dimensional structures which is the main reason for the growing interest in this this field during the last decade.

2.2.2 Reason for Meniscus appearance

The particle weight (together with the Archimedes force) gives rise to an interfacial deformation and lateral capillary attraction (flotation force). This appears when floating "heavy" particles of size greater than ca 10 μm, menisci appear also around colloids that are partially immersed in a liquid film because of the different wettability of the particles by the two neighboring fluid phases interfacial deformations can be produced by an undulated contact line on the particle surface due, for example, to surface roughness or to non-spherical particle shape (ellipsoids, polyhedrons, etc.) interfacial deformations can be produced by electric charges at the particle surface. Like-charged particles electrostatically repel each other

The balance of the latter two (undulated contact line on the particle surface and electric charges at the particle surface) forces would lead to the appearance of an energy minimum, corresponding to the equilibrium position of the particle in a two-dimensional colloid lattice

Most of the experimentally observed electric effects with particles at oil/water and air/water interfaces are due to the presence of electric charges at the boundary particle/nonpolar fluid. Because of the absence (or very low concentration) of ions in the nonpolar fluid, the electric interaction between two particles across the nonpolar phase are not screened. Consequently, the electric repulsion between like-charged particles has a long-range. Different approaches have led to the conclusion that the electric-field-induced capillary force is attractive, but it has been unclear whether it could prevail over the direct electric repulsion between like-charged particles

2.3 Lateral capillary forces between particles attached to an interface

When a colloidal particle is attached to a liquid interface, the latter usually deforms in the vicinity of the particle.

The overlap of meniscus from two particles gives rise to lateral capillary force between them

The range of these capillary forces is usually much longer than the range of the van der Waals and double-layer surface forces Figure.,.)

Lateral capillary forces play an important role for the production of two-dimensional (2D) arrays of colloidal particles,

Depending on the physical origin of the meniscus, we can distinguish several kinds of lateral capillary forces, which are illustrated in Figure 2.1 and considered separately below.

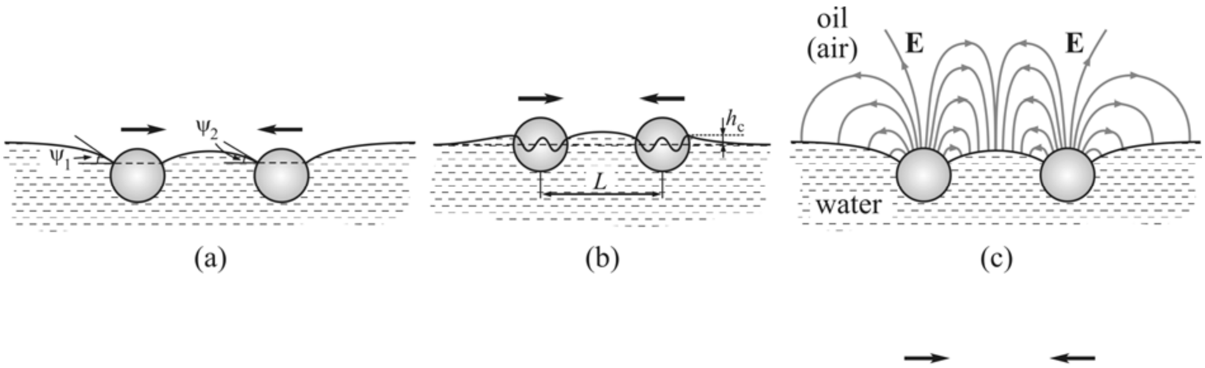

Figure 2.1: Different types of lateral capillary forces

2.4 Flotation Capillary Forces

The interfacial deformation around two floating particles can be due to gravitational effects, that is, the particle weight minus the buoyancy force (Figure 2.1a). In this case, we are dealing with a gravity-induced lateral capillary force.

The flotation capillary force is essential for particle diameters greater than 5–10 μm depending on the particle and liquid-phase mass densities. The meniscus shape around an isolated particle of rotational symmetry is described by equation (2.6)

Expression:

$$\xi(r) = QK_0(qr),\ q \equiv (\frac{\Delta\rho g}{\gamma})^{1/2} \tag{2.6}$$

Where $z = \zeta(r)$ describes the meniscus profile; r and z are cylindrical coordinates, $K0$ is the modified Bessel function of the second kind and zero order. The force of capillary interaction q is the inverse capillary length

$F = -\,d\Delta W/dL$

With $\Delta W = -2\pi\gamma Q_1 Q_2 K_0(qL)$ (2.7)

The minus sign in equation (2.7) means that the capillary interaction corresponds to attraction and is represented by equation (2.8)

$$Q_1 = \mp r_1 \sin\Psi_1 \quad Q_2 = \mp r_2 \sin\Psi_2 \tag{2.8}$$

Where F: force of capillary interaction, r_1, r_2 are the radii of the three-phase contact lines on particles 1 and 2, Ψ_1 and Ψ_1 Meniscus-slope angles, ΔW the capillary interaction energy

L is the center-to-center distance between the two particles and q is the inverse capillary length.

Differentiating equation (2.7) gives

$$F = -2\pi\gamma Q_1 Q_2 K_1(qL)$$

$K1$ is the modified Bessel function of the second kind and first order

For qL<<<1

$K_1(qL) \sim 1$

2.8 becomes (2.9)

$$F = -2\pi\gamma \frac{Q_1 Q_2}{L} \text{ for } qL<<<1 \tag{2.9}$$

Equation (2.6) looks like a two-dimensional analog of the Coulomb's law of electricity, and for this reason the quantities Q1 and Q2 have been called capillary charges

This analogy between capillary and electric forces has been further extended by introducing "capillary multipoles" as analogs of the electric multipoles

The "capillary charge" for floating particles can be estimated from the expression

$$Q_1 \approx \frac{1}{6} q^2 R_i^3 \,(2 - 4D_i + 3\cos\alpha_i - \cos\alpha_i^3) \text{ (i =1.2)} \tag{2.10}$$

Di = (ρi − ρII)/ (ρI − ρII), ρi, ρI and ρII are the mass densities of the particle lower and upper fluid phases, respectively. Equation 2.10 allows one to calculate the capillary charge Qi directly from the particle radius Ri and the central angle αi (by definition, sin αi = ri/R)

2.5 Forces between Capillary Multipoles

The weight of particle of microns size is not sufficient to deform the fluid interface and to yield capillary force between the particles. However, interfacial deformation appears if the contact line at the particle surface has undulated or irregular shape (Figure 2.1b).

This may happen when the particle surface is rough, angular or heterogeneous. In such cases, the contact line sticks to edges or to boundaries between domains on the heterogeneous surface. The undulated contact line induces undulations in the surrounding fluid interface

2.6 Electric-Field-Induced Capillary Forces

Except the gravitational field (Figure 2.1a), the electric field can induce interfacial deformations around an adsorbed particle, if this particle is electrically charged (Figure 2.1c). The overlap of the interfacial deformations around such two charged particles gives rise to electric-field-induced capillary force. Charges located near the boundary between two phases of different dielectric constants experience image-charge forces which cause electro-dipping force (F_{ED}) acting on each particle in direction toward the phase of greater dielectric constant in our case – toward water. At equilibrium, the electro dipping represented in equation (2.11) force is counterbalanced by the interfacial tension force

$$F_{ED} = 2\pi r_c \gamma \sin\Psi_c \tag{2.11}$$

Where Ψ_c: meniscus slope angle at the contact line; γ: the interfacial tension; r_c: is the radius of the contact line on the particle surface. F_{ED} can be determined from the experimental values Ψ_c, γ, and r_c.

This approach was used to obtain the values of F_{ED} for salinized glass particles of radii 200–300 μm from figure (2.3) the particles at an oil-water or air-water interface where

F_{ED} is the electrodipping force, due to the image-charge effect, that pushes the particles into water and deforms the fluid interface around the particles, F_{ER} is the direct electric repulsion between the two like-charged particles, F_{EC} is the electro capillary attraction, related to deformations in the fluid interface created by the electric field. F_{ED} was found to be much greater than the gravitational force acting on the particles.

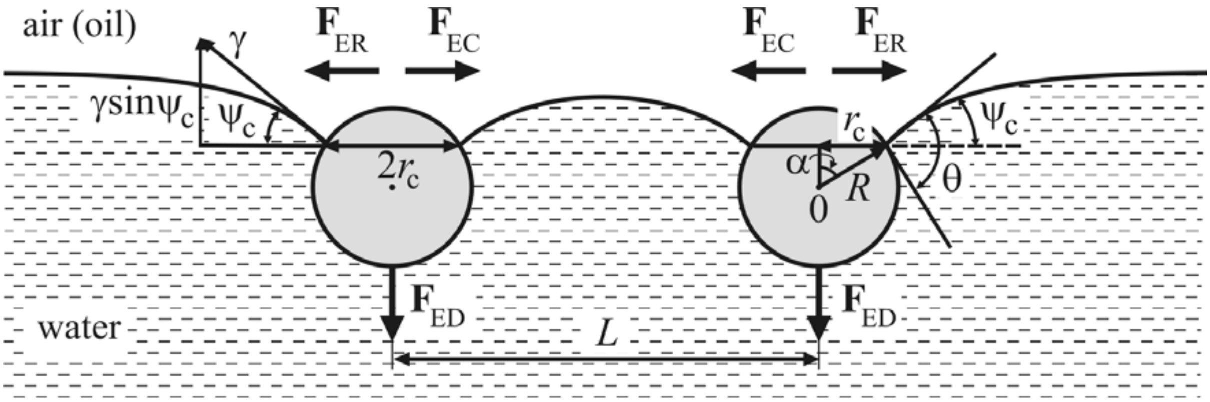

Figure 2.3: Sketch of two electrically charged particles attached to an oil-water interface.

In figure 2.4 the profiles of the liquid menisci around a noncharged particle and a charged particle are compared. The particles represent hydrophobized glass spheres of density ρp = 2.5 g/cm3. The oil phase is purified soybean oil of density *ρ*oil = 0.92 g/cm3.

The oil-water interfacial tension is γ = 30.5 mN/m.

The calculated surface tension force, 2*πr*cγ sin ψc, which counterbalances the gravitational force (particle weight minus the Archimedes force) corresponds to meniscus slope angle ψc = 1.5°, the deformation of the liquid interface caused by the particle is hardly visible (Figure 2.4a).

In contrast, for the charged particle

(Figure 2.4b), the meniscus slope angle is much greater, ψc = 26°.

This is due to the fact that the electro dipping force, *F*ED, which pushes the particle toward the water phase, has to be counterbalanced by the interfacial-tension force, 2*πr*cγ sin ψc.

(a) Uncharged particle of radius *R* = 235 μm: the meniscus slope angle due to gravity is relatively small, ψc= 1.5°. (b) Electrically-charged particle of radius *R* = 274 μm: the experimental meniscus slope angle is ψc = 26° owing to the electrodipping force, F_{ED} (see Figure 2.3). If this force were missing, the gravitational slope angle of this particle would be only ψc = 1.9°.

Experimentally, it has been found that the angle ψc is insensitive to the concentration of NaCl in the aqueous phase, which means that (in the investigated case) the electro dipping force is due to charges situated at the particle-oil interface.58,60 With similar particles, the magnitude of F_{ED} at the air-water interface was found to be about six times smaller than at the oil-water

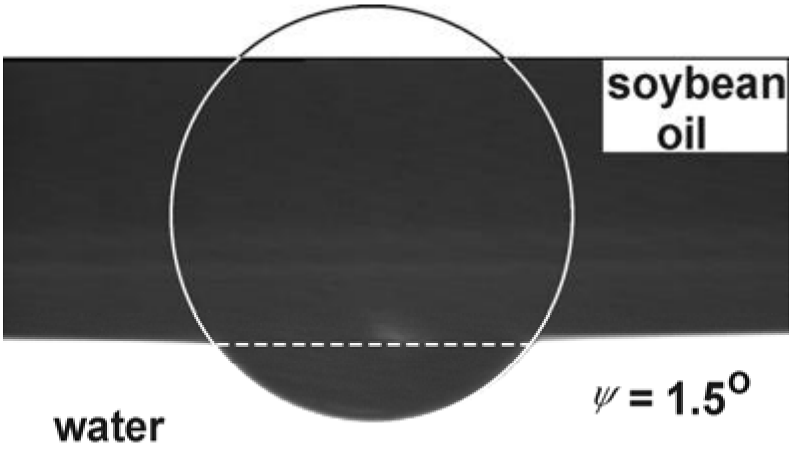

(a) noncharged particle

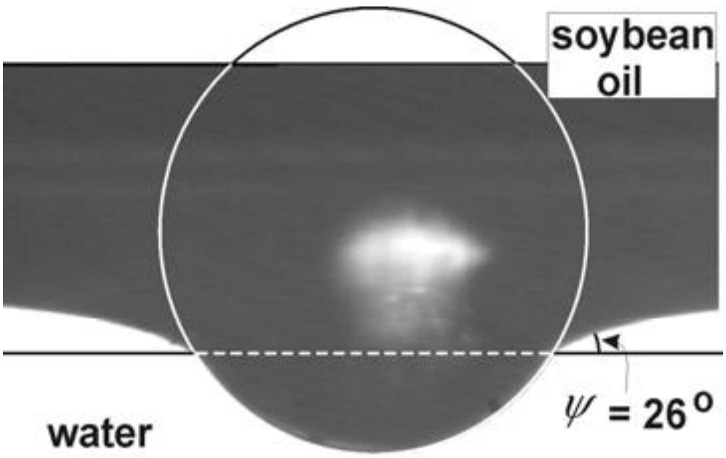

(b) charged particle

Figure 2.4: Side-view photographs of hydrophobized spherical glass particles at the boundary water/soybean oil (no added surfactants).

interface. In the case when the electrostatic interactions are dominated by the field of charges situated at the particle/nonpolar-fluid interface, F_{ED} can be calculated from the expression in equation (2.9):

$$\mathbf{F_{ED}} = (\mathbf{4\pi/\varepsilon_n})\,(\boldsymbol{\sigma}_{\mathbf{pn}}\mathbf{R})^2(\mathbf{1} - \mathbf{cos\alpha})\mathbf{f}(\boldsymbol{\theta}, \boldsymbol{\varepsilon}_{\mathbf{pn}}) \quad (2.12)$$

Where R is the particle radius, $\boldsymbol{\varepsilon}_{\mathbf{n}}$**;** the dielectric constant of the nonpolar fluid (oil, air); $\boldsymbol{\sigma}_{\mathbf{pn}}$**:** the surface charge density at the boundary particle–nonpolar fluid, the ratio of the respective two dielectric constants is represented by (equation 2.13)

$$\varepsilon_{pn} = {}^{\varepsilon_p}/_{\varepsilon_n}\text{: (2.10)} \quad (2.13)$$

Where the ratio of the respective two dielectric constants $\boldsymbol{\alpha}$**:** central angle and $\theta = \alpha + \Psi_c$: the contact angle (see Figure 2.3). In the other limiting case, when the electrostatic interactions are dominated by the field of surface charges of density σpw situated at the particle/water interface, F_{ED} can be calculated from the expression in equation (2.14)

$$F_{ED} = \frac{16\pi {r_c}^2 kTC}{ƙR}\left[cosh\left(\frac{e\varphi_{pw}}{2kT}\right) - 1\right], \sigma_{pw} = \frac{4eC}{ƙ} sinh\left(\frac{e\varphi_{pw}}{2kT}\right) \;\; (ƙR \gg> 1 \quad (2.14)$$

Where k is the Boltzmann constant, *T* is the temperature, *C* is the bulk concentration of 1:1 electrolyte; *e* is the elementary electric charge; $ƙ = (2e^2/\varepsilon_0\varepsilon_w kT)^{1/2}$: Debye screening parameter, ε_0 is the dielectric constant of vacuum, φ_{pw}: the electric potential at the particle/water boundary with respect to the bulk water phase

Two like-charged particles at a liquid interface (Figure 2.1c) experience both direct electric repulsion, F_{ER} and electrocapillary force. F_{EC}. Note that F_{ED} acts on each individual particle, while F_{ER} and F_{EC} are interaction forces between two (or more) particles (Figure 2.3). For a particle in isolation, the charges at the particle/nonpolar-fluid interface create electric field in the nonpolar fluid (oil, air) that asymptotically resembles the electric field of a dipole, because of the image-charge effect (Figure 2.5).

In the nonpolar fluid (oil, air), the electric field of each separate particle is asymptotically identical to the field of a dipole of moment *p*d. This field is created by charges at the particle/nonpolar-fluid interface. This field practically does not penetrate into the water phase, because it is reflected by the oil-water boundary owing to the relatively large dielectric constant of water. For a single particle, the respective electrostatic problem has been solved. The asymptotic behaviour of the force of direct electric repulsion between two such particles-dipoles is determined through equation (2.15).

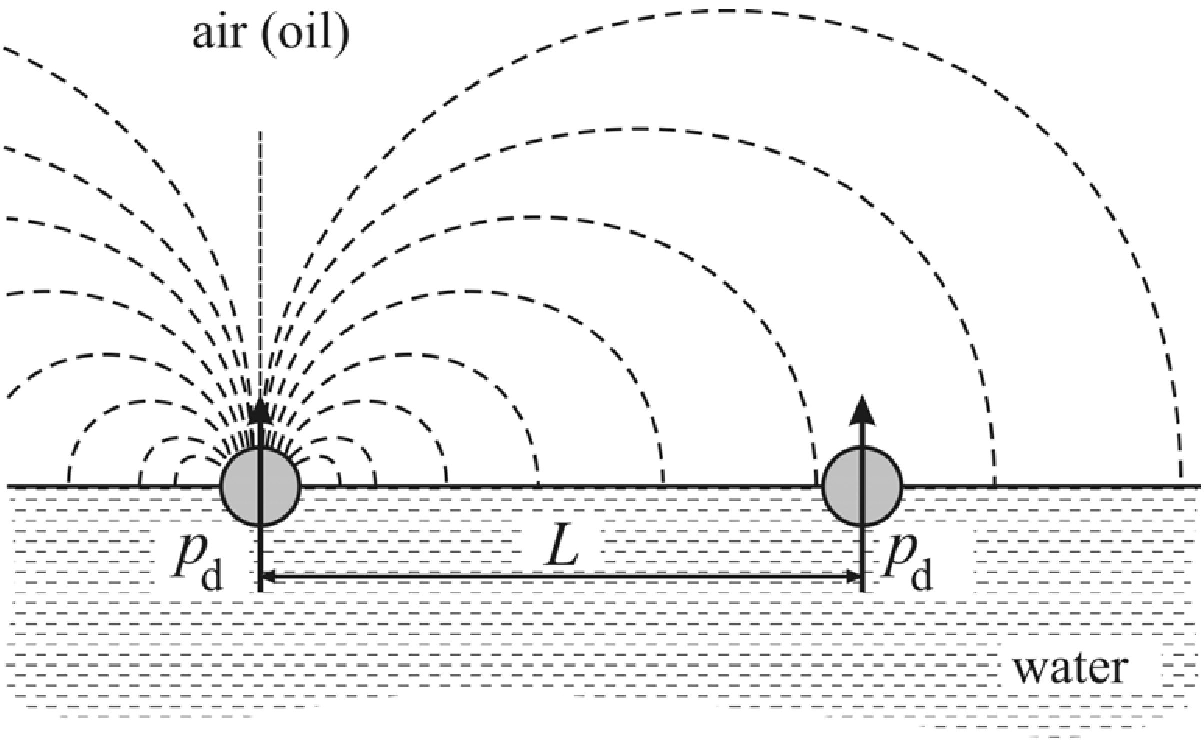

Figure 2.5: Two particles attached to the boundary water–nonpolar fluid and separated at a center-to-center distance *L*.

$$F_{ER} = \frac{3{p_d}^2}{2\varepsilon_n L^4} \quad (L/r_c \gg 1) \qquad (2.15)$$

Where L is the center-to-center distance between the two particles; the quantity,

The effective particle dipole moment is given by equation (2.16)

$$p_d = 4\pi\sigma_{pn} DR^3 \sin^3\alpha \qquad (2.16)$$

Where R is the particle radius, α is central angle , σpn is the electric charge density at the particle/nonpolar-fluid interface, D = D(α,εpn) is a known dimensionless function,

$\varepsilon_{pn} = {}^{\varepsilon_p}/_{\varepsilon_n}$ is the ratio of the dielectric constants of the two phases

Equation 2.15 shows that F_{ER} asymptotically decays as $1/_{L^4}$ like the force between two-point dipoles. However, at shorter distances, the finite size of the particle is expected to lead to a Coulombic repulsion, $F_{ER} \sim 1/_{L^2}$

Equation 2.16 is derived for the case, when the surface charges are located at the particle/nonpolar-fluid interface. In this case, the total interaction force between the two particles (Figure 15.1c), of both electric and capillary origin, is given by equation (2.17)

$$F = F_{ER} + F_{EC} = \frac{3p_d^2}{2\varepsilon_n L^4}\left[1 - \frac{\delta}{5} + O\left(\frac{r_c}{L}\right)^2\right] \quad L/r_c \gg 1 \tag{2.17}$$

$$\delta = \frac{p_d^2}{32\pi\gamma\varepsilon_n r_c^5} = \Psi_c \tag{2.18}$$

Considering equation 2.15, the force of electro capillary attraction determined using equation (2.19)

$$F_{EC} = -\frac{3p_d^2}{5\varepsilon_n L^4}\left[\delta + O\left(\frac{r_c}{L}\right)^2\right] \quad L/r_c \ggg 1 \tag{2.19}$$

$\delta = \sin\Psi_c$ can be either measured experimentally from photographs like figure 2.4, or calculated from equation 2.18.

2.7 Capillary Immersion Forces

Capillary interaction appears also when the particles (instead of being freely floating) are partially immersed (confined) in a liquid film; this is the *immersion* capillary force (Figure 2.6 (a, b).

a b

Figure 2.6: Partially immersed particles a. with tensions, b with distance

The deformation of the liquid surface in this case is related to the wetting properties of the particle surface that is, to the position of the contact line and the magnitude of the contact angle, rather than to gravity. The immersion capillary force, resulting from the overlap of such interfacial deformations, can be large enough to cause 2D aggregation and ordering of small colloidal particles

In the particular case, when the particle radii are equal, $R_1 = R_2 = R$ and $r_k \ll L \ll q^{-1}$, from Equation 2.5 we can derive equation (2.17, a, b) respectively for and floatation force and for immersion force

$$F = \left(\frac{R^6}{\gamma}\right)K_1(pL) \tag{2.21}$$

$$F = \gamma R^2 K_1(qL) \quad (2..22)$$

The equation 2.22 derives from Equation 7, whereas (2.21) follows from Equation 2.10

Equation 2.21 and 2.22 show that the flotation force decreases, while the immersion force increases, when the interfacial tension γ increases

2.8 Capillary Forces in the Case of Finite Menisci

Equation 2.1, which describes a meniscus decaying at infinity, is not valid for all physically possible cases. For example, when the particle diameter is much greater than the thickness of the surrounding liquid film (2.9), the meniscus profile near an isolated particle, $z = \zeta(r)$, obeys the Laplace equation of capillarity in the form equation (2.23)

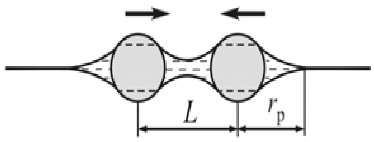

Figure 2.7: Meniscus the particle diameter much greater than the thickness of the surrounding liquid film

$$\frac{\gamma}{r}\frac{d}{dr}\left(r\frac{d\xi}{dr}\right) = P_c = constant \qquad (2.23)$$

The capillary pressure, Pc, is the pressure jump across the meniscus. For particle diameters between 1 μm and 1 mm, Pc is constant because the effects of the gravitational hydrostatic pressure and molecular disjoining pressure are both negligible

Then, the solution of Equation Equation 2.23

$$\boldsymbol{\xi(r) = A + Blnr + (\frac{P_c}{4\gamma})r^2}$$

Hence, in the considered case the Laplace equation has no axisymmetric solution that is finite at infinity (r → ∞). The latter fact implies that the meniscus around the particle must end at a peripheral contact line (of radius rp), out of which the film is plane-parallel (ζ ≡ 0), see figure 2.7. In other words, we are dealing with a finite meniscus. In this case, the overlap of the menisci, and the interaction between the particles, begins when they come at a distance $L <$ 2rp from each other.

This type of interaction is obviously different from that described by Equation 2.6. The respective capillary force can be calculated from the derived integral expressions by means of numerical integration

CHAPTER III

MINERAL LIBERATIONS

Minerals recovery is based on their physical or chemical properties. Complete liberation corresponds to particle containing only one mineral. Separating minerals at the particulate level is referred to as liberation since the individual minerals are liberated from each other in a physical way. In practice comminution processes are not selective and the particles that are formed consist of mixtures of the mineral components

During comminution particles that are smaller than the mineral grains in the ore can appear as a single mineral. Mineralogical textures have random in size, shape, orientation, and position geometries as the particles generated by comminution operations.

However, the distributions of particles with respect to composition show some regular features.

Minerals can be considered as having a characteristic size depending on the size of individual grains. Except in the most regular crystalline structures, it is not possible to assign a unique size to a grain of irregular shape. It was observed that the distribution of particles over the grade range changes from a distribution that is higher around the average grade to one that shows considerable dispersion towards the liberated ends over a comparatively small particle size range Figure as shows figure 3.1.

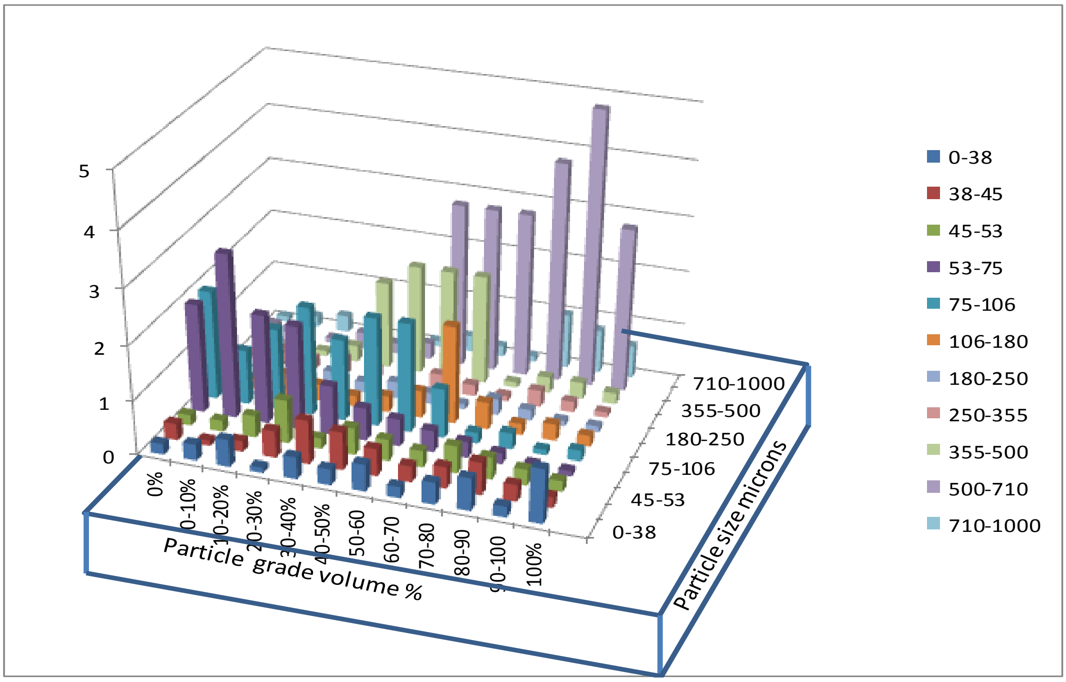

Figure 3.1: Distribution of particles over the grade

3.1 The Beta Distribution for Mineral Liberation

When describing a population of particles that contain minerals, four parameters at least are essential: average grade of mineral in the population($\bar{g}$), Standard deviation about the mean in the populationσ_g, mass fraction of the population that consists of liberated gangue particles.(L_0), mass fraction of the population that consists of liberated mineral (L_1)

The distribution density for particle grade is given by equation (3.1):

$$p(g) = 1 - L_o - L_1 \frac{g^{\alpha-1}(1-g)^{\beta-1}}{B(\alpha,\beta)} \; for \; 0 < g < 1 \qquad (3.1)$$

Properties of the Beta distribution is presented by equation (3.2)

$$B(\alpha, \beta) = \int_0^1 g^{\alpha-1}(1-g)^{\beta-1}dg \qquad (3.2)$$

α and β are two parameters that characterize the distribution and B(α, β) is the Beta function. Two Dirac delta functions must be added at each end to complete this distribution.

The mean of the interior distribution is given by equation (3.3):

$$\bar{g}^M = \frac{\alpha}{\alpha+\beta} \qquad (3.3)$$

The variance of the interior distribution is defined as in equation (3.4)

$$(\sigma^2)^M = \int_0^1 (g - \bar{g}^M)^2 \frac{g^{\alpha-1}(1-g)^{\beta-1}}{B(\alpha,\beta)} dg \qquad (3.4)$$

The parameters α and β are related to the mean and the variance through the expressions in equation (3.5), (3.6) and (3.7)

$$\alpha = \bar{g}^M \gamma \qquad (3.5)$$

and

$$\beta = (1 - \bar{g}^M)\gamma \qquad (3.6)$$

where γ is given by:

$$\gamma = \frac{\bar{g}^M - (\bar{g}^M)^2 - (\sigma^2)^M}{(\sigma^2)^M} \qquad (3.7)$$

Both α and β must be positive numbers and therefore equations 3.5 and 3.6 require $\gamma > 0$

This in turn imposes an upper limit on the variance of the distribution by equation (3.8)

$$(\sigma^2)^M < \bar{g}^M(1 - \bar{g}^M) \qquad (3.8)$$

The corresponding cumulative distribution is given by equation (3.9)

$$P(g) = L_0 + (1 - L_o - L_1)I_g(\alpha, \beta) \qquad (3.9)$$

$I_g(\alpha, \beta)$ is the incomplete beta function defined by equation (3.10)

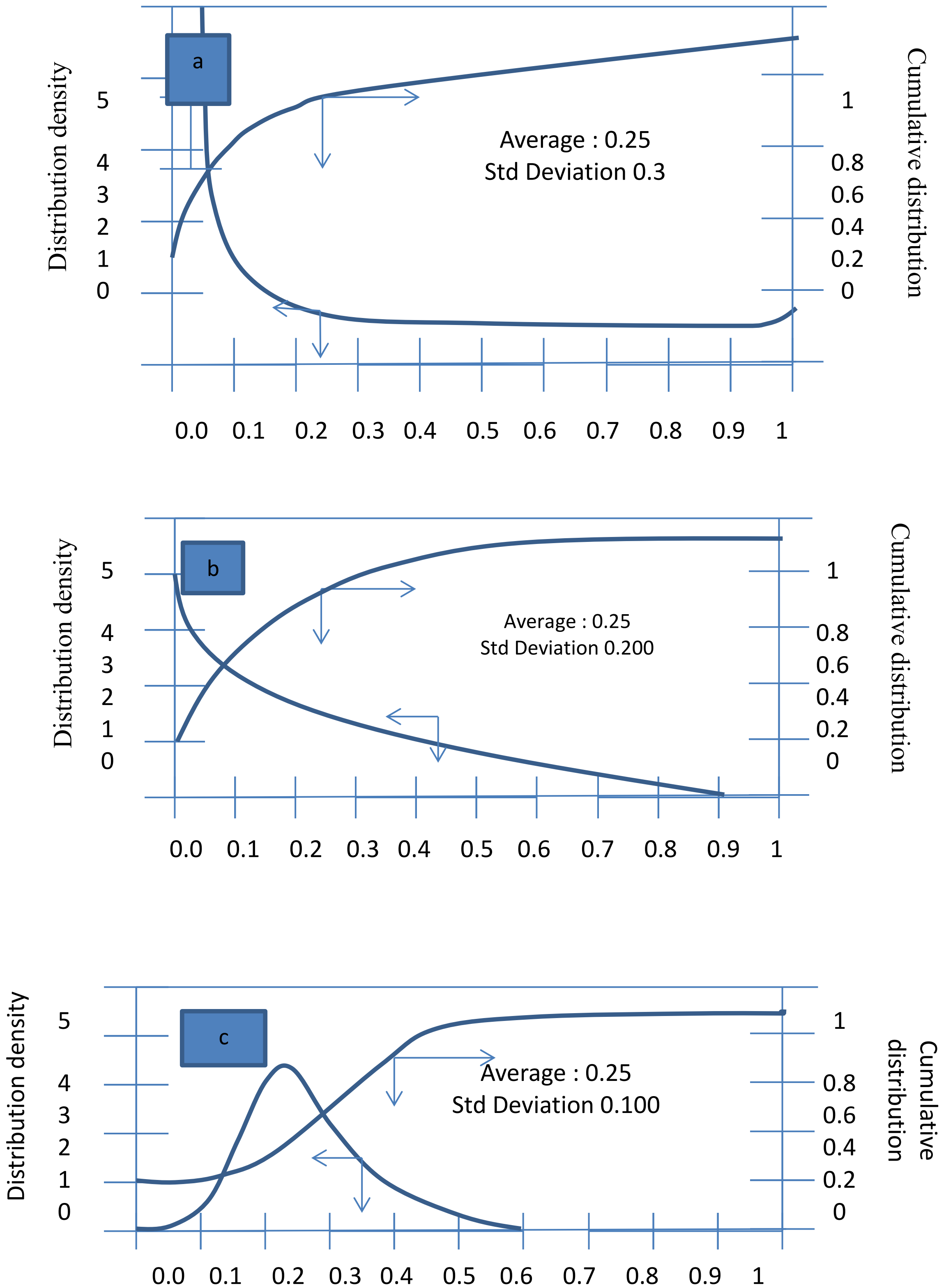

Figure 3.2: The beta distribution function (Figure 3.2) for different α and β .

$$I_g(\alpha, \beta) = \frac{1}{B(\alpha,\beta)} \int_0^g x^{\alpha-1}(1-x)^{\beta-1} dx \tag{3.10}$$

When $\alpha = \beta$ the distribution is symmetrical around the grade g = 0.5. In practice particle grade distributions are generally asymmetric. The beta distribution function (Figure 3.2) for different α and β .

The distribution densities and cumulative distributions are ploted above. The cumulative distribution is discontinued at each ends where there either completely liberated guangue or mineral and grade are $g =$ and $g = 1$. The distribution density changes from bell-shaped to U-shaped as the variance of the inner distribution varies from 0.1 (3.1 c) to 0.3 (3.1 a). This is an essential requirement for the description of mineral liberation distributions for different particle sizes.

A bell shaped means the particle size is larger than the sizes of the mineral in the ore and most particles in the population have grade close to the average grade of the ore.

U shape means the particle size is smaller than the sizes of the mineral, particles appear more as liberated.

If the variance reaches the aximum value $\bar{g}^M(1-\bar{g}^M)$, then Beta distribution describes a population consisting of completely liberated particles only.

These properties of the Beta distribution help to develop models for the liberation process.

Liberated material are often represented in terms of the fraction of the available liberated mineral as show equation (2.11).

$$\mathfrak{L}_1 = \bar{g}\, L_1 \tag{2.11 a}$$

$$\mathfrak{L}_o = (1-\overline{g)}\, 0 \tag{3.11 b}$$

3.2 Graphical Representation of the Liberation Distribution

The distribution density does not efficiently represent liberated material at each end, this can be done by using either the cumulative distribution or as a histogram. The three distributions in Figure 3.1 are represented as histograms in Figure 3.3.

Histogram cannot be used to make accurate estimates of the average grade of particles in the population, instead equation (3.12) used:

$$\bar{g} = \sum_{i=1}^{12} g_i p_i(g) \tag{3.12}$$

However, this estimates contain error because it uses representative grade gi of the grade class i. An alternative equation (3.13) is based on the cumulative distribution

$$\bar{g} = \int_0^1 gp(g)dg = 1 - \int_0^1 P(g)dg \tag{3.13}$$

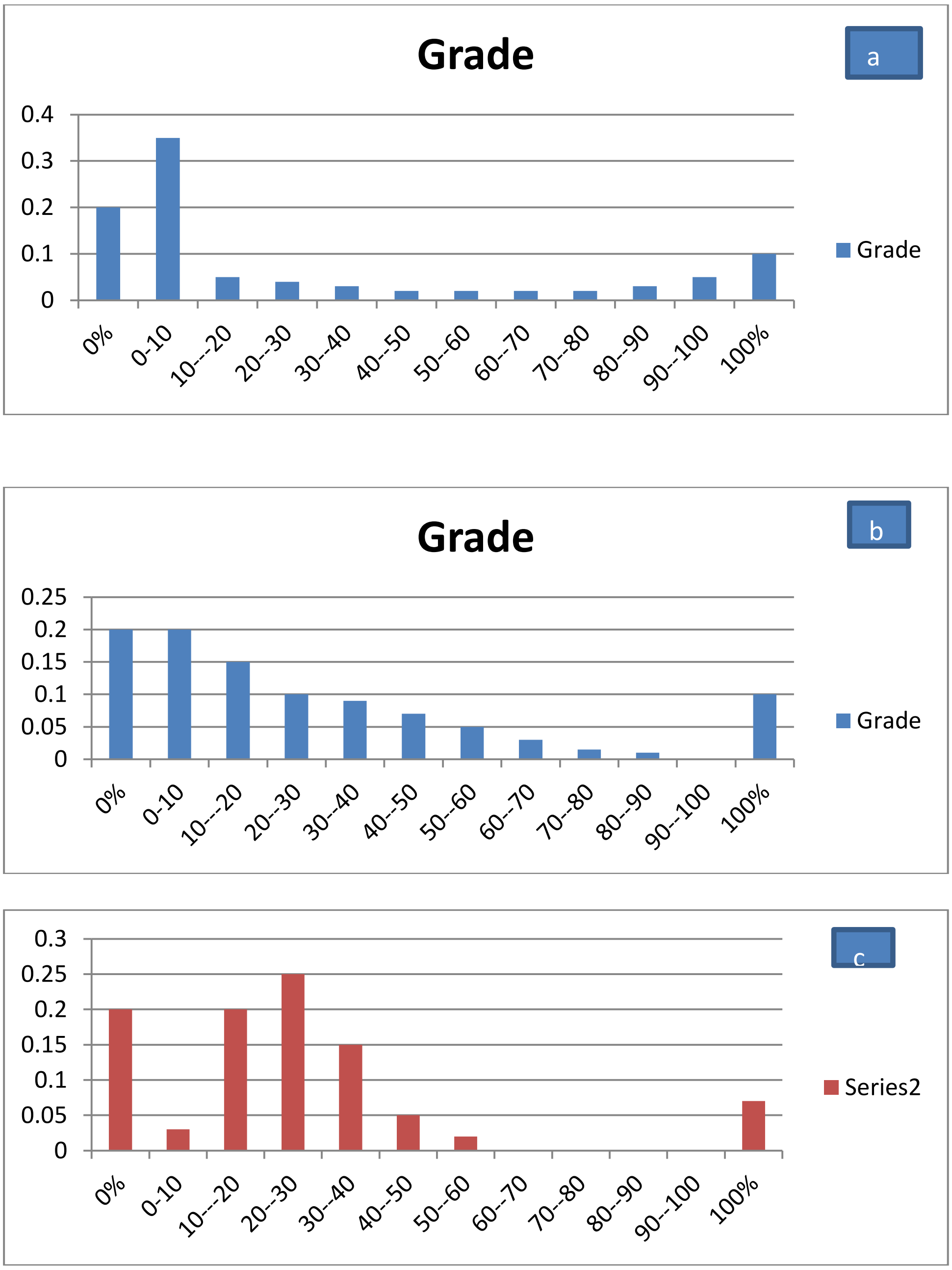

Figure 3.3: The liberation distributions of Figure 3.1 shown as histograms over the grade classes

This integral can be evaluated numerically from a knowledge of the cumulation distribution, P(g) at equidistant values of g.

This can be generated easily from the histogram data as shown in the following example

Example 3.1

The histogram data for the distribution shown in the upper graph in figure 3.2 is given in table . Use equation 3.12 and 3.13 to make estimates of the average grade and compare these to the true average.

G- class	Grade range	$p_i(g)$	P(g)	g_i
1	0	0.2	0.2	0.00
2	0-10	0.3478	0.5478	0.05
3	10-20	0.0737	0.6215	0.15
4	20-30	0.0512	0.6727	0.25
5	30-40	0.0410	0.7137	0.35
6	40-50	0.0351	0.7488	0.45
7	50-60	0.0315	0.7803	0.55
8	60-70	0.0292	0.8095	0.65
9	70-80	0.0280	0.8375	0.75
10	80-90	0.0282	0.8657	0.85
11	90-100	0.0343	0.9000	0.95
12	100	0.1	1	1

$\bar{g} = \sum_{i=1}^{12} g_i p_i(g)$ = 0x0 + 0.05x0.3475 + 0.15x0.0737 + 0.25x0.0512 + 0.35x0.0410 …. = 0.285

Using Simson's rule to calculate Intergral 3.13

$$\int_a^b P(g)dg \approx \frac{b-a}{6}\left[P(a) + 4P\left(\frac{a+b}{2}\right) + P(b)\right]$$

$$\int_0^1 P(g)dg \approx \frac{1-0}{6}\left[P(0) + 4P\left(\frac{0+1}{2}\right) + P(1)\right]$$

$$\frac{a+b}{2} = \frac{0+1}{2} = 0.5$$

$$\frac{0.5-0.45}{0.55-0.45} = \frac{f(0.5)-0.7488}{0.7803-0.7488}$$

P(0.5) = 0.76455

$$\int_0^1 P(g)dg \approx \frac{1-0}{6}\left[P(0) + 4P\left(\frac{0+1}{2}\right) + P(1)\right] = \frac{1}{6}(0.2 + 4x0.76455+1)$$

$$\bar{g} = 1 - \int_0^1 P(g)dg \approx \frac{1-0}{6}\left[P(0) + 4P\left(\frac{0+1}{2}\right) + P(1)\right] = 0.2903$$

3.3 Quantitative Prediction of Mineral Liberation

Minerals are liberated by grinding and liberation is purpose of comminution. Crushing and grinding are a vast network of fractures of heterogeneous mineralogical texture of the ore.

The relationship between the network of fractures and the mineralogical texture determines the mineral distribution in the population after fracture. In figure 3.4, Bright phase is pyrite, grey phases are silicates.

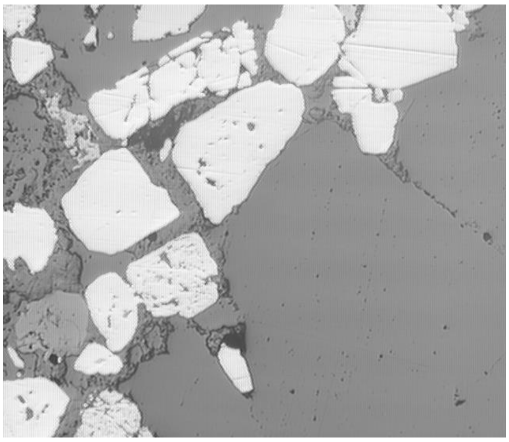

Figure 3.4 : Typical image of a section through mineral-bearing ore.

Mathematical model of the liberation process help to calculate the liberation distribution that can be expected when mineral ores are broken. The most effective tool for the quantitative characterization of texture is image analysis. Samples of the ore are obtained and these are sectioned and polished to reveal a plane section through the material (ref. electron Microscope).

3.4 Simulating Mineral Liberation During Comminution Boundaries of the Andrews-Mika diagram.

The Andrews-Mika diagrams show what type of progeny particles will be generated when a single parent particle breaks in a milling environment. The diagrams are useful because graphs are easy to interpret and the diagrams explicitly include a number of essential constraints that must be applied to the breakage process in the population balance modelling method. A geometric approach is taken and the nature of the function is described by reference to the two dimensional g - dp plane as shown in Figure 3.9 Any particle is located in this plane according to the values of its mineral grade g and its size dp.

We wish to investigate how the progeny particles of a single parent will dispose themselves in this two-dimensional phase space after breakage when the location of the parent particle is known. Of course this can be determined only in a probabilistic sense because the fracture process is random in character.

Consider a parent particle at point A in Figure 3.9. When this particle is broken, the progeny particles cannot appear at every point in the phase space. They are restricted by definite physical constraints:
progeny can appear only below point A, because every progeny particle must be smaller than the parent. The progeny particles must satisfy the law of conservation of phase volume.
This means that no progeny particle can contain a greater volume of mineral than the volume of mineral in the parent particle. In addition no progeny particle can contain more gangue than the parent particle. These restrictions lead to the two inequalities in equations (3.14) and (3.15)

$$g v_p \leq g' v'_p \tag{3.14}$$

$$(1 - g) v_p \leq (1 - g') v'_p \tag{3.15}$$

Where v_p is the volume of the progeny particle, v'_p the volume of the parent particle
Because similarity of particle shape in comminution, these inequalities can be written in the form of equations (3.16) and (3.17)

$$g {d_p}^3 \leq g' {d'_p}^3 \tag{3.16}$$

$$(1 - g) {d_p}^3 \leq (1 - g') {d'_p}^3 \tag{3.17}$$

These inequalities define two regions R and R1 in the phase space like those shown in the right hand panel of Figure 3.5
When the parent particle is too smaller than the average “grain size” of the mineral, the parent will appear under the microscope as shown in image D of Figure 3.5a. and will typically contain only a single region of mineral and a single region of gangue.
This is not true when the parent particle is significantly larger than the mineral “grain size”.
Two other cases can be distinguished: the parent size is comparable to the mineral “grain size” Figure 3.5 b and the situation when the parent size is much larger than the mineral “grain size”.Figure 3.5 c.

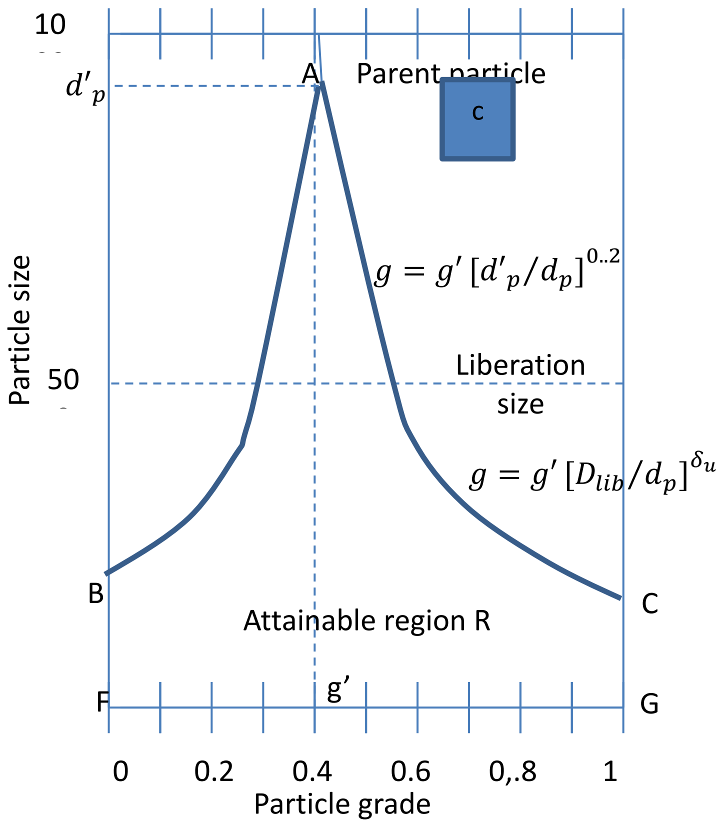
10
d'_p
A
Parent particle
c
$g = g' [d'_p/d_p]^{0..2}$
Particle size
50
Liberation
size
$g = g' [D_{lib}/d_p]^{\delta_u}$
B
C
Attainable region R
F
g'
G
0
0.2
0.4
0.6
0,.8
1
Particle grade

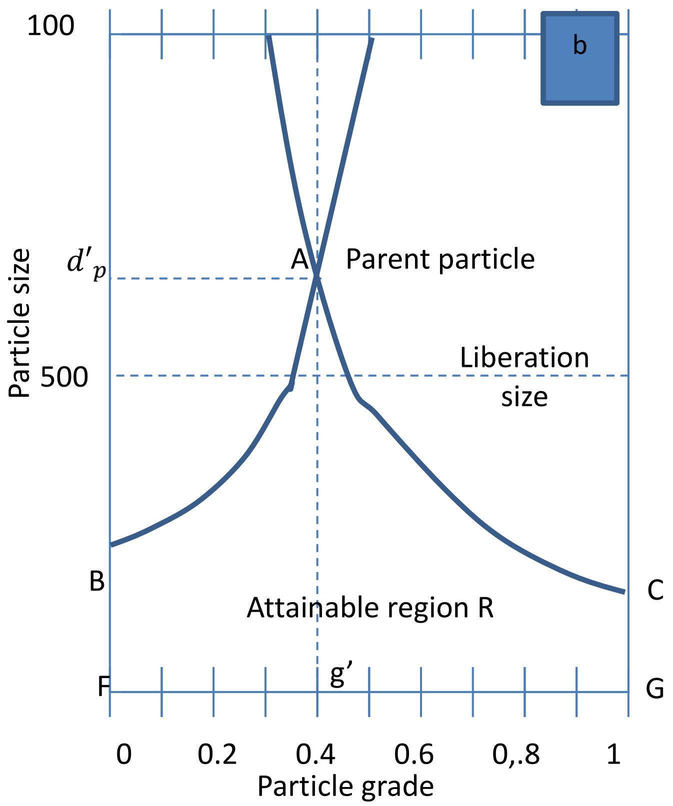
100
b
Particle size
d'_p
A
Parent particle
500
Liberation
size
B
C
Attainable region R
F
g'
G
0
0.2
0.4
0.6
0,.8
1
Particle grade

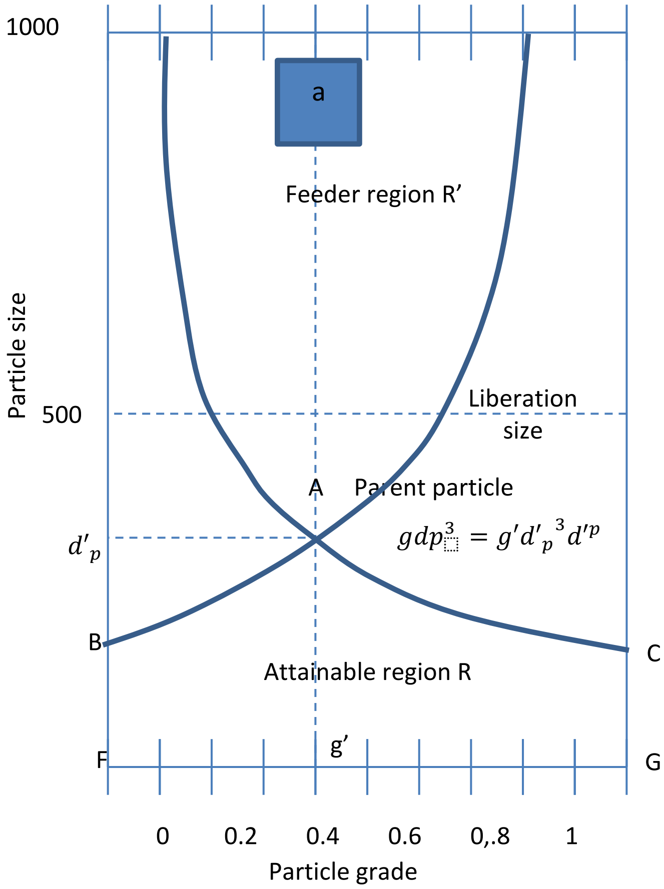

Figure 3.5: Boundaries of the Andrews-Mika diagram for the three cases: parent particle size > liberation size, parent particle size _ liberation size and parent particle size < liberation size.

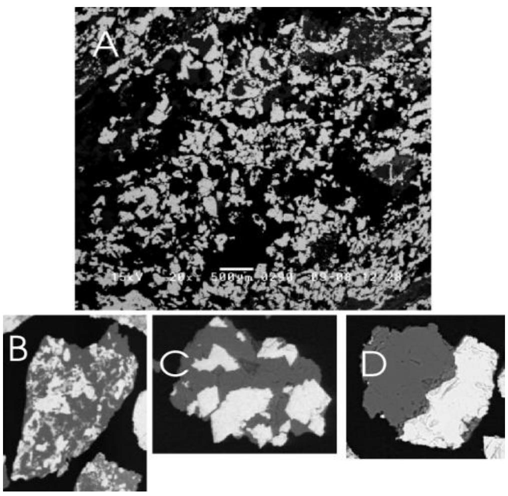

Figure 3.6: Images that show the non-fractal nature of a typical mineralogical texture.

A is a section through the unbroken ore, B is a section through a single particle from the 950-1180 μm screen fraction at 20× magnification, C is from the (212-300) μm screen fraction at 70× magnification, D is from the (53-75) μm screen fraction at 300× magnification

Progenities of the parent particle at A will belong to the region R, **called the attainable region**.

Liberated edges of the region, represented by BF and CG in the diagram, are included in the attainable region because an unliberated particle can generate completely liberated particles.

However, a parent at A cannot generate any liberated particles larger than dpC or liberated gangue particles larger than dpB. The region R' contains parent particles that could produce a progeny at point A. This region is called **the feeder region** for progeny at A.

The boundaries of the feeder region do not intersect or touch the vertical sides of the diagram at g = 0 and g = 1 because unliberated progenity cannot be produced from a liberated parent.

The shape of the boundaries of R and R' vary considerably with the location of the parent particle in the phase space. When the parent particle is too smaller than the average "grain size" of the mineral, the parent will appear under the microscope as shown in image D of Figure 3.6. Under these conditions the parent will typically contain only a single region of mineral and a single region of gangue. If the parent size is close to the mineral "grain size" the image appears like in (B) and if the parent size is much larger than the mineral "grain size" the image appears like in C.

Textures that appear differently in different sizes are called **non-fractal** to distinguish them from **synthetic textures** which appear to be qualitatively similar no matter the magnification used to observe them.

These geometrical properties of textures affect the boundaries of the feeder and attainable regions. Point C reflects the principle that the largest completely liberated progeny particle cannot exceed the total size of the mineral phase in the parent. If the parent particle contains only a single mineral grain as is suggested, the largest grain is proportional to $g'{d'_p}^3$which is reflected in inequality 3.16.

However, when the parent particle contains several separate mineral grains as shown in the upper diagram in Figure 3.5a, the intersection of the attainable region boundary with g = 1 must reflect the principle that the size of the largest liberated mineral particle in the progeny population cannot exceed the size of the largest single coherent mineral grain in the parent particle.

If there is more than one grain in the parent, the size of the largest single grain must be smaller than $g'{d'_p}^3$ and the upper boundary of the attainable region must fall below$g'{d'_p}^3$. This is illustrated in the left hand and center panels of Figure 3.5c. Similar arguments can be made for the gangue phase, which is reflected in the left hand boundaries of the attainable regions shown in Figure 3.5a. Boundaries for the feeder and attainable regions for this situation can be defined by analogy to inequalities 3.18 and 3.19 as

$$g{d_p}^{\delta} \leq g'{d'_p}^{\delta} \tag{3.18}$$

$$(1-g){d_p}^{\delta} \leq (1-g'){d'_p}^{\delta} \tag{3.19}$$

$$\delta \leq 3$$

The exponent δ varies with parent size and a model for this variation that has been found to be useful in practice is given by equation (3.20)

$$\delta = \min\left[\delta_0\left(\frac{D_{lib}}{d'_p}\right)^{x}, 3\right] \tag{3.20}$$

Where $d'_p \leq D_{lib}$; D_{lib} parameter referred to as the liberation size for the ore. It is roughly equal to the particle size at which the mineral starts to liberate significantly when the ore is comminuted; x is a parameter which is approximately 0.5. The upper limit of $\delta = 3$ represents the law of conservation of phase volume and must never be exceeded. The symmetry of the texture is also an important factor in fixing the boundaries of the attainable and feeder regions. A symmetrical texture is one in which the different mineral phases cannot be distinguished from geometrical factors alone. The most common asymmetric texture is one in which distinct grains of one mineral are imbedded in a more or less continuous phase of another mineral. To account for this effect the exponent δ can be different for the mineral and the gangue. Thus inequalities 3.30 and 3.31 are written in form of equation (3.21)

$$g{d_p}^{\delta_u} \leq g'{d'_p}^{\delta_u}$$

$$(1-g){d_p}^{\delta_l} \leq (1-g'){d'_p}^{\delta_l} \quad (3.21)$$

The asymmetry factor for the texture is the ratio δ_u/δ_1 with $\delta_1\delta_1 = \delta$

When the parent size is much greater than the liberation size D_{lib}, and when the progeny particles are also larger than D_{lib}, these will retain the parent composition or at most will be only slightly less or slightly greater than the parent composition. The attainable region is narrow for these progeny and useful approximations to the boundaries are shown in the left hand panel of Figures 3.5 and are represented by equations (3.22) and (3.23):

$$g_u \leq max\left[g'\left(\frac{d'_p}{d_p}\right)^{0.2}, g'\left(\frac{D_{lib}}{d_p}\right)^{\delta_u}\right] \tag{3.22}$$

$$1 - g_l \leq max\left[(1 - g')\left(\frac{d'_p}{d_p}\right)^{0.2}, (1 - g')\left(\frac{D_{lib}}{d_p}\right)^{\delta_l}\right] \tag{3.23}$$

In spite of the empirical nature of these relationships, the parameters can be estimated reliably from batch comminution tests on two-component ores.

3.5 Internal structure of the Andrews-Mika diagram

The boundaries of the Andrews-Mika diagram are not sufficient to define how progeny particles are distributed when a parent of given size and grade is broken. The internal structure of the diagram contains this information and a useful model for this internal structure is developed here which is based on the Beta distribution as shows figure 3.7.

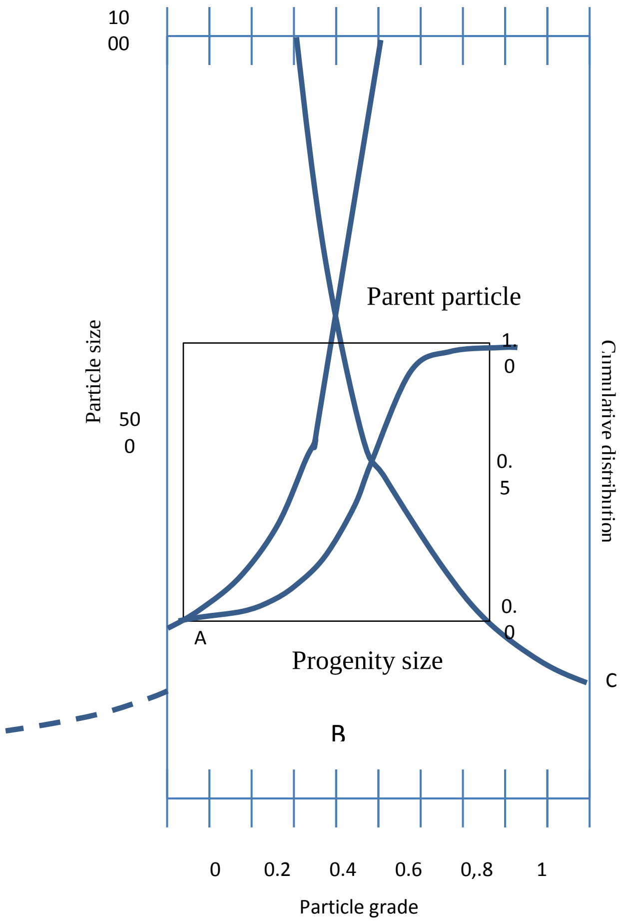

Figure 3.7: The internal structure of the Andrews-Mika diagram

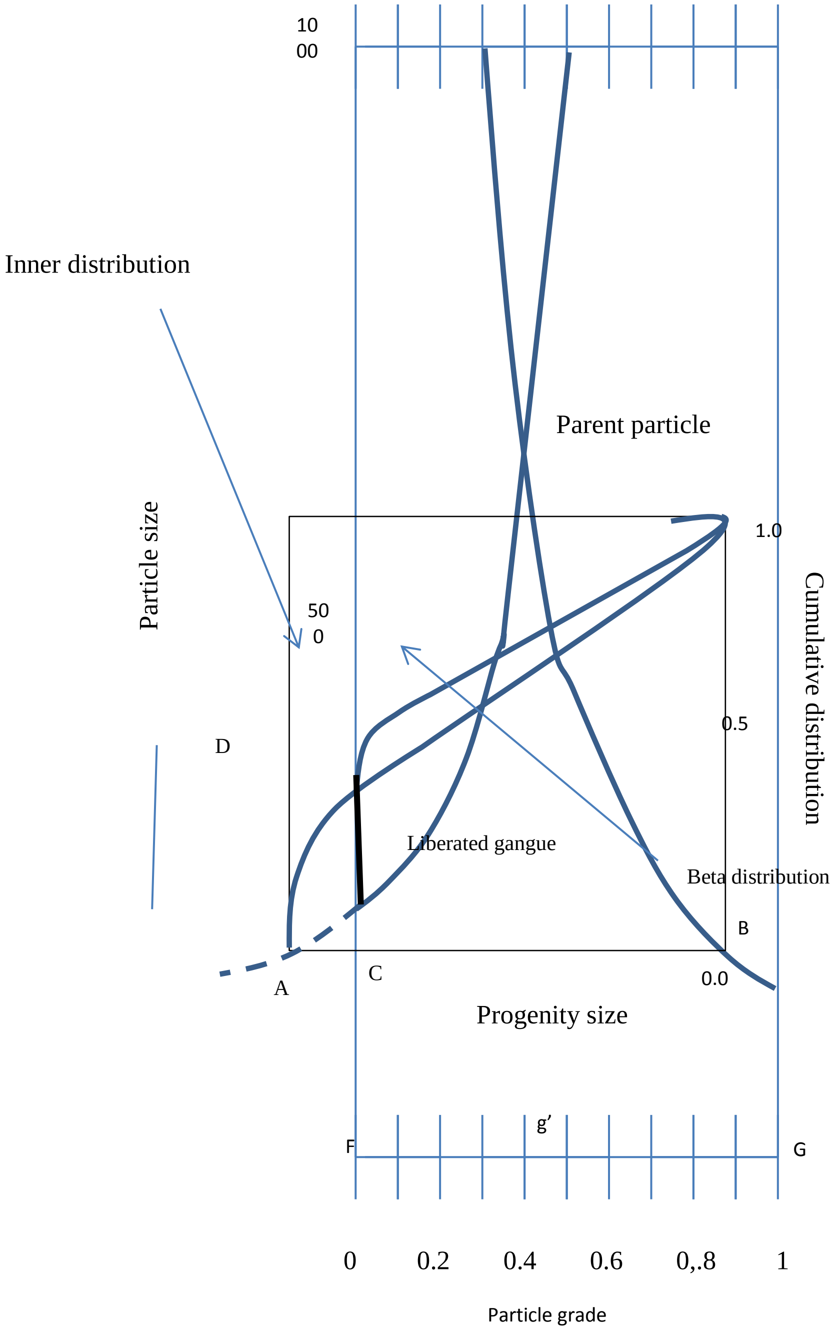

Figure 3.8: Shapes of progenities distribution

Assumption in this model: the progeny particle population at any size will have a Beta distribution with respect to particle grade.

The progenities with size close to the parent, will have a bell-shaped distribution around the parent particle grade. As the progeny size goes far below the parent size, they show more liberation and the distribution tends to U-shape as shows figure 3.8.

This behaviour is better modelled by Beta distribution and the change from bell-shaped to U-shaped distribution is modelled by increasing variance as the progeny size decreases.

The Beta distribution itself does not account for completely liberated material at g = 0 and g = 1.

At any horizontal level in the Andrews-Mika diagram where the boundaries of the attainable region are inside the limits $g = 0$ and $g = 1$ as shown for example by line A-B in Figure 3.12 there are no liberated particles and the total distribution is given by the inner Beta distribution alone which extends from A to B. At progeny particle sizes where at least one of the boundaries of the attainable region is a vertical edge at g = 0 or g = 1, liberated particles are present in the population. It is necessary to calculate what fraction of the particle population appears as liberated particles at grades $g = 0$ and $g = 1$ and this is achieved by the following method.

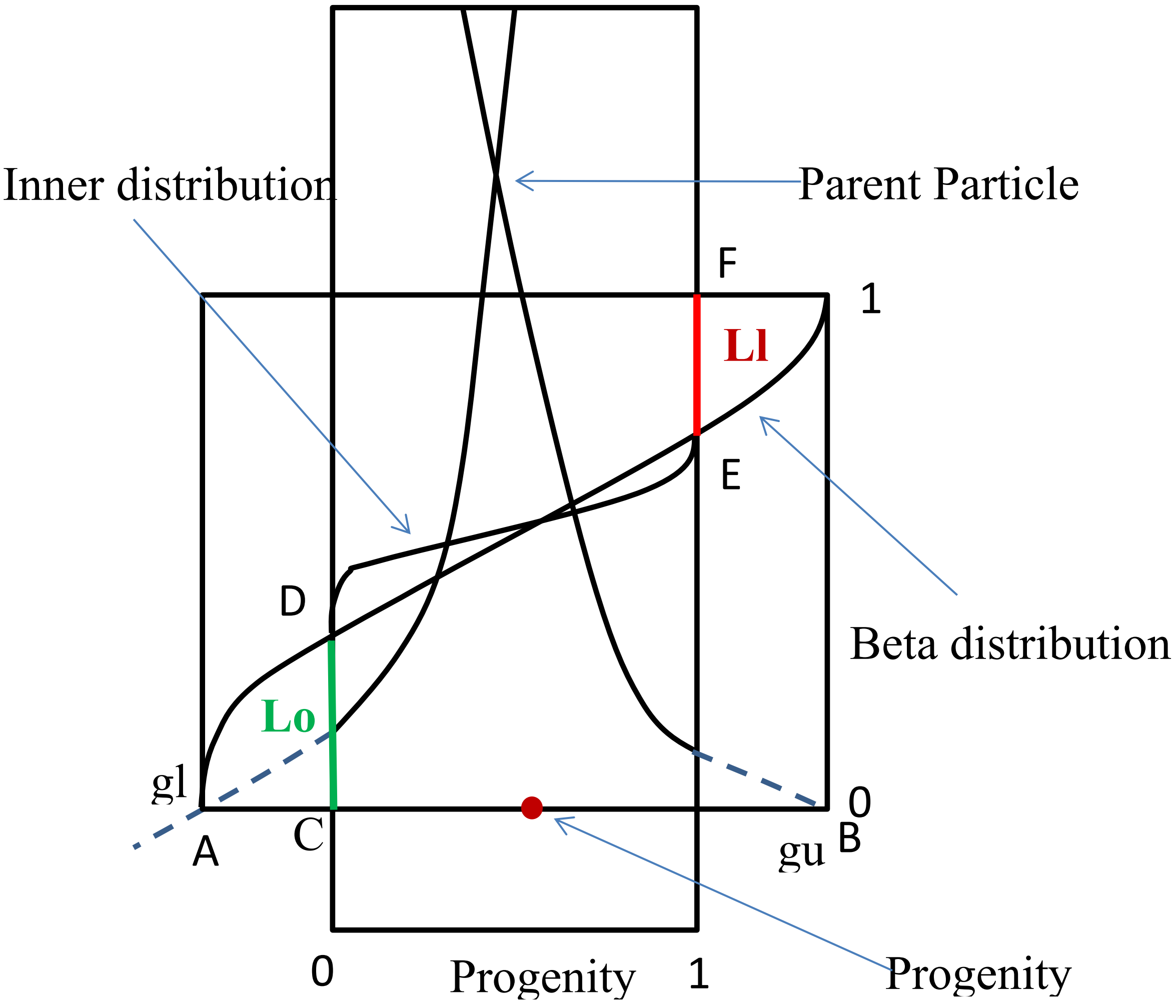

Figure 3.9: extended the curved boundaries of the attainable region

The curved boundaries of the attainable region are extended out past $g = 0$ and $g = 1$ as shown by the broken lines in Figures 3.8 and 3.9 At any progeny size, the grade distribution is assumed to be beta distributed from one extended boundary to the other but the distribution is truncated at g = 0 and g = 1 with all the probability mass in the distribution from $g = gl$ (point A) to g = 0 concentrated at g = 0 and all the probability mass in the distribution from g = 1 to $g = gu$ (point B) concentrated at g = 1. This represents the liberated gangue and liberated mineral respectively. The liberated gangue, *L0,* is given by the length of the line CD in Figures 3.13 and 3.14. The liberated mineral is given by the length of the line FE in Figure 3.14 The remainder of the particle population is then distributed internally as a Beta distribution as described in Section 3.1 There is an upper limit to the amount of liberated mineral or liberated gangue in the particle population. This is clearly the amount of mineral or gangue respectively in the parent.

CHAPTER IV

CRUSHING MECHANISMS, PRODUCT SIZE DISTRIBUTION AND SIZE CLASSIFICATION

4.1 Crushing mechanism

The crushing action of a crushing machine is described most usefully through the classification - breakage cycle model. The operation of a crusher is periodic with each period consisting of a nipping action and an opening action. During the opening part of the cycle material moves downward into the crusher and some material falls through and out. A certain amount of fresh feed is also taken in.

Let us now describe this behaviour quantitatively. It is best to work with a discrete size distribution. So define: $\mathbf{p_i}^{\mathbf{F}}$ **:** fraction of the feed in size class i, $\mathbf{p_i}$ **:** fraction of the product in size class i, **M:** mass of material held in the crusher, $\mathbf{b_{ij}}$ **:** fraction of particles breaking in size class j but that end up in size class i. $\mathbf{m_i}$ **:** fraction of material in the crusher in size class I, $\mathbf{c_i}$ **:** $\mathbf{c(c_i)}$**:** fraction of material in size class i that is retained for breakage during the next nip of the crusher, W: Mass of total feed that is accepted during a single opening, mass of product discharged. Size class 1 contains the largest particles.

Let us follow the fortunes of material in the largest size class starting with an amount Mm_1 in the crusher. During an opening phase of the cycle: Material discharged from the crusher is $(1-c_1)Mm_1$; Material positioned for breakage in the breakage zone during next nip is c_1Mm_1; Accepted from feed is $Wp_i{}^F$; After the next nip the crusher must again have an amount Mm_1in the crushing zone since the operation is at steady state $Mm_1 = Wp_1{}^F + c_1Mm_1b_{11}$

$$\frac{Mm_1}{W} = \frac{p_1{}^F}{1-c_1b_{11}}$$

Product discharged = Wp_1 = (1- c_1) Mm_1

$$p_1 = (1-c_1)\frac{Mm_1}{W} \qquad (4.1)$$

Now consider the next size down:

During an opening phase of the cycle: Material discharged = (1- c_2)Mm_2; Material positioned for breakage during next nip =c_2Mm_2; Accepted from feed is $Wp_2{}^F$

After next nip: $Mm_2 = Wp_2{}^F + c_2Mm_2b_{22} + c_1Mm_1b_{21}$

$$\frac{Mm_2}{W} = \frac{1}{1-c_2b_{22}}\left(p_2{}^F + c_1\frac{Mm_1}{W}b_{21}\right)$$

Product discharged is $Mm_2 = (1 - c_2)\,Mm_2$

$$p_2 = (1 - c_2)\frac{Mm_2}{W} \tag{4.2}$$

The next size down can be handled in exactly the same way to give

$$Mm_3 = Wp_3{}^F + c_3 Mm_3 b_{33} + c_2 Mm_2 b_{32} + c_1 Mm_1 b_{31}$$

$$\frac{Mm_3}{W} = \frac{1}{1 - c_3 b_{33}}\left(p_3{}^F + c_2 \frac{Mm_2}{W} b_{32} + c_1 \frac{Mm_1}{W} b_{31}\right) \ (4.5)$$

This procedure can be continued from size to size. In general

$$\frac{Mm_i}{W} = \frac{1}{1 - c_i b_{ii}}\left(p_i{}^F + \sum_{j=1}^{i=1} c_j \frac{Mm_j}{W} b_{ij}\right) \tag{4.3}$$

The series of equations (4.3) can be easily solved recursively for the group Mmi/W starting from size class number 1. The size distribution in the product can then be calculated from

$$p_i = \frac{(1 - c_1)Mm_i}{W} = \frac{1 - c_i}{1 - c_i b_{ii}} p_i{}^F + \sum_{j=1}^{i=1} c_j \frac{Mm_j}{W} b_{ij} \tag{4.4}$$

And the distribution of sizes in the product is completely determined from the size distribution in the feed and a knowledge of the classification and breakage functions 1.

The classification function is usually of the form shown in Figure 4.1.

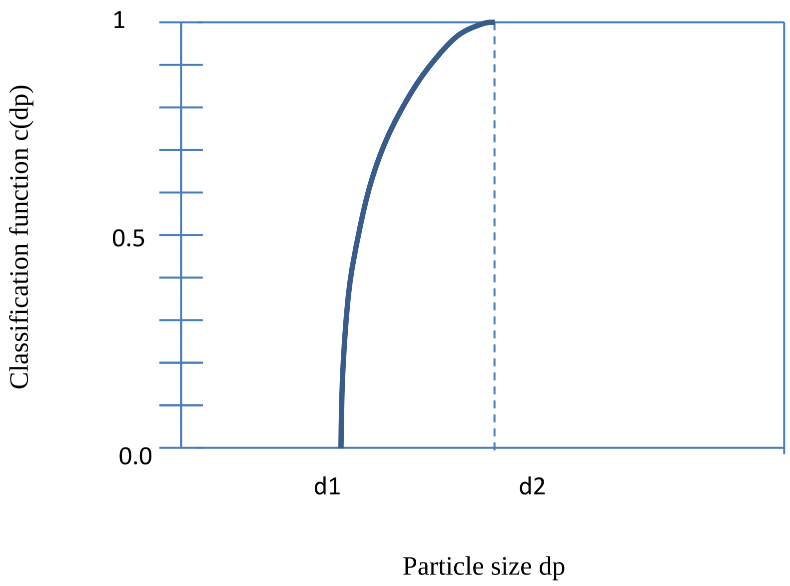

Figure 4.1 A typical internal classification function for a crusher

d_1 and d_2 are parameters that are characteristic of the crusher. They are determined primarily by the setting of the crusher. Data from operating crusher machines indicate that both d_1 and d_2 are proportional to the closed side setting. d_1 is the smallest size particle that can be retained in the crushing zone during the opening phase of the cycle. d_2 is the largest particle that can fall through the crushing zone during the opening phase of the cycle.

A useful form of the classification function is determined through equations (4.5) $c_i = 1 - \left(\frac{d_{pi} - d_2}{d_i - d_2}\right)^n$ for $d_1 < d_{pi} < d_2$ (4.5)

$c_i = 0$ for $d_1 = \alpha_1 CSS$; $d_2 = \alpha_2 CSS + d^*$

α_1 varies from about 0.5 to 0.95 and α_2 varies from about 1.7 to 3.5. n is usually approximately 2 but can be as low as 1 and as high as 3. Higher values of n usually require higher values of α_2, d^* is usually set to 0. Breakage functions of the type presented in equation (4.6) are normally used to describe crusher behaviour.

$$B(x, y) = K\left(\frac{x}{y}\right)^{n_1} + (1 - K)\left(\frac{x}{y}\right)^{n_2} \quad (4.7)$$

The values of bij can be obtained from the cumulative breakage function by equation (4.8) and (4.9)

$$b_{ij} = B(D_{i-1}; d_{pj}) - B(D_i; d_{pj}) \quad (4.8)$$

$$b_{ij} = 1 - B(D_i; d_{pj}) \quad (4.9)$$

represents the fraction of material that remains in size interval j after breakage. These relationships are illustrated in figure 4.2. n_1 is approximately 0.5 for both standard and short-head crushers and n_2 is approximately 2.5 for short-head and 4.5 for standard crushers.

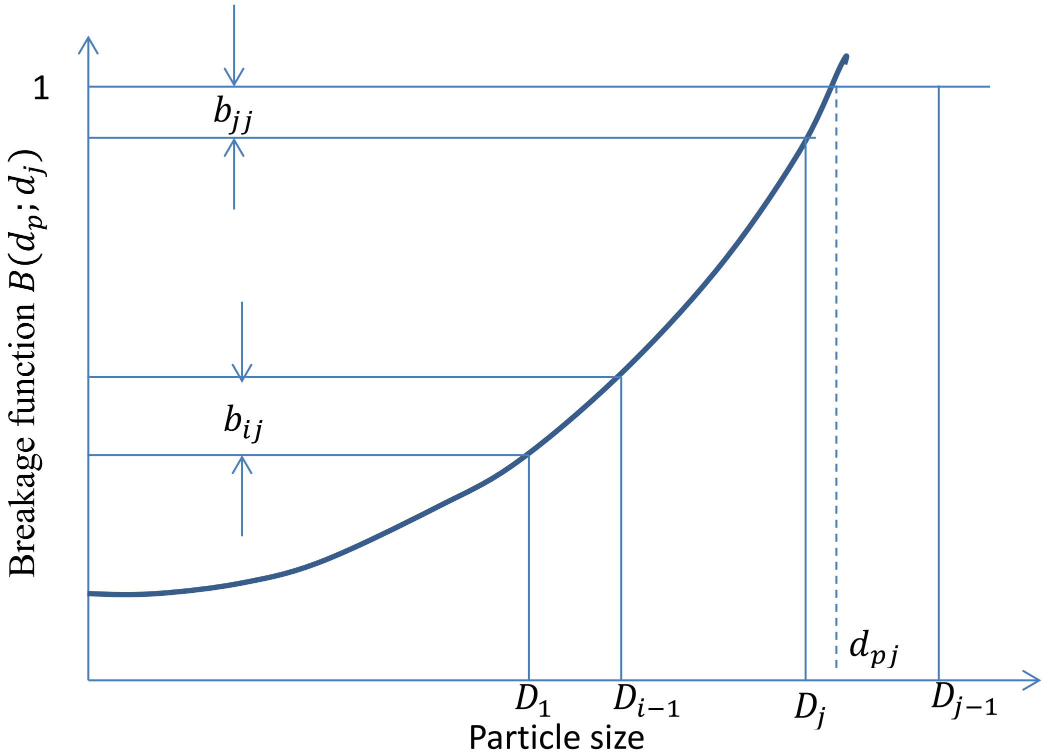

Figure 4.2: Breakage function against size intervals

Example 4.1

The breakage function in a crusher machine was determined to be given by

$B(x,y) = 0.3\left(\frac{x}{y}\right)^{0.45} + 0.7\left(\frac{x}{y}\right)^{3.2}$

If size class 2 has mesh sizes boundaries 13.4 cm and 9.5 cm and size class 5 has boundaries 7.50 cm and 5.60 cm, calculate $b52$.

$b_{ij} = B\big(D_{i-1}; d_{pj}\big) - B(D_i; d_{pj})$

$$d_{p2} = \sqrt{13.4x9.4} = 11.28\ cm$$

$$b_{52} = 0.3\left(\frac{7.5}{11.28}\right)^{0.45} + 0.7\left(\frac{7.5}{11.28}\right)^{3.2} - 0.3\left(\frac{5.6}{11.28}\right)^{0.45} - 0.7\left(\frac{5.6}{11.28}\right)^{3.2}$$

=0.4393-0.2934=0.1459

4.2 Size classification

In most cases, size classification equipment is designed to split a feed into a coarse and a fine product. Occasionally one or two product streams of intermediate size may be produced (e.g double or triple deck screen. Probably the most common application of size classification is its use to prevent oversize material leaving a comminution circuit.

There is no clean cut at a particular size equipments will always pass a proportion of oversize and retain a portion of undersize material. Size classification equipment are limed in capacity and this must be considered when evaluating the performance of new or existing classification equipment. The performance evaluation relies on capacity limitations and other procedures. There are two types of classifier available for process operation: screens and classifiers that rely on the variation of terminal settling velocities of particles of varying size when these are immersed in a viscous fluid

4.2.1 Models of evaluating screen performance based on screen capacity

This model represents the ability of the screen to accept and handle the feed tonnage of material. The screen capacity is assumed to be directly proportional to its surface and the basic capacity (Iu) is specified at tons of feed per hour per square meter of screen.

The basic capacity of any screen is determined under standard operating conditions using a predefined standard feed material. The actual screen capacity changes with the operating conditions which are accounted for through capacity factors $\mathrm{K_i}$.

The rated feed capacity $= \mathrm{I_u K_1 K_2 K_3 K_4 K_5 K_6 K_7 K_8 K_9 \quad tons/hr\ m^2}$ (4.10)

The basic capacity is related to the screen opening h by equation (4.11):

$I_u = 0,.783h + 37$ for h ≥ 25 mm and $I_u = 20.0\ h^{0.33-1.28}$ for $h \leq 25$ mm (4.11)

I_u: is in tons/hr m^2 and h is in mm

The individual capacity factors are provided by screen manufacturers. The following factors are typical for woven wire mesh screens.

The open area factor $K_1 = \frac{\%\ \text{open area}}{50}$

4.2.2 Screen transmission efficiency

Ideally the screen should transmit all the undersize material in the feed but is not happening in practice. The fraction of the feed undersize passing through is called the screen efficiency.

The efficiency is determined primarily by the actual feed loading on the screen relative to the rated feed capacity as calculated by equation (4.1). The efficiency decreases if the screen must handle feed in excess of 80% of the rated tonnage because the access of individual particles to the screen surface is hindered. The efficiency also decreases as the actual feed tonnage falls below 80% of rated capacity because particles tend to bounce on the lightly loaded screen and make fewer contacts with the screen surface.

If WF represents the actual feed tonnage, then the rating ratio is given by equation (4.12)

$$RR = \frac{W^F}{I_u \prod_i K_i \text{x screen area}} \tag{4.12}$$

the efficiency of transmission is given by equations (4.13) and (4.14)

$$e = 0.95 - 0.25(RR - 0.8) - 0.05\ (RR - 0.8)^2 \text{ for } RR \geq 0.8 \tag{4.13}$$

$$e = 0.95 - 1.67\ (0.8 - RR)^2 \text{ for } RR < 0.8 \tag{4.14}$$

The actual tonnage passed to the undersize stream is determined through equation (4.15)

$$W^U = eP^F(h)W^F \tag{4.15}$$

Each size class smaller than the mesh size is subject to the same efficiency factor e so that the particle size distribution in the underflow stream is calculated in discrete form as provided by equation (4.16)

$$p_i{}^U = \frac{ep_i{}^F W^F}{eP^F(h)W^F} = \frac{p_i{}^F}{P^F(h)} \text{ for } d_{pi} < h \tag{4.16}$$

$$p_i{}^U = 0 \text{ for } d_{pi} \geq h$$

Where $p_i{}^U$ is the fraction of the underflow stream in the size class I; $p_i{}^F$ is the fraction of the underflow stream in the size class i in the feed

The actual tonnage passed to the overflow stream is determined through equation (4.17) and (4.18)

$$W^o = \left(1 - P^F(h)\right)W^F + (1 - e)P^F(h)W^F \tag{4.17}$$

$$W^o = W^F\left(1 - P^F(h)\right) \tag{4.18}$$

and the discrete size distribution in the overflow stream is given by equation (4.19) and (4.20)

$$p_i{}^o = \frac{(1-e)p_i{}^F}{\left(1-eP^F(h)\right)} \text{ for } d_p < h \tag{4.19}$$

$$p_i{}^o = \frac{p_i{}^F}{1-eP^F(h)} \text{ for } d_p \geq h \tag{4.20}$$

The simple capacity model allow the calculation of the total screen area required for a specific duty. The aspect ratio of the screen (length/width ratio) must be determined by considering the depth of the bed of particles on the screen. An approximate guide is the restriction of the bed depth at the discharge end to no more than 4 times the mesh size. The thickness of the bed is determined by the total flowrate over the screen surface as how equation (4.21), the width of the screen, b, and the velocity of travel of the material along the screen.

$$t_b = \frac{W^o}{bu\rho_b} \tag{4.21}$$

t_b is the bed thickness; W^o the mass flowrate across the discharge and b the screen width; u the velocity of travel across the screen surface; ρ_b the bulk density. The velocity of travel depends primarily on the angle of inclination and the amplitude and mode of vibration.

4.2.3 The Classification Function

The performance of a classification device is also provided by the classification (partition) function. The classification function c(dpi) is defined as the mass fraction of material in size interval i in the feed which finally leaves in the oversize stream. Once the partition function is known, the size distribution in both overflow and underflow can be calculated by a simple mass balance over the solids in size class I as shows equation 4.22 and (4.23).

$$W^U p_i{}^U = (1 - c(d_{pi}))W^F p_i{}^F \qquad \text{I (4.22)}$$

$$W^o p_i{}^o = c(d_{pi}))W^F p_i{}^F \qquad \text{ii (4.23)}$$

where the superscripts O, U and F refer to oversize, undersize and feed respectively

The total flowrates of solid in the oversize and the undersize are given respectively by equation (4.24)

$$W^U = \sum_i W^U p_i{}^U = \sum_i (1 - c(d_{pi}))W^F p_i{}^F \tag{4.24}$$

$$W^o = \sum_i W^o p_i{}^o = \sum_i c(d_{pi}))W^F p_i{}^F \tag{4.25}$$

$$p_i{}^U = \left[1 - c(d_{pi})\right]\frac{W^F}{W^U} p_i{}^F = \frac{[1-C(d_{pi})]p_i{}^F}{\sum_i[1-C(d_{pi})]p_i{}^F} \tag{4.26}$$

$$p_i^{o} = c(d_{pi})\frac{W^F}{W^o}p_i^{F} = \frac{C(d_{pi})]p_i^{F}}{\sum_i C(d_{pi})]p_i^{F}} \qquad (4.27)$$

Equations (4.26) and (4.27) are often written in terms of the total yield of solids to the overflow as show equation (4.28)

$$Y_s = \frac{W^o}{W^F} \qquad (4.28)$$

$$p_i^{U} = \frac{[1-c(d_{pi})]p_i^{F}}{1-Y_s} \qquad (4.29)$$

$$p_i^{o} = \frac{C(d_{pi})]p_i^{F}}{Y_s} \qquad (4.30)$$

$$Y_s = \sum_i C(d_{pi})]p_i^{F} \qquad (4.31)$$

Theoretically, the screens can transmit the amount:

$T_h = ABCDEFG_c$

B: account for the amount of over size in the feed, C: account for the amount of half size in the feed; D: account for the location of the deck; E: account for wet screening; F: account for material bulk density; G_c : accounts for the amount of near size material

In standard operating conditions these factors all have a value of unity.

In a well designed screen, T_h will correspond to the amount of undersize in the feed

4.3 Performance of the screen in the Karra Model

The basic capacity is determined in the Kara model through equation (4.32) and (4.33), where the effective through fall aperture h_T is determined through equation (4.34), provided the diameter of the wire d_w and the angle of inclination of the screen θ ,

$$A = 12.13h_T^{0.32} - 10.3 \text{ for } h_T < 51\ mm \qquad (4.32)$$

$$A = 0.34\ h_T + 14.41 \text{ for } h_T \geq 51 \text{ mm} \qquad (4.33)$$

$$h_T = (h + d_w)\cos\theta - d_w \qquad (4.34)$$

Where h_T is in mm; A in $\text{metric ton/hr} . m^2$

For a screen treating x tons per hr then the size of the screen will be $x/A . m^2$

This value of A applies for woven screens, for others, it has to be modified as follow:

First determine the open area for light medium wire mesh trough equation (4.35): $OA = 21.5 \log_{10}h + 37$, (4.35)

h: mm

Then measure the actual % of the open area (% actual OA)

Then determine the adjusted basic capacity through equation (4.36) adjusted basic capacity $= \frac{\text{A \% actual OA}}{\text{OA}}$

The oversize factor B is determined through equations (4.37) and (4.38) .

$B = 1.6 - 1.2P^F(hT)$ for $P^F(hT) \leq 0.87$ (4.37)

$B = 4.275 - 4.25P^F(hT)$ for $P^F(hT) > 0.87$ (4.38)

The half size factor C is determined through series of equations (4.39) - (4.40)

$C = 0.7 + 1.2P^F(0.5hT)$ for $P^F(0.5hT) \leq 0.3$ (4.39)

$C = 2{,}053P^F(0.5hT)^{0.564}$ for $0.3 < P^F(0.5hT) \leq 0.55$ (4.40)

$C = 3.35P^F(0.5hT)^{1.37}$ for $0.55 < P^F(0.5hT) \leq 0.8$ (4.41)

$C = 5.0\ P^F(0.5hT) - 1.5$ for $P^F(0.5hT) > 0.8$ (4.42)

The deck location factor D is determined through equation (4.43)

D=1.1-0.1s (4.43)

S=1 for top deck , 2 for second deck etc.

The wet screens factor E while applies for material that are sprayed with water and is determined series of equation (4.44)-(4.53)

If $T = 1.26h_T$ (h_T in mm)

$E = 1$ for $T < 1$ (4.44)

$E = T$ for $1 \leq T < 2$ (4.45)

$E = 1.5 + 0.25T$ for $2 \leq T < 4$ (4.46)

$E = 2.5$ for $4 < T < 6$ (4.47)

$E = 3.25 - 0.125T$ for $6 \leq T < 10$ (4.48)

$E = 4.5 - 0.25T$ for $10 \leq T < 12$ (4.49)

$E = 2.1 - 0.05T$ for $12 \leq T < 16$ (4.50)

$E = 1.5 - 0.0125T$ for $16 \leq T < 24$ (4.51)

$E = 1.35 - 0.00625T$ for $24 \leq T < 32$ (4.52)

$E = 1.15$ for $T > 32$ (4.53)

The bulk density factor F is determined through equation (4.54)

$F = \frac{\rho_B}{1600}$ (4.54)

The near size factor Gc is determined through equations (4.55) and (4.56)

Near size material in in the feed is in the range $0.75h_T$ and $1.25h_T$

$G_c = 0.975(1 - \text{near size fraction in the feed})^{0.511}$ (4.55)

$G_c = 0.975(1 - P^F(1.25hT) + P^F(0.75hT))^{0.511}$ (4.56)

Example

Determine the theoretical amount transmitted by a screen

The feed to the screen is 50 dry t/hr

h=55mm

The slope is 9 degrees

4.4 The screen classification function

This the fact that not all undersize is transmitted to the underflow is described by the classification or partition function. Karra uses the function given in equation (4.57)

$$c(d_p) = 1 - \exp\{-0.693\,(d_p/d_{50})^{5.9} \tag{4.57}$$

$c(d_p)$ is the efficiency of transfer of particles of size dp to oversize

Karra determines d_{50} by the relationship in equation (4.58)

$$\frac{d_{50}}{h_T} = \frac{G_c}{K^{0.148}} \tag{4.58}$$

Where $K = \frac{\text{tons of undersize in the}\frac{\text{feed}}{\text{unit}}\text{of screen area}}{\text{ABCDEF}}$; $K = \frac{\frac{W^F P(h_T)}{\text{Screen}}\text{area}}{\text{ABCDEF}}$

d_{50} can be substituted in equations (4.50) and i-vi to determine the size distributions in the two product streams as presented in equation (4.59) and (4.60)

$$p_i{}^U = \frac{[1-C(d_{pi})]p_i{}^F}{\sum_i[1-C(d_{pi})]p_i{}^F} \tag{4.59}$$

$$p_i{}^o = \frac{C(d_{pi})]p_i{}^F}{\sum_i C(d_{pi})]p_i{}^F} \tag{4.60}$$

The model provides a simulation of the actual performance of the screen in the circuit. This performance can be compared with the design capacity of the screen and the screen performance evaluated. In particular, the actual operating efficiency can be calculated from equation (4.61) and (4.62)

$$\text{simulated efficiency} = \frac{\text{tonnage transmitted to the undersize}}{\text{tonnage of undersize in the feed}} \tag{4.61}$$

$$\text{simulated efficiency} = \frac{\sum_i[1-C(d_{pi})]p_i{}^F}{P^F(h)} \tag{4.62}$$

The effective utilization (AUF) of the screen area can be calculated from equation (4.63) and (4.64)

$$\text{AUF} = \frac{\text{tonnage transmitted to undersize}}{\text{theoretical ability of the screen to pass undersize}} \tag{4.63}$$

$$AUF = \frac{W^F P^F x \text{ simulated efficiency}}{ABCDEFG_c x \text{ screen area}} \quad (4.64)$$

An AUF equal to unity indicates that the screen capacity is exactly balanced to the required duty. AUF > 1 indicates that the screen is overloaded while AUF < 1 indicates that the screen is underloaded. $c\left(d_{pi}\right)$ mass fraction of material in size interval i in the feed which finally leaves in the oversize stream

CHAPTER V

GRINDING

5.1. Grinding action

In Tumbling mills (rod, ball, pebble autogenous and semi - autogenous) the grinding action is induced by relative motion between the particles of media - the rods, balls or pebbles (Figure 5.1) This motion can be: Collision with breakage induced by impact rolling with breakage induced by crushing and attrition. In autogenous grinding machines fracture of the media particles also occurs by both impact (self breakage) and attrition.

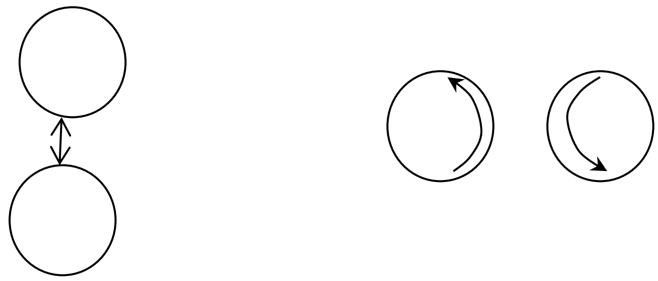

(a) Collision (b) Rolling with nipping

Figure 5.1: Simulation of relative motion between the particles of media

The relative motion of the media is determined by the tumbling action which in turn is quite strongly influenced by the liners and lifters that are always fixed inside the shell of the mill. Liners and lifters have two main purposes:

Liners protect the outer shell of the mill from wear and they are renewable. Lifters prevent slipping between the medium and slurry charge in the mill and the mill shell. Slippage will consume energy wastefully but more importantly it will reduce the ability of the mill shell to transmit energy to the tumbling charge. This energy is required to cause grinding of the material in the mill. The shape and dimensions of the lifters control the tumbling action of the media. The tumbling action is difficult to describe accurately but certain regions in the mill can be characterized in terms of the basic pattern of motion of material in the mill.

The motion of an individual ball in the charge is complicated in practice and it is not possible to calculate the path taken by a particular particle during station of the charge. However the general pattern of the motion of the media can be simulated by discrete element methods which provide valuable information about the dynamic conditions inside the mill. Some of the terms that are often used to describe the motion of the media in a tumbling mill are shown in the figure 5.2

…

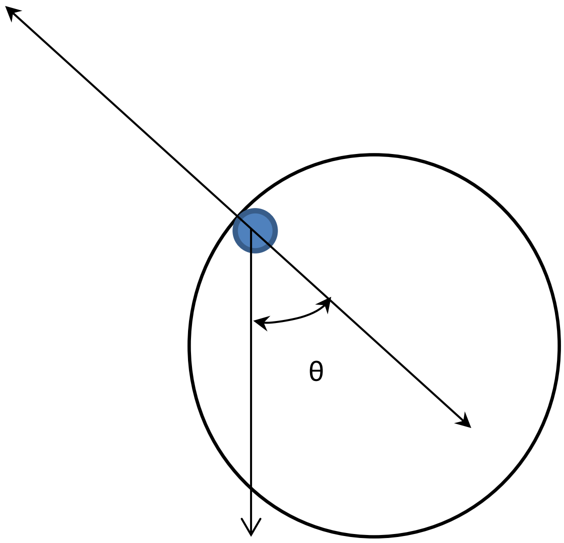

Figure 5.2: Media motion in the tumbling mill.

5.1.1. Critical speed of rotation

The force balance on a particle against the wall is given by equation (5.1)

Centrifugal force outward

$$F_c = m_p\omega^2\frac{D_m}{2} \tag{5.1}$$

Where ω: the angular velocity, m_p: the mass of any particle (media or charge) in the mill

D_m: the diameter of the mill inside the liners

Knowing the gravitational force: $F_g = m_p g$, the particle will remain against the wall if these two forces are in balance ie. $F_c = F_g Cos\theta$

Thus a particle will separate from the wall at the point where

$$Cos\theta = \frac{F_c}{F_g}$$

The critical speed of the mill, ω_c is defined as the speed at which a single ball will just remain against the wall for a full cycle. At the top of the cycleθ =0 and

$$F_c = F_g$$

$$m_p\frac{\omega_c{}^2 D_m}{2} = m_p g$$

$$\omega_c = \left(\frac{2g}{D_m}\right)^{1/2}$$

The critical speed is usually expressed in terms of the number of revolutions per second as shows equation (5.2)

$$N_c = \frac{\omega_c}{2\pi} = \frac{1}{2\pi}\left(\frac{2g}{D_m}\right)^{1/2} = \frac{(2x9.81)^{1/2}}{2\pi {D_m}^{1/2}}$$

$$N_c = \frac{0.705}{{D_m}^{1/2}} \text{ rev/sec}$$

$$N_c = \frac{0.705}{{D_m}^{1/2}} \text{ rev/min} \tag{5.2}$$

The liner profile and the stickiness of the pulp in the mill can have a significant effect on the actual critical velocity. Mills usually operate in the range 65 - 82% of critical but values as high as 90% are sometimes used.

A crucial parameter that defines the performance of a mill is the energy consumption. The power supplied to the mill is used primarily to lift the load (medium and charge). Additional power is required to keep the mill rotating.

5.1.2 Power drawn by ball, semi-autogenous and autogenous mills

A simplified picture of the mill load is shown in Figure 5.3 And this can be used to establish the essential features of a model for mill power. The torque required to turn the mill is given in equation (5.2):

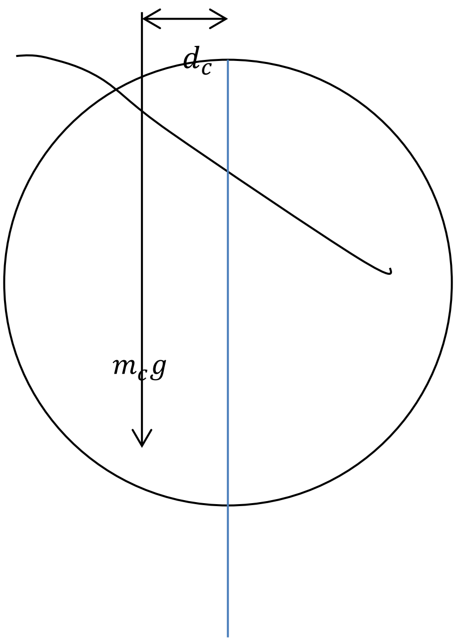

Figure 5.3: Simulation of the torque required to turn the mill

$$\text{Torque} = \text{T} = \text{M}_\text{c}\text{gd}_\text{c} + \text{T}_\text{f} \tag{5.3}$$

Where M_c: the total mass of the charge in the mill; T_f: the torque required to overcome friction.

Power $= 2\pi NT$

For mills of different diameter but running at the same fraction of critical speed and having the same fractional the net power is given by equation (5.4)

Filling

$$\text{Net power} = 2\pi N M_c d_c = \alpha N_c M_c d_c = \alpha \frac{1}{{D_m}^{0.5}} L{D_m}^2 D_m = \alpha L {D_m}^{2.5} \quad (5.4)$$

The effect of varying mill speed on the power drawn by the mill is shown graphically in figure 5.4

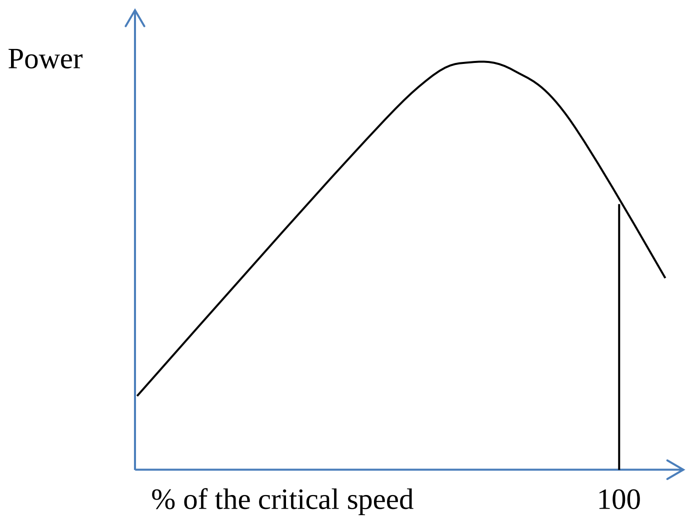

Figure 5.4: The effect of mill speed on the power drawn by a rotating mill.

The speed of rotation of the mill influences the power draft through two effects:

the value of N

the shift in the center of gravity with speed.

The center of gravity first starts to shift to the left as the speed of rotation increases but as critical speed is reached the center of gravity moves towards the center of the mill as more and more of the material is held against the shell throughout the cycle. Since critical speed is larger at smaller radii the centrifuging layer gets thicker and thicker as the speed increases until the entire charge is centrifuging and the net power draw is zero.

The effect of mill charge is primarily through the shifting of the center of gravity and the mass of the charge. As the charge increases the center of gravity moves inward. The power draft is more or less symmetrical around the 50% value.

Another equation for calculating net power draft is represented in equation (5.5)

$$P = 2\varphi_c D_m{}^{2.5} K_i \quad \text{KW} \tag{5.5}$$

Where K_i: the loading factor of the mill; φ_c: the mill speed measured as a fraction of the critical speed. Knowing that Gross power = No-load power + Net power drawn by the charge

The net power is calculated from equation (5.6)

$$\text{Net power} = KD^{2.5} L_e \rho_c \alpha \delta \quad \text{Watts} \tag{5.6}$$

Where D is the diameter inside the mill liners; L_e: the effective length of the mill including the conical ends; ρ_c: the specific gravity of the charge; α: factor that account for the fractional filling; δ: factors that account for speed of rotation; K is a calibration constant that varies with the type of discharge

For overflow mills K = 7.98

and for grate mills K = 9.10.

K_i depend on the type of mill discharge and is determined graphically through figure 5.5 which represents the constant against loading percentage

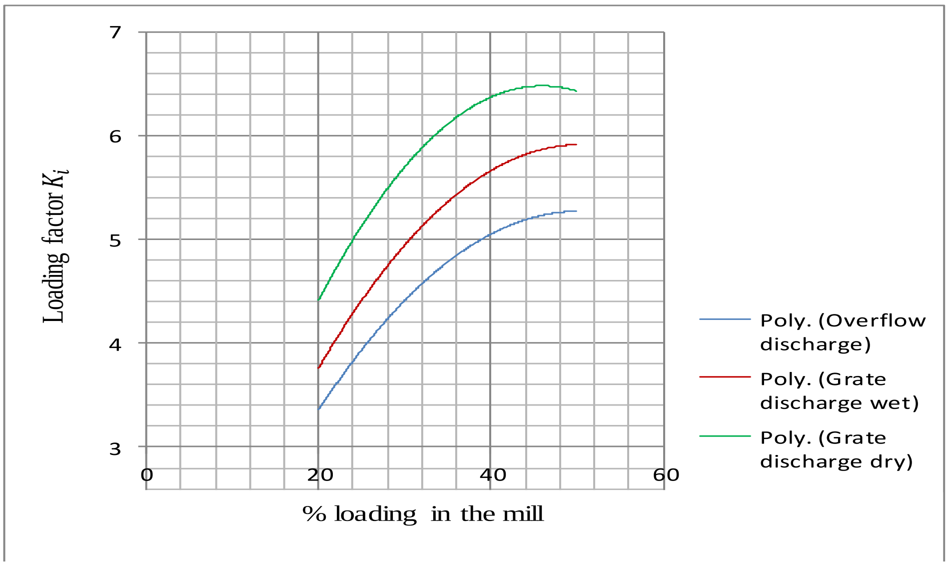

Figure 5.5: the loading factor K_i against percentage loading (%)

The no-load power accounts for all frictional and mechanical losses in the drive system of the mill and can be calculated from equation (5.7)

$$\text{No} - \text{load power} = 1.68 D^{2.05} [\varphi_c (0.667 L_d + L)]^{0.82} \text{ KW} \tag{5.7}$$

Where L_d is the mean length of the conical ends and is calculated as half the difference between the center-line length of the mill and the length of the cylindrical section(belly length) and determined through equation (5.8)

$$L_d = \frac{L_c - L}{2} \tag{5.8}$$

The geometry of a mill with conical ends is shown in Figure 5.6

The total volume inside the mill is given by equation (5.9)

$$V_m = \frac{\pi}{4} D_m{}^2 L \left(1 + \frac{2(L_c - L)}{L} \frac{1-\left(\frac{D_t}{D_m}\right)^3}{1-\frac{D_t}{D_m}}\right) \tag{5.9}$$

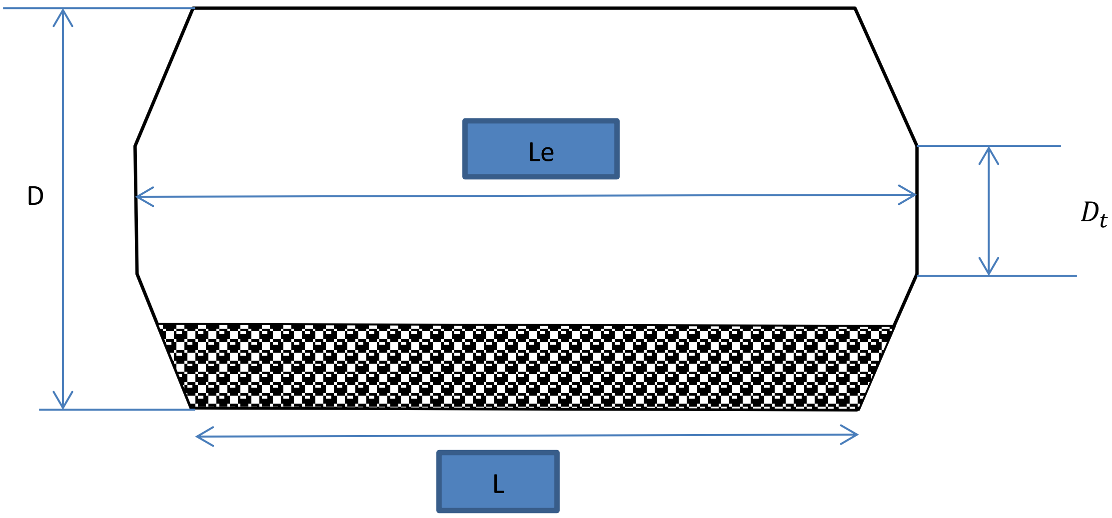

Figure 5.6: Geometry of a mill with cylindrical ends.

Where all dimensions are inside liners: Le = centerline length (effective length); L =belly length; D = mill diameter; Dt = trunnion diameter.

The density of the charge must account for all of the material in the mill including the media which may be steel balls in a ball mill, or large lumps of ore in an autogenous mill or a mixture in a semi-autogenous mill, as well as the slurry that makes up the operating charge

Let Jt be the fraction of the mill volume that is occupied by the total charge, Jb the fraction of the mill volume that is occupied by steel balls and E the voidage of the balls and media. U is the fraction of the voidage that is filled by slurry. φ_V is the volume fraction of solids in the slurry. Let VB be the volume of steel balls in the mill, V_{med} be the volume of autogenous media and V_s the volume of slurry, they are respectively calculated using equation (5.10), (5.11) and (5.12)

$$V_B = J_b(1-E)V_m \tag{5.10}$$

$$V_s = J_t U E V_m \tag{5.11}$$

$$V_{Med} = (J_t - J_b)(1-E)V_m \tag{5.12}$$

The charge density is calculated from equation (5.13)

$$\rho_c = \frac{V_B\rho_b + V_{Med}\rho_m + V_s(1-\varphi_v)1000 + V_s\varphi_v\rho_0}{J_t V_m} \tag{5.13}$$

Where ρ_b: the density of the balls; ρ_m: density of the media (used as grinding media in autogenous mill; ρ_o: density of the ore

The effective length of the mill is dependent on the load and is calculated from:

the Morell equation (5.14)

$$L_e = L\left[1 + 2.28J_t(1-J_t)\frac{L_d}{L}\right] \tag{5.14}$$

And Austin equation (5.15)

$$L_e = L(1+f_3) \tag{5.15}$$

Where is determined through equation (5.16) $f_3 = \frac{0.092}{J_t(1-1.03J_t)}\left\{\frac{L_d}{L(1-\frac{D_t}{D})}\left[\left(\frac{0.625}{0.5-J_t}\right)^{0.1} - \left(\frac{0.625}{0.5-J_t}\right)^{-4}\right]\right\}$ (5.16)

α and δ can be determined according to Morell by equation (5.17) - (5.20):

$$\alpha = \frac{J_t(\omega - J_t)}{\omega^2} \tag{5.17}$$

$$\omega = 2(2.986\varphi_c - 2.213\varphi_c{}^2 - 0.4927) \tag{5.18}$$

$$\delta = \varphi_c(1 - [1-\varphi_{max}]\exp(-19.42(\varphi_{max} - \varphi_c))) \tag{5.19}$$

$$\varphi_{max} = 0.954 - 0.135J_t \tag{5.20}$$

And according to Austin by equation (5.21) and (5.22)

$$\alpha = J_t(1 - 1.03J_t) \tag{5.21}$$

$$\delta = \varphi_c\left(1 - \frac{0.1}{2^{9-10\varphi_c}}\right) \tag{5.22}$$

Example 5.1

Determine the Net power of the SAG grinding mill for the different diameters 1, 1.2 , 1.3 …up to 2 according to:

Austin

L= 0.5D, J_b = 0.04

L=2D; J_b = 0.04

Morell

L=0.5D; J_b = 0.04

L=0.5D; J_b = 0.1

L=2D; J_b = 0.1

J_t = 0.35,

E = 0.4,

U= 1.0,

φ_c = 0.72,

Dt = 0.1D,

Ld = 0.25D,

ρ_b = 7800,

ρ_o = 2750,

φ_v = 0.459

K=7.98

Solution

Austin

$$L_e = L(1 + f_3)$$

$$f_3 = \frac{0.092}{J_t(1-1.03J_t)}\left\{\frac{L_d}{L(1-\frac{D_t}{D})}\left[\left(\frac{0.625}{0.5-J_t}\right)^{0.1} - \left(\frac{0.625}{0.5-J_t}\right)^{-4}\right]\right\}$$

$$f_3 = \frac{0.092}{0.35(1-1.03x0.35)}\left\{\frac{0.25D}{0.5D(1-\frac{0.1D}{D})}\left[\left(\frac{0.625}{0.5-0.35}\right)^{0.1} - \left(\frac{0.625}{0.5-0.35}\right)^{-4}\right]\right\}$$

f_3= 0.411(0.556(1.153-0.003)) = 0.263

$L_e = 0.5D(1 + 0.263)$ = 0.632D

$$V_m = \frac{\pi}{4}D^2L\left(1 + \frac{2(L_e-L)}{L}\ \frac{1-\left(\frac{D_t}{D}\right)^3}{1-\frac{D_t}{D}}\right)$$

$$L = 0.5D$$

$$V_m = \frac{\pi}{4}D^2 0.5D\left(1 + \frac{2(0.63D-0.5D)}{0.5D}\ \frac{1-\left(\frac{0.1D}{D}\right)^3}{1-\frac{0.1D}{D}}\right)$$

$$V_m = 0.393D^3(1 + 0.52x1.11) = 0.620\ D^3$$

$V_B = J_b(1 - E)V_m$

$V_B = 0.04(1 - 0.4)V_m = 0.024Vm = 0.015\ D^3$

$V_s = J_t UEV_m$

$V_s = 0.35x1x0.4Vm = 0.14Vm = 0.087D^3$

$V_{Med} = (J_t - J_b)(1 - E)V_m$

$V_{Med} = (0.35 - 0.04)(1 - 0.4)V_m = 0.186Vm = 0.115D^3$

$$\rho_c = \frac{V_B\rho_b + V_{Med}\rho_m + V_s(1-\varphi_v)1000 + V_s\varphi_v\rho_0}{J_t}$$

$$\rho_c = \frac{0.015\ D^3\ x7800 + 0.115D^3x2750 + 0.087D^3(1 - 0.459)1000 + 0.087D^3x0.459x2750}{0.217D^3}$$

$\rho_c = (117D^3 + 316.250D^3 + 47.067D^3 + 109.816D^3)/0.217D^3$

$\rho_c = 2719.506$

$\alpha = J_t(1 - 1.03J_t)$

$\alpha = 0.35(1 - 1.03x0.35) = 0.224$

$$\delta = \varphi_c\left(1 - \frac{0.1}{2^{9-10\varphi_c}}\right)$$

$$\delta = 0.72x\left(1 - \frac{0.1}{2^{9-10x0.72}}\right) = 0.699$$

Net power $= KD^{2.5}L_e\rho_c\alpha\delta$ Watts

Net power $= 7.98D^{2.5}\ x\ 0.632Dx2719.506\ x\ 0.224x\ 0.699$ Watts

Net power $= 2147.510D^{3.5}$

Diameter	Net Power (W) Austin
1	2147
1.1	2998
1.2	4065
1.3	5379
1.4	6972
1.5	8877
1.6	11126
1.7	13726
1.8	16803
1.9	20304
2	24296

Morel

Net power $= \mathrm{KD}^{2.5}\mathrm{L_e}\rho_c\alpha\delta$ Watts

$$\mathrm{L_e} = \mathrm{L}\left[1 + 2.28\mathrm{J_t}(1-\mathrm{J_t})\frac{\mathrm{L_d}}{\mathrm{L}}\right]$$

$$\mathrm{L_e} = 0.5\mathrm{D}\left[1 + 2.28\mathrm{x}\,0.35(1-0.35)\frac{0.25\mathrm{D}}{0.5\mathrm{D}}\right]$$

$\mathrm{L_e}$= 0.63D

For overflow mill K = 7.8

$$\mathrm{V_m} = \frac{\pi}{4}\mathrm{D}^2\mathrm{L}\left(1 + \frac{2(\mathrm{L_e}-\mathrm{L})}{\mathrm{L}}\ \frac{1-\left(\frac{\mathrm{D_t}}{\mathrm{D}}\right)^3}{1-\frac{\mathrm{D_t}}{\mathrm{D}}}\right)$$

$$L = 0.5D$$

$$\mathrm{V_m} = \frac{\pi}{4}\mathrm{D}^2 0.5\mathrm{D}\left(1 + \frac{2(0.63\mathrm{D}-0.5\mathrm{D})}{0.5\mathrm{D}}\ \frac{1-\left(\frac{0.1\mathrm{D}}{\mathrm{D}}\right)^3}{1-\frac{0.1\mathrm{D}}{\mathrm{D}}}\right)$$

$$\mathrm{V_m} = 0.393\mathrm{D}^3(1 + 0.52\mathrm{x}1.11) = 0.620\ \mathrm{D}^3$$

$$\mathrm{V_B} = \mathrm{J_b}(1-\mathrm{E})\mathrm{V_m}$$

$\mathrm{V_B} = 0.04(1-0.4)\mathrm{V_m}$ = 0.024Vm = 0.015 D^3

$$\mathrm{V_s} = \mathrm{J_t}\mathrm{UEV_m}$$

$\mathrm{V_s}$ = 0.35x1x0.4Vm= 0.14Vm = 0.087D^3

$$\mathrm{V_{Med}} = (\mathrm{J_t}-\mathrm{J_b})(1-\mathrm{E})\mathrm{V_m}$$

$\mathrm{V_{Med}} = (0.35-0.04)(1-0.4)\mathrm{V_m}$ = 0.186Vm = 0.115D^3

$$\rho_c = \frac{\mathrm{V_B}\rho_b + \mathrm{V_{Med}}\rho_m + \mathrm{V_s}(1-\varphi_v)1000 + \mathrm{V_s}\varphi_v\rho_0}{\mathrm{J_t}\mathrm{V}_m}$$

$$\rho_c = \frac{0.015\ \mathrm{D}^3\ \mathrm{x}7800 + 0.115\mathrm{D}^3\mathrm{x}2750 + 0.087\mathrm{D}^3(1-0.459)1000 + 0.087\mathrm{D}^3\mathrm{x}0.459\mathrm{x}2750}{0.217\mathrm{D}^3}$$

ρ_c = (117D^3+316.250D^3+47.067D^3+109.816D^3)/0.217D^3

ρ_c =2719.506

$$\alpha = \frac{\mathrm{J_t}(\omega-\mathrm{J_t})}{\omega^2}$$

$$\omega = 2(2.986\varphi_c - 2.213{\varphi_c}^2 - 0.4927)$$

$$\omega = 2(2.986(0.72) - 2.213(0.72)^2 - 0.4927)$$

$$\omega = 1.02$$

$$\alpha = \frac{0.35(1.02-0.35)}{1.02^2} = 0.225$$

$$\delta = \varphi_c(1 - [1-\varphi_{max}]\exp(-19.42(\varphi_{max}-\varphi_c)))$$

$\varphi_{max} = 0.954 - 0.135J_t$

$\varphi_{max} = 0.954 - 0.135x0.35 = 0.907$

$\delta = 0.72(1 - [1 - 0.907]\exp(-19.42(0.907 - 0.72)))$

$\delta = 0.72(1 - [0.093]\exp(-3.63)) = 0.718$

Net power $= KD^{2.5}L_e\rho_c\alpha\delta$ Watts

Net power $=$ 7.98 $D^{2.5}$ x $0.63D\ x$ 2719.506 x 0.225x0.718

Net power $=$ 2208.719 $D^{3.5}$

Diameter	Net Power (W) Morel	Net Power (W) Austin
1	2209	2147
1.1	3083	2998
1.2	4181	4065
1.3	5533	5379
1.4	7171	6972
1.5	9130	8877
1.6	11444	11126
1.7	14149	13726
1.8	17282	16803
1.9	20882	20304
2	24989	24296

5.2 Power drawn by rod mills

The power drawn by a rod mill is given by equation (5.23)

$P = 1.752D^{0.33}(6.3 - 5.4V_p)\varphi_c$ KWhr/tonne of rods charged (5.23)

Where V_p: fraction of the mill volume that is loaded with rods; Rod mills operate typically at φ_c between 0.64 and 0.75. Typical rod loads are 35% to 45% of mill volume and rod bulk densities range from about 5400 kg/m3 to 6400 kg/m3

5.3 The impact energy spectrum in a mill

The impact energy spectrum of the mill is distribution of impact energies through mill load, it it determines the kinetics of the comminution process in the mill. The breakage energy is supplied by the drive motor and is converted to kinetic and potential energy of the grinding media. The media particles are lifted and they fall and tumble over the charge crushing each of the particles. The overall breakage energy is delivered by large number of individual impact or crushing events. Each impact event delivers a finite amount of energy unequally distributed and transmitted from particles to particles.

Not all impacts are alike. Some will be more energetic (such as the impact caused by a steel ball falling in free flight over several meters) other less (between media pieces as they move relative to each other with only little relative motion). It is possible to calculate the distribution of impact energies using discrete element methods to simulate the motion of the media particles including all the many collisions in an operating mill

5.4 Kinetics of Breakage

The process engineering of milling circuits is linked with the rate at which material of given size is broken in a comminution machine. This rate is a function of the amount of that size of material present. The rate of breakage varies with size.

It is usual to use discrete size classes which provides an adequate approximation for practical computation.

Rate of breakage of material out of size class = $k_i M m_i$

k_i: the specific rate of breakage

Material breaking out of class i distributes itself over all other classes according to the breakage function.

It is common practice to normalise the breakage function to the lower mesh size of the interval so that breakage means breakage out of a size class. If the breakage function is described by the standard form of equations (5.24) and (5.25)

$$B(x,y) = \left(\frac{x}{y}\right)^{n_1} + (1-K)\left(\frac{x}{y}\right)^{n_2} \tag{5.24}$$

$$b_{ij} = B\left(D_{i-1}; D_j\right) - B(D_i; D_j) \tag{5.25}$$

$$b_{ij} = 0$$

The relationship between the cumulative breakage function and *bij* is shown in Figure (5.7)

The breakage function has the value 1.0 at the lower boundary of the parent size interval. This reflects the convention that breakage is assumed to occur only when material leaves the parent size interval.

.

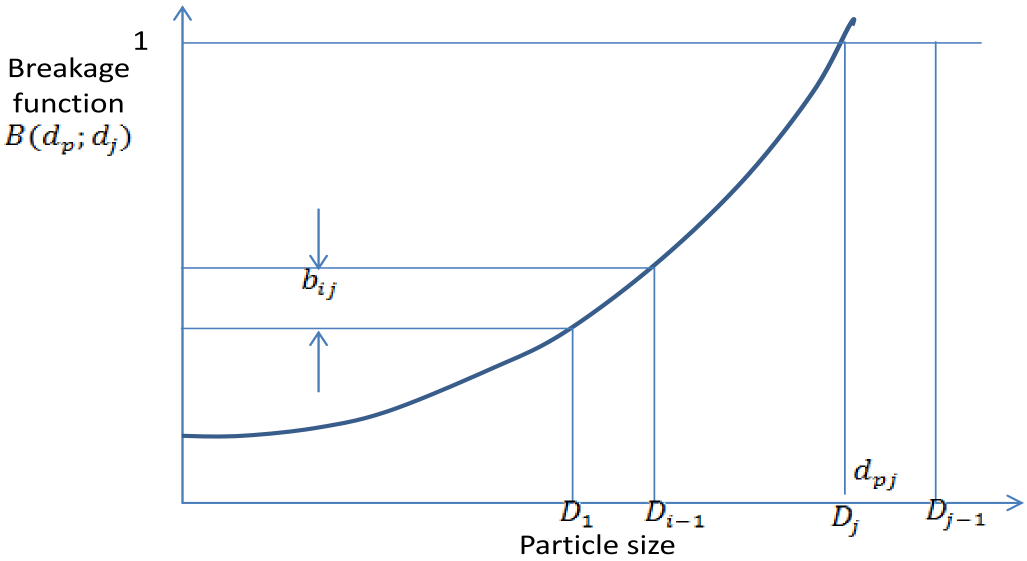

Figure 5.7: The relationship between the cumulative breakage function and *bij*

K represents the fraction of fines that are produced in a single fracture event. It is in general a function of the parent size and can be determined using equation (5.26)

$$K = K_1 \left(\frac{d_{pi}}{d_{p1}}\right)^{-n_3} \tag{5.26}$$

If normalisation is satisfactory and if a strictly geometric progression is used for the mess size then bij is a function only of the difference i-j.

Example 5.2

If a root 2 series is used for the size classes.

$$\frac{D_i}{D_j} = \frac{D_i}{(\sqrt{2})^{i-j} D_i} = (\sqrt{2})^{j-i}$$

$$b_{ij} = K\left(\frac{D_{i-1}}{D_j}\right)^{n_1} + (1-K)\left(\frac{D_{i-1}}{D_j}\right)^{n_1} - K\left(\frac{D_i}{D_j}\right)^{n_1} + (1-K)\left(\frac{D_i}{D_j}\right)^{n_2}$$

$$b_{ij} = K\left[(\sqrt{2})^{n_1(j-i+1)} - (\sqrt{2})^{n_1(j-i)}\right] + (1-K)\left[(\sqrt{2})^{n_2(j-i+1)} - (\sqrt{2})^{n_2(j-i)}\right]$$

$$= K(\sqrt{2})^{n_1(j-i)}(\sqrt{2}-1) + (1-K)(\sqrt{2})^{n_2(j-i)}(\sqrt{2}-1)$$

$$= 0.414K(\sqrt{2})^{n_1(j-i)} + 0.414(1-K)(\sqrt{2})^{n_2(j-i)}$$

5.5 The Continuous Mill.

Industrial grinding mills always process material continuously so that models must simulate continuous operation. Suitable models are developed in this section.

The population balance model for a perfectly mixed mill.

The equations that describe the size reduction process in a perfectly mixed ball mill can be is represented as shows figure 5.8 and can be derived directly from the master population balance equation that was developed in Chapter 2. However, the equation is simple enough to derive directly from a simple mass balance for material in any specific size class.

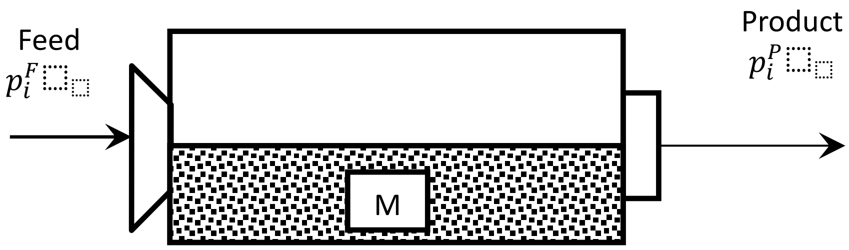

Figure 5.8: The perfectly mixed continuous mill

Lets define: p_i^F : fraction of the feed in size class I; p_i^p : fraction of the product in size class i,; m_i : fraction of the mill contents in size class I; mass of material in mill; W: Mass flowrate through the mill; b_{ij} : fraction of particles breaking in size class j but that end up in size class I; m_i : fraction of material in the crusher in size class I; A mass balance on size class i is developed by noting that the contents of the mill receives material in size class i from the feed and from the breakage of material in the mill that is of size greater than size i. Material of size i is destroyed in the mill by fracture and are represented by equation (5.27) and (5.28).

$$\mathrm{W}p_i^{p} = \mathrm{W}p_i^{F} + \mathrm{M}\sum_{j=1}^{i=1} b_{ij}k_j\, m_j - \mathrm{M}k_i m_i \tag{5.27}$$

$$p_i^{p} = p_i^{F} + \tau\sum_{j=1}^{i=1} b_{ij}k_j\, m_j - \mathrm{M}k_i m_i \tag{5.28}$$

Where $\tau = \mathrm{M/W}$ is the average residence time of the material in the mill

If the contents of the mill are assumed to be perfectly mixed, then $m_i = p_i^p$ equations (5.27) and (5.28) are converted into equations (5.29) and (5.30)

$$p_i^{p} = p_i^{F} + \sum_{j=1}^{i=1} b_{ij}k_j\, \tau\, p_j^{p} - k_i\tau\, p_i^{p} \tag{5.29}$$

$$p_i^{P} = \frac{p_i^{F} + \sum_{j=1}^{i=1} b_{ij} k_j \tau\, p_j^{P}}{1 + k_i^{\tau}} \text{ for all I} \tag{5.30}$$

These can be solved by a straightforward recursion relationship starting with size class 1 and lead to equations (5.31), (5.32), (5.33)

$$p_1^{P} = \frac{p_i^{F}}{1 + k_1^{\tau}} \tag{5.31}$$

$$p_2^{P} = \frac{p_2^{F} + b_{21} \tau k_1 p_2^{P}}{1 + k_2^{\tau}} \tag{5.32}$$

$$p_3^{P} = \frac{p_3^{F} + b_{31} \tau k_1 p_1^{P} + b_{32} \tau k_2 p_2^{P}}{1 + k_3^{\tau}} \text{ etc} \tag{5.33}$$

5.6 The mill with post classification.

In practice the material in the mill does not have unrestricted ability to leave in the outlet stream. Larger

particles are prevented from leaving by the discharge grate if one is present and even in overflow discharge mills, the larger particles do not readily move upward through the medium bed to the discharge. On the other hand very small particles move readily with the water and are discharged easily. Thus the discharge end of the mill behaves as a classifier which permits the selective discharge of smaller particles and recycles the larger particles back into the body of the mill. This is illustrated schematically in Figure (5.10). The operation of such a mill can be modeled as a perfectly mixed mill with post classification as shown in Figure (5.10).

.Applying equation $p_i^{P} = \frac{p_i^{F} + \sum_{j=1}^{i=1} b_{ij} k_j \tau\, p_j^{P}}{1 + k_i^{\tau}}$ to the perfectly mixed milling section lead to equation (5.34)

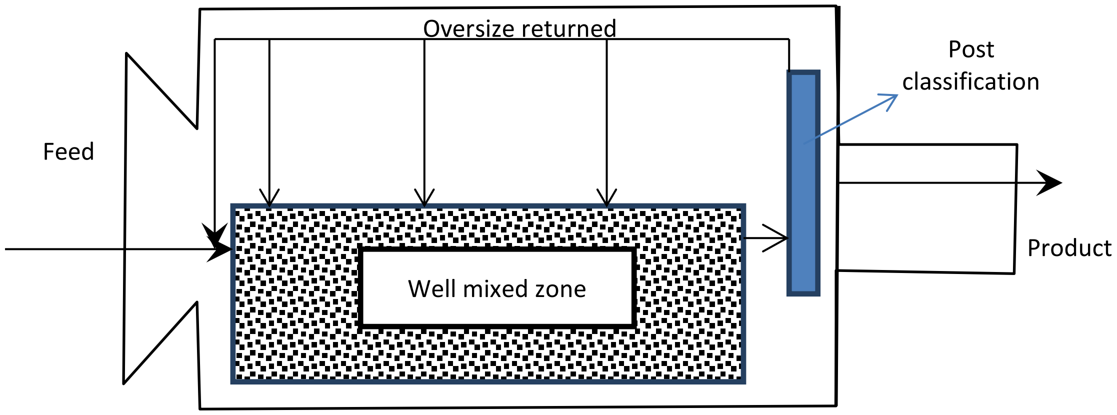

Figure 5.9: The classification mechanism at the mill discharge

$$p_i^{P} = \frac{f_i' + \sum_{j=1}^{i=1} b_{ij} k_j \tau'\, m_j}{1 + \tau' k_i} \tag{5.34}$$

Where τ' is the effective residence time in the mixed section of the mill and represented by equation (5.35)

$$\tau' = \frac{M}{W(1+C)} = \frac{\tau}{(1-C)} \quad (5.35)$$

Where C: is the ratio of recirculation rate to feed rate.

A mass balance on size class i at the point where the post classified material re-enters the mill gives leads to equation (5.36)

$$(1+C)\mathrm{f_i}' = c_i m_i (1+C) + \mathrm{p_i}^{\mathrm{F}} \quad (5.36)$$

Where ci is the classification constant for the particles of size i at the mill discharge.

Substituting the expression for $\mathrm{f_i}'$ into equation (5.34) gives, after some simplification equation (5.37), (5. 38) and (5.39)

$$m_i(1+C) = \frac{\mathrm{p_i}^{\mathrm{F}} + \sum_{j=1}^{i=1} \mathrm{b_{ij}k_j}\tau' m_j(1+C)}{1+\tau' m_j - c_i} \quad (5.37)$$

$$\text{If } m_i^* = m_i(1+C) \quad (5.38)$$

$$\mathrm{m_i}^* = \frac{\mathrm{p_i}^{\mathrm{F}} + \sum_{j=1}^{i=1} \mathrm{b_{ij}k_j}\tau' m_j^*}{1+\tau' k_i - c_i} \quad (5.39)$$

Equation (5.37) can be solved using the same recursive procedure as that used for (8.32) starting from the largest size. The size distribution in the product can be obtained from the calculated values of $\mathrm{m_i}^*$ using the properties of the classifier through equation (5.40).

$$\mathrm{p_i}^{\mathrm{F}} = (1-c_i)(1+C)(1+C)m_i = (1-c_i)\mathrm{m_i}^* \quad (5.40)$$

This solution is complicated a little because the modified residence time is not usually known. It can be calculated only after the size distribution in the mixed section has been evaluated. This requires an iterative solution for convenient implementation starting with an assumed value of τ' to calculate $\mathrm{m_i}^*$from equation (5.41) and (5.42)

$$\mathrm{m_i}^* = \frac{\mathrm{p_i}^{\mathrm{F}} + \sum_{j=1}^{i=1} \mathrm{b_{ij}k_j}\tau' m_j^*}{1+\tau' k_i - c_i} \quad (5.41)$$

C is calculated from

$$\boldsymbol{C} = \sum_{\boldsymbol{i}} c_i(1+C)m_i = \sum_i c_i \mathrm{m_i}^* \quad (5.42)$$

The actual residence time can be obtained from the load of solid in the mill and the mass flowrate of the solid through the mill or from a dynamic tracer experiment. It is usually easier to trace the liquid phase than the solid but the residence time of the liquid will be considerably shorter because of the holdback of the solid by the classification mechanism of the discharge. The precise form of the classification function can be determined by measuring the size distribution of the material in the mill contents and in the product stream using equation (5.43)

$$(1 - c_i) = \frac{\mathrm{p_i}^P}{(1+C)m_i} \quad (5.43)$$

The presence of post classification in a mill is noted from the difference in particle size distribution between the mill contents and the discharged product

5.7 Mill Power and Mill Selection.

5.7.1 The Bond method

The correlation between material toughness and power required in the comminution machine is expressed by the empirical Bond equation. The work done in reducing a mass of material from representative size *d80F* to representative size *d80 P* is given by the Bond equation (5.44)

$$\mathrm{P_o} = \mathrm{K}\left(\frac{1}{\left(\mathrm{d_{80}}^{\mathrm{P}}\right)^{1/2}} - \frac{1}{\left(\mathrm{d_{80}}^{\mathrm{F}}\right)^{1/2}}\right) \text{Kwhr/ton} \quad (5.44)$$

A reference condition is the hypothetical reduction of 1 ton of material from a very large size to a representative size of 100 microns. This reference energy is calculated through equation (5.45) and is called the work index of the material WI. Table 5.1 shows Work index for different material [6]

$$\mathrm{WI} = \mathrm{K}\left(\frac{1}{(100)^{1/2}} - 0\right) = \frac{\mathrm{K}}{10} \rightarrow \mathrm{K} = 10\mathrm{WI} \quad (5.45)$$

Substituting equation (5.45) into equation (5.44) leads to equation (5.46)

$$\mathrm{P_o} = 10\mathrm{WI}\left(\frac{1}{\left(\mathrm{d_{80}}^{\mathrm{P}}\right)^{1/2}} - \frac{1}{\left(\mathrm{d_{80}}^{\mathrm{F}}\right)^{1/2}}\right) \quad (5.46)$$

in equation (5.46), d_{80} must be specified in microns

The work index for the ore as measured using the standard laboratory method must be adjusted to account for various operating conditions before applying it to calculate the energy requirements of an industrial mill that differ from this standard.

This is done by multiplying the measured work index by a series of efficiency factors to account for differences between the actual milling operation and the standard conditions against which the work index was originally calibrated

The efficiency factors are:

EF1: Factor to apply for fine grinding in closed circuit

in ball mills = 1.3.

EF2: Open circuit factor to account for the smaller size reduction that is observed across the mill itself (open circuit condition) as opposed to the size reduction obtained across the closed

Table 5.1 Work index kWh/t

Material	WI
Basalt	18.9
Bauxite	9.7
Copper ore	14
Copper zinc ore	9.8
Dolomite	
Hematite	14.3
Magnetite	11.5
Takonite	16.1
Limestone	13.8
Manganese ore	12.2
Pyrite ore	9.8
Quartzite	10.6
Rutile	14
Sandstone	11
Silicon carbide	28.5
Silver ore	17
Slag	12.2

circuit. If two ball mill circuits, one open and the other closed, as shown in Figure 8.23. If both circuits produce the same $d80$

P the power required for the closed circuit is given directly by the Bond formula equation (5.47) and (5.48)

$$P_{cc} = 10WI\left(\frac{1}{({d_{80}}^{P})^{1/2}} - \frac{1}{({d_{80}}^{F})^{1/2}}\right) \quad (5.47)$$

and the power required by the open circuit is given by

$$P_{oc} = 10xEF_2\left(\frac{1}{({d_{80}}^{P})^{1/2}} - \frac{1}{({d_{80}}^{F})^{1/2}}\right) \quad (5.48)$$

with EF2 = 1.2

The Bond work index efficiency factors are represented in table 5.2

Table: 5.2: Bond work index efficiency factor for wet open circuit milling

Reference % Passing	Open circuit efficiency factor EF2
50	1.035
60	1.05
70	1.1
80	1.2
90	1.4
92	1.46
95	1.57
98	1.7

EF3: Factor for variation in mill diameter. Larger mills are assumed to utilize power somewhat more efficiently than smaller mills. This factor is calculated from equation (5.49)

$$EF_3 = \left(\frac{2.44}{D_m}\right)^{0.2} \; for\ D_m < 3.81 \; and\ EF_3 = 0.914\, for\ D_m \geq 3.81 \tag{5.49}$$

EF4: Oversize feed factor. The optimal $d80F$ size for a ball mill that grinds material having a work index of WI kW hr/tonne is given by equation (5.50)

$$F_o = 4x\left(\frac{14.3}{WI}\right)^{1/2} \text{ mm} \tag{5.50}$$

When the feed has a size distribution coarser than the optimum, the mill must draw more power to achieve the desired product size. The appropriate efficiency factor is given by equation (5.51) and (5.52)

$$EF_4 = 1 + \frac{(WI-7)({d_{80}}^F - F_o)}{R_r F_o} \tag{5.51}$$

R_r: the reduction ratio $\frac{{d_{80}}^F}{{d_{80}}^P}$ (5.52)

EF5: The work index in a ball mill increases when the reduction ratio decreases below 3 and the efficiency factor is
given by equation (5.53)

$$EF_5 = 1 + \frac{0.013}{R_r - 1.35} \tag{5.53}$$

5.8 Procedure to size a ball or rod mill

To size a ball mill or rod mill that must process W tons/hr it is necessary to calculate the mill power required from equation (5.54)

$$P= Po \times W \quad (5.54)$$

and find a mill from the manufacturers catalogue that can accept that power.

If manufacturers' data is not available use equation (5.55) and (5.56)

$$P = 2\varphi_c {D_m}^{2.5} K_i \quad KW \quad (5.55)$$

$$\text{Net power} = KD^{2.5} L_e \rho_c \alpha \delta \text{ Watts} \quad (5.56)$$

This will not produce a unique design for the mill because many combinations of Dm and L will satisfy these equations and the aspect ratio of the mill must be chosen to ensure that the mill will provide sufficient residence time or specific power input to produce the required product size distribution

It is important to note that the geometry of the mill will determine the power input not the tonnage through the mill. The power consumed will give a certain amount of size reduction and the output size will be a function of the tonnage

Example

Copper ore is to be ground in an overflow ball operating in closed circuit to reduce the ore from a p80 of 10mm to a p80 of 130 microns.

FE1= 1.3

FE2=1

FE3=1

5.9 The Batch Mill

Batch grinding of homogeneous solids

The comminution properties are often determined from batch mill. The size distribution in the mill changes continuously with time. The mass balance must be written for each size class.

For the top size it is represented by equation (5.57)

$$M\frac{dm_1}{dt} = -k_1 M m_1 \quad (5.57)$$

Where k_1: the specific rate of breakage; m_i : fraction of the mill contents in size class i, M: mass of material in mill, It is usually adequate to assume that k1 does not vary with time and this equation can be easily integrated to give equation (5.58)

$$m_1 = m_1(0)e^{-k_1 t} \quad (5.58)$$

This solution plots as a straight line on log-linear coordinates.

For the next size down equation (5.59) leads to equation (5.60)

$$M\frac{dm_2}{dt} = -k_2Mm_2 + k_1Mm_1b_{21} \tag{5.59}$$

$$\frac{dm_2}{dt} + k_2m_2 = k_1b_{21}m_1 = k_1b_{21}m_1(0)e^{-k_1t} \tag{5.60}$$

This is a first order linear differential equation which has a solution of the form equation (5.61):

$$m_2 = Ae^{-k_2t} + Be^{-k_1t} \tag{5.61}$$

A and B are constants that must be determined from the form of the differential equation and from the initial conditions as follows. First the proposed solution is differentiated as show equation (5.62)

$$\frac{dm_2}{dt} = -Ak_2e^{-k_2t} - k_1Be^{-k_1t} \tag{5.62}$$

Equations (5.61) and (5.62) into equation (5.60) gives

$$-Ak_2e^{-k_2t} - Bk_1e^{-k_1t} + -k_2Ae^{-k_2t} + k_2Be^{-k_1t} = k_1b_{21}m_1(0)e^{-k_1t}$$

which simplifies to equation (5.63)

$$-k_1B + k_2B)e^{-k_1t} = k_1b_{21}m_1(0)e^{-k_1t} \tag{5.63}$$

$$B = \frac{k_1b_{21}m_1(0)}{k_2-k_1}$$

A must be evaluated from the initial condition as show equation (5.64) and (5.65) resultin g into equations (5.66) and (5.67)

$m_1(0) = A + B$ (5.64)

$A = m_1(0) - B$ (5.65)

And

$$m_2 = m_2(0)e^{-k_2t} + B(e^{-k_2t} - e^{-k_2t}) \tag{5.66}$$

$$m_2 = m_2(0)e^{-k_2t} - \frac{k_1b_{21}m_1(0)}{k_2-k_1}(e^{-k_2t} - e^{-k_2t}) \tag{5.67}$$

The solution can be continued in this way to develop the solution from size to size

CHAPTER VI
CONCENTRATION

6.1 Magnetic Concentration

6.1.1 Behaviour of particles in magnetic field

Permanent magnets are familiar object and the fact that the opposite poles of two magnets attract each other strongly is a manifestation of the magnetic field that is generated in the space surrounding a magnetic pole. All solid material reacts with a magnetic field and display definite properties when placed in a magnetic field.

Ferromagnetic (iron and magnetite) react strongly and are attracted toward magnetic pole Paramagnetic are much less affected by magnetic field, but attracted toward a magnetic pole.

Diamagnetic are repelled from a magnetic pole but this tendency is always very week. The magnetic strength H describes the magnetic field that surrounds a magnet or an electric line.

H is measured in Amps/m, it reflect the strength of the electric current flowing through a unit length of conductor. H is a vector and has a direction and magnitude. The field strength is then defined by three components Hx, Hy and Hz. The force exerted on a pole of strength m Wb is given by equation (6.1)

F= mH (6.1)

Oested is the commonly used unit of H

In the SI system $\mathrm{T} = \frac{\mathrm{Wb}}{\mathrm{m}^2} = \frac{\mathrm{kg}}{\mathrm{AS}^2} = \frac{\mathrm{N}}{\mathrm{Am}}$

$\mathrm{Wb} = \frac{\mathrm{Nm}}{\mathrm{A}}$

$\mathrm{H} = \frac{Wb}{A} = \frac{m^2kg}{A^2S^2}$

$\mathrm{m}\delta\cos\theta$ is the effective moment parallel to the x coordinate direction and cab be written in the form equation (6.2)

$\mathrm{m}\delta\cos\theta = \mathrm{J'}_{\mathrm{x}}$ (6.2)

Equation (6.2) can be developed into equation (6.3)

$\mathrm{J'} = \mu_o ƙ\mathrm{H'}$ (6.3)

Where $\mathrm{H'}$ field strength in the particle; J' magnetic polarization; ƙ the volume susceptibility of the material. The field strength in the particle can be related to the induction by equation (6.4), (6.5) and (6.6) while it relates to the external magnetic field strength through equation (6.7)

$$\mathrm{B'} = \mu_o\mathrm{H'} + \mu_o ƙ\mathrm{H'} = \mu_o(1 + ƙ)\mathrm{H'} \quad (6.4)$$

$$\mu = \mu_o(1 + ƙ) \quad (6.5)$$

$$\boldsymbol{\mu_r} = \frac{\boldsymbol{\mu}}{\boldsymbol{\mu_o}} = \mathbf{1} + ß \quad (6.6)$$

$$H' = \frac{H}{1+ßN} \quad (6.7)$$

Where μ_r is the relative permeability of the particle; H' the magnetic field strength inside the particle; H the external magnetic field strength. The three are related through equation (6.8) and (6.9)

$$H' = H - NJ'/\mu_o = H - NßH' \quad (6.8)$$

$$H'_x = \frac{H_x}{1+ßN_x} \quad (6.9)$$

H'_x is not perfectly parallel to H unless the particle is free to orient itself parallel to the field

Forces experienced by a particle in a magnetic field xcan be represented as shows figure 6.1

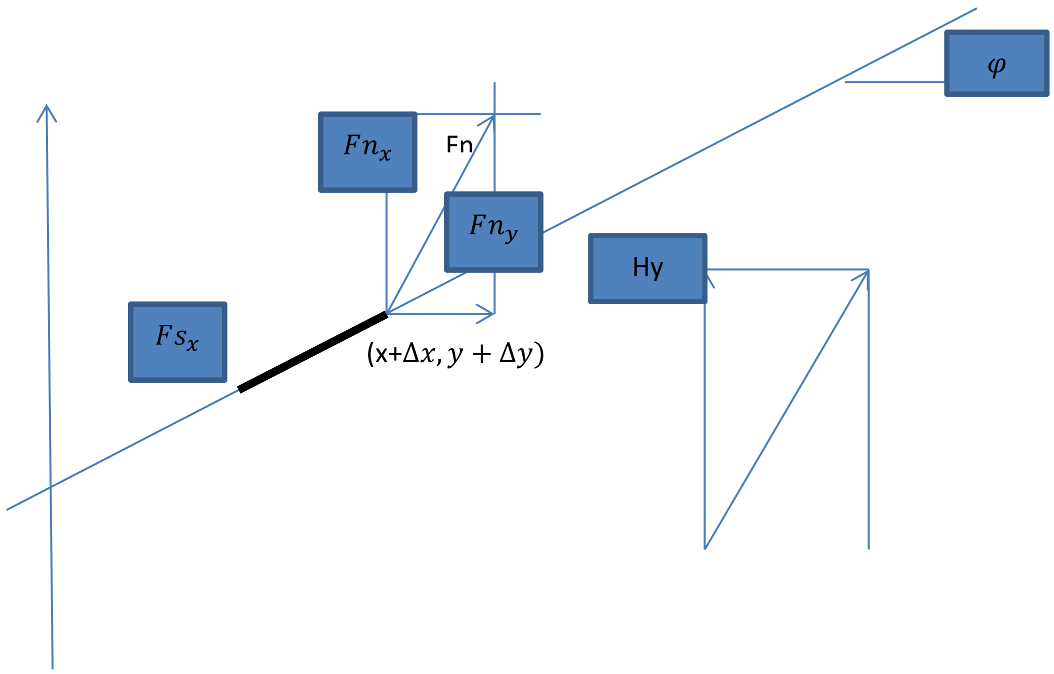

Figure 6.1: A dipole representation in two dimensions

In horizontal axis,

$F_x = Fn_x - Fs_x$ (6.10)

$F_x = mH_x(x + \Delta x, y + \Delta y) - mH_x(x, y)$ (6.11)

$F_x = m\Delta H_x$ (6.12)

$F_x = m\frac{\partial H_x}{\partial x}\Delta x + \frac{\partial H_x}{\partial}\Delta y$ (6.13)

And

$\frac{\partial H_x}{\partial y} = -\frac{\partial^2 \varphi}{\partial y\, \partial x} = \frac{\partial H_y}{\partial x}$ (6.14)

Thus $F_x = \frac{v_p \mu_o ꞣ}{1+(\mu_r - 1)N}\left(H_x \frac{\partial H_x}{\partial x} + H_y \frac{\partial H_y}{\partial x}\right)$ this can be written

$F_x = \frac{0.5 v_p \mu_o ꞣ \, \partial H^2}{1 + ꞣN \, \partial x}$ (6.15)

The square of the magnetic field strength is determined from equation (6.16)

$H^2 = {H_x}^2 + {H_y}^2 + {H_z}^2$ (6.16)

Equivalent expression can be written for y and z components

If χ is the mass susceptibility of the particle and m_p the mass of the particle, then they are represented by equations (6.17) and (6.18)

$$v_p ꞣ = m_p \chi \tag{6.17}$$

$$ꞣ = \rho_p \chi \tag{6.18}$$

Where ρ_p is the density of the particle and the magnetic volume of the particle is determined from equation (6.19)

$$V_m = \frac{0.5 v_p ꞣ}{1 + ꞣN} \tag{6.19}$$

V_m is magnetic volume of the particle (m^3)

And

$$f_m = \mu_o \nabla H^2 \tag{6.20}$$

f_m magnetic force density (N/m^3) is related to the magnetic volume of the particle through equation (6.21) and to the volume of the particle through equation (6.22)

$$F = V_m f_m \tag{6.21}$$

$$V_{mi} = \frac{v_i v_p ꞣ_i}{1 + Nꞣ_p} \tag{6.22}$$

Where v_i volume fraction of component i ; v_p: volume susceptibility of the particle; $ꞣ_p$ magnetic susceptibility of the particle; N: geometric factor (demagnetization factor) that depends on the shape of the particle and is *N* = 0.333 for spherical particles,

N= 0.27 for a cylinder of length equal to its diameter

N = 0.0172 for cylinders of length equal to 10 times the diameter.

Example 6.1

Calculate the radial component of the force on a small spherical paramagnetic particle of diameter 100 microns in the neighbourhood of a magnetically saturated ferromagnetic wire of radius a. The magnetic field has the following components in cylindrical coordinates.

$H_r = \left(H_s \frac{a^2}{r^2} + H_o\right) \cos \emptyset$

$H_o = \left(H_s \frac{a^2}{r^2} - H_o\right) \sin\varphi$

$H_z = 0$

H_s is the field inside the magnetically saturated wire and Ho is the strength of the magnetizing field.

Use the following data

$H_s = 2x10^3 \text{ A/m}$

$H_o = 3x10^3 \text{ A/m}$

$H_z = 0$

a = 1 mm

The Magnetic susceptibility of the particle is $ƙ_p = 1.36.10^{-3}$

The particle situated at coordinates location r =1.05 mm and Ø =0^o

Solution

Since particle is spherical, the shape factor or demagnetisation is: N = 0.333

The force on the particle is given by:

$F = \frac{0.5 v_p \mu_o ƙ v_p}{1+ƙN} \nabla H^2$ where vector notations are used represent F and H

The square of the field strength is obtained from the components of the field strength vector

$H^2 = {H_r}^2 + {H_\emptyset}^2 + {H_z}^2$

$H^2 = \left(H_s \frac{a^2}{r^2} + H_o\right)^2 \cos^2\emptyset + \left(H_s \frac{a^2}{r^2} - H_o\right)^2 \sin^2\emptyset$

The radial component of the force is given by

$F_r = \frac{0.5 v_p ƙ \mu_o}{1+ƙN} \frac{\partial H^2}{\partial r}$

$\frac{\partial H^2}{\partial r} = -4\left(H_s \frac{a^2}{r^2} + H_o\right) H_s \frac{a^2}{r^3} \cos^2\emptyset - 4\left(H_s \frac{a^2}{r^2} + H_o\right) H_s \frac{a^2}{r^3} \sin^2\emptyset$

$\frac{\partial H^2}{\partial r} = -4\left(H_s \frac{a^2}{r^2} + H_o\right) H_s \frac{a^2}{r^3} \cos^2\emptyset - 4\left(H_s \frac{a^2}{r^2} + H_o\right) H_s \frac{a^2}{r^3} \sin^2\emptyset$

$\frac{\partial H^2}{\partial r} = -4\left(2000 \frac{(0.0011)^2}{(0.00105)^2} + 3000\right) 2000 \frac{(0.001)^2}{(0.00105)^3} \cos^2 0^o = -3.33.10^{10}$

The magnetic volume of the particle is

$V_{mi} = \frac{v_i v_p ƙ_i}{1+Nƙ_p}$

$V_m = \frac{0.5x\ (1.36x10^{-3})x\frac{\pi(100.10^{-6})^3}{6}}{1+0.333x1.36x10^{-3}} = 3.559x10^{-16} m^3$

The magnetic force density is

$$f_m = \mu_0 \frac{\partial H^2}{\partial r}$$

$$f_m = 4\pi x10^{-7} x3.327x10^{10} = 4.18x10^4 N/m^3$$

The radial component of the force experienced by the particle is

$$F_r = 3.559x10^{-16} x4.18x10^4 = 1.49x10^{-11} N$$

6.1.2 Magnetic properties of minerals

The difference in magnetic susceptibility is used to separate minerals in separators. The separator allow particles to move under the influence of magnetic field, gravity or shear in flowing liquid. Particle with higher susceptibility will be strongly influenced by magnetic field. Particles of different susceptibility will follow different path and thus be separated

Dry magnetic separation

In dry magnetic separators d the more highly magnetic particles are carried into the concentrate discharge. Many points of high field intensity are produced on the surface of a drum separator.

6.1.3 Hopstock model for the dry low intensity magnetic separator

The particulate material is fed to the top of the drum and is carried downward as the drum rotates. The paramagnetic particles are attracted by the magnetic field inside the drum. The nonmagnetic particles tend to be lifted from the surface of the drum by centrifugal force. The particles can be separated depending on the position of separation and a tailing, a middling and a magnetic concentrate are usually produced.

A simple analysis can be used to develop a simple model for this type of magnetic separator..

Near the surface of the drum the magnetic field strength can be described by two components in cylindrical coordinates with origin at the center of the drum as show equations (6.23) and (6.24)

$$H_r = H_0 \cos\left(\pi \frac{\varphi}{\varphi_0}\right) \exp\left(\frac{-\pi(r-R)}{\varphi_o R}\right) \tag{6.23}$$

$$H_\varphi = H_0 \sin\left(\pi \frac{\varphi}{\varphi_0}\right) \exp\left(\frac{-\pi(r-R)}{\varphi_o R}\right) \tag{6.24}$$

H_0 is the field strength at the drum surface.

The model based on the value of the radial force that is experienced by a particle near the surface of the drum. This can be calculated as the product of the magnetic force density and the magnetic volume of the particle.

The square of the field strength close to the surface of the drum is obtained from Equations (6.25) and (6.26)

$$H^2 = {H_r}^2 + {H_\emptyset}^2 + {H_z}^2 \tag{6.25}$$

$$H^2 = {H_0}^2 \exp\left(-\frac{2\pi(r-R)}{\varphi_o R}\right) \tag{6.26}$$

The radial component of force on a particle near the drum surface is given by equation (6.27) and (6.28)

$$F_r = V_m \mu_0 \frac{\partial H^2}{\partial r} \tag{6.27}$$

$$F_r = -V_m \mu_0 {H_0}^2 \exp\left(-\frac{2\pi(r-R)}{\varphi_o R}\right) \tag{6.28}$$

The negative sign indicates that the radial component of the force on a paramagnetic particle is directed inward.

At the surface of the drum, r = R and the radial force is determined from equation (6.29)

$$F_r = -V_m \mu_0 {H_0}^2 \frac{2\pi}{\varphi_o R} \tag{6.29}$$

The radial component of the magnetic force density at the surface of the
drum is determined from equation (6.30)

$$f_m = \mu_0 \frac{2\pi \mu_0 {H_0}^2}{\varphi_o R} \tag{6.30}$$

The behaviour of a particle on the surface of the drum is governed by a force balance.

The centrifugal force which is determined using equation (6.30)

$$F_C = \rho_p v_p \omega^2 R \tag{6.30}$$

and the radial component of the gravitational force is determined through equation (6.31)

$$F_{Gr} = \rho_p v_p g \sin\varphi \tag{6.31}$$

The particle will detach from the surface of the drum when the centrifugal and the gravity force are equal overcome the radial force as shows equation (6.32)

$$F_C + F_{Gr} > F_r \tag{6.32}$$

The critical rotation speed for detachment of a particle of magnetic volume Vm is obtained by equating the magnetic and centrifugal forces equation (6.33) can be obtained:

$$\omega_{Crit} = \left(\frac{2\pi V_m \mu_0}{\varphi_0 \rho_p v_p}\right)^{1/2} \frac{H_0}{R} \tag{6.33}$$

Because the ratio Vm/vp is independent of particle size, this model predicts that the separating action of the rotating drum magnetic separator is independent of particle size and this has been confirmed by experiment over a size range from about 1 mm to 6 mm.

The theoretical point of detachment of a particle magnetic volume Vm is given by equation (6.34)

$$\text{Sin } \varphi_d = \frac{V_m f_m}{\rho_p v_p} - \frac{\omega^2 R}{g} \tag{6.34}$$

In theory all particles with $\varphi_T < \varphi_d$ and all particle with $\varphi_T < \varphi_d$ < 90 will be in middling.

In practice it is not the case. Significant variations in the magnetic field strength on the surface of the drum caused by serrations and grooves or other design features. In fact the value of the magnetic force density will be distributed over a range of values within the particle bed on the surface of the drum and the model should reflect this.

Imperfect separation of the desired mineral also results from the imperfect correlation between particle composition and the magnetic susceptibility or magnetic volume of the particle. The conditional distribution density of Vm for particles of mineral grade g can be quite wide and this should be reflected in the model. If p(fm) is the distribution density for the magnetic force density within the particle bed on the surface of the drum and p(Vm|g) is the conditional distribution of particle magnetic volume for particles of grade g, the yield to tailing is given by equation (6.35):

$$Y_T = \int_0^{\varphi_T} \int_0^{\infty} \int_0^{\infty} \int_0^{\infty} \sin^{-1}\left(\frac{V_m f_m}{\rho_p v_p} - \frac{\omega^2 R}{g}\right) p(f_m) p(V_m/g) df_m dV_m dg d\varphi \tag{6.35}$$

6.1.4 Capacity of the separator

Tonnage hundled by the separator is given by equation (6.36)

$$\text{Tonnage} = \omega R \rho_b b \tag{6.36}$$

Where ρ_b is the bulk density of layer; b is depth of bed.

Generally a bed depth equal to particle diameter is desirable but this might lead to capacities that are too low. Then a depth of several particle layers will be used. To increase tonnage, the drum should rotate at a rate close to the critical value for separation of the lowest grade particle that should report to the tailing.

Then the tonnage is determined using equation (6.37)

$$\text{Tonnage} = \rho_b b \left(\frac{\pi k \mu_0}{\varphi_o \rho (1 + kN)}\right)^{1/2} H_0 \tag{6.37}$$

which is independent of R!

6.1.5 Wet high intensity magnetic separation

The recovery of magnetic particles in a whims is dependent on the magnetic susceptibility and size of each particle. The probability of capture is proportional to the ratio of the magnetic capture force and the hydrodynamic force that tends to dislodge the particle.

${d_p}^3 \rho\chi HG/d_w$

$G = H \text{ if } H < H_s$

Or

$G = H_s \text{ if } H > H_s$

Where F_u is hydrodynamic force proportional to $d_p \mu \mu_f$; d_w is the diameter of matrix wire and H_s the saturation magnetic field strength; U is the average velocity of the slurry through the matrix; d_p Particle size; χ Magnetic susceptibility

The recovery of a particle of size dp and magnetic susceptibility χ should be a function of the group and is determined through equation (6.38)

$$\frac{F_M}{F_H} = \frac{{d_p}^2 \rho\chi H^2}{\mu u} \quad (6.38)$$

Their experimental data are correlated better by the group as hsow equation (6.39)

$$M_L = \frac{HG(\rho\chi)^{1.2}{d_p}^{2.5}}{u^{1.8}{L_m}^{0.8}} \quad (6.39)$$

where

$$L_m(\text{ the mixing matrix}) = \frac{\text{Mass fraction of magnetics in the feed}}{\text{Mass of matrix}} \quad (6.40)$$

The recovery of particle of size dp and volumetric magnetic susceptibility ƙ is modelled by equation (6.41), (6.42) and (6.43)

$$R_M(\chi, d_p) = 0.5 + B\log_{10}\frac{M_L}{M_{50}} \text{ for } M_{50}10^{-0.5/B} \le M_L \le M_{50}10^{0.5/B} \quad (6.41)$$

$$R_M(\chi, d_p) = 0 \text{ for } M_L < M_{50}10^{0.5/B} \quad (6.42)$$

$$R_M(\chi, d_p) = 1.0 \text{ for } M_L > M_{50}10^{0.5/B} \quad (6.43)$$

M_{50} is the magnetic cut point at which the recovery is 0.5

B=0.348 and $M_{50} = 1.269\text{x}10^{-2}$ for the machines that was tested in litterature

6.2 Gravity separation

Differences in the density of individual particles can used for concentration.

The driving force can be the gravitational force or centrifugal force.

6.2.1 Types of gravity concentration

The two groups of gravity concentrations are manufactured medium and autogenous medium devices.

In manufactured medium, the medium used can be ground magnetite or ferrosilicon in water, silica (2.7), barite (4.5), magnetite (5.18), ferrosilicon (6.8) and galena (7.8).) that have densities values between those of the materials to be separated.

In autogenous medium devices, the medium consist of materials to be separated themselves. Eg in jigs, the sluice, the Reichert cone etc..

6.2.2 Quantitative Models for Dense-Media Separators

Four factors define the separating performance of manufactured media separators:

the separating density or cutpoint,

the separating efficiency,

the short circuit of feed to underflow

the short circuit of feed to overflow.

These effects are best described by means of a partition curve. Three typical partition curves for a dense medium cyclone are shown in Figure 6.2. These curves show how material of different specific gravity (1.32; 1.37; 1.42) will partition to the float fraction. Other dense-medium separators have similar partition curves. These partition curves reveal the four operating characteristics.

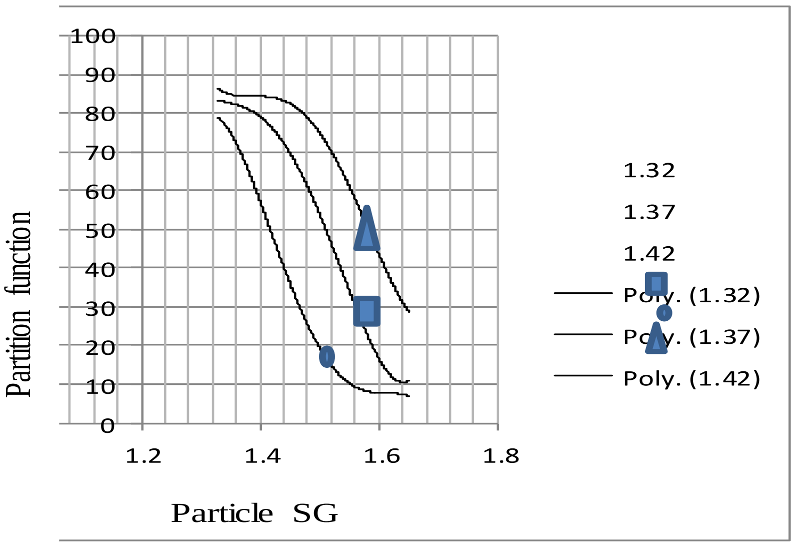

Figure 6.2: typical partition curves for a dense medium cyclone

6.2.3 The Cutpoint

The cutpoint is defined as the density ρ_{50} at which the partition function has the value 0.5. A particle having the density ρ_{50} has equal chance of reporting to sink or float fraction. In a static bath of dense medium the cutpoint is always equal to the density of the medium while in continuously operating equipment this is not always the case, it depends on whether the lighter or heavier fraction must move counter to the prevailing bulk flow of the medium in the equipment. Any heavy particles that leave the cyclone in the underflow, move against the medium flow and therefore require a net negative buoyancy to overcome the viscous drag of the medium. Thus any particle located in equilibrium orbit in the cyclone is denser than the medium. Since the particles on equilibrium orbits define the cut point $\rho_{50} > \rho_m$

ρ_m: density of the medium and $\rho_{50} - \rho_m$ is called the cut point shift and this can be normalized with respect to the medium density to form the normalized cut point shift given in equation (6.44)

$$NCPS = \frac{\rho_{50}-\rho_m}{\rho_m} \tag{6.44}$$

The normalized cut point shift must obviously increase as particle size decreases and experimental data for coal in a dense-medium cyclone are correlated by the simple power law $NCPS = 0.4{d_p}^{-0.32}$ over the range $0.015<d_p < 1\,mm$. When the lighter fraction move counter to the medium flow, the NCPS is negative but when sink material moves against medium flow NSPS is positive. In general the NCPS can be neglected for dense-medium drum type separators for particles larger than a few millimeters. The cut point shift increases with increased media density differential. The partition curves usually normalize well with respect to the cut point density so that partition curves determined at different medium densities will overlap when they are plotted using a normalized abscissa ρ/ρ_{50} and the data fall on a single curve. A model that describes the underflow density in the dense-medium cyclone, for smaller diameter cyclones is determined through equation (6.45) and (6.46)

$$\frac{\rho_u+E}{\rho_m} = 1.872{Re_i}^{0.0891}\left(\frac{D_u}{D_c}\right)^{-0.0872}\left(\frac{D_o}{D_c}\right)^{1.919} \tag{6.45}$$

Where

$$Re_i = \frac{\rho_m V_i D_i}{\mu_a} \tag{6.46}$$

where ρ_u is the underflow density; E: Error introduced by cyclone diameter; D_u spigot diameter; D_c cyclone diameter; D_o vortex finder diameter; V_i the velocity in the cyclone inlet; D_i inlet diameter; μ_a apparent viscosity of the medium

6.2.4 Short circuit flows

Figure 6.3 shows the Partition cuves against particle size and 6.4 shows the Partition function against normalised density. 6.3 is the normalized partition curve and it is represented by the symbol R(x) where x represents the normalized density ρ/ρ_{50}.

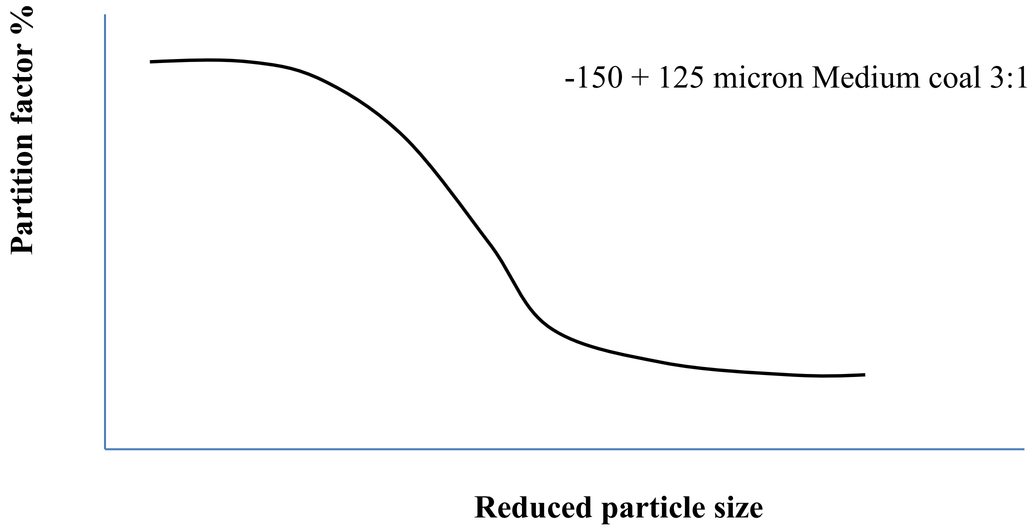

Figure 6.3: Partition cuves against particle size

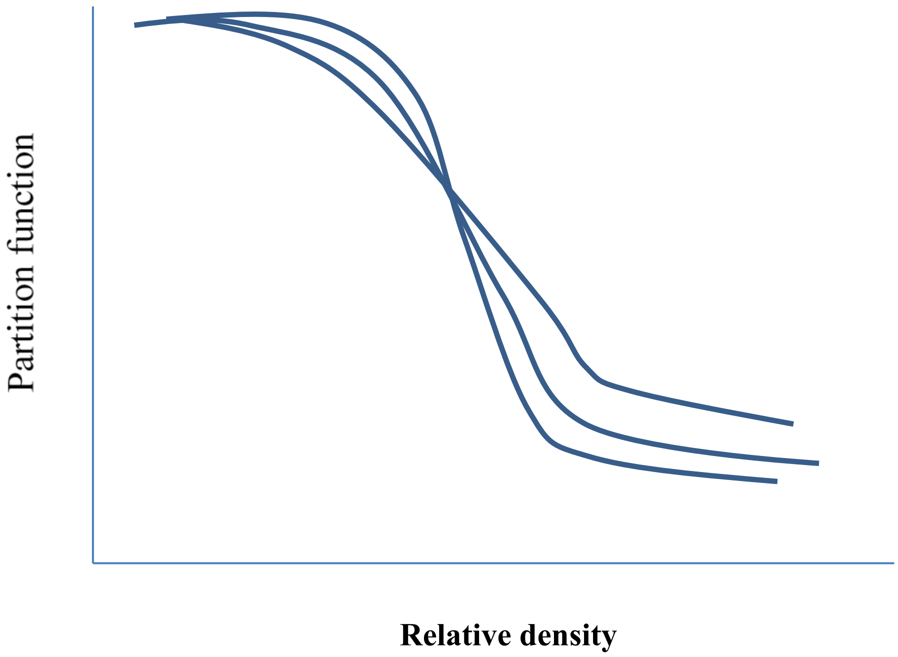

Figure 6.4: Partition function against normalised density

Practically the low- and high- density asymptotes are not at 100% and 0% respectively. A fraction of the feed is assumed to pass directly to the underflow and another fraction to the overflow directly. I f α is the short circuit fraction to sinks and β the short circuit flow to floats, the actual partition factor R can be related to an ideal or corrected partition factorR_c by equation (6.47)

$$R(x) = \beta + (1 - \alpha - \beta)R_c(x) \tag{6.47}$$

Short circuited flows are functions of particle size. An exponential dependence with size has been found in a 150 mm dense-medium cyclone, $\alpha = R_f e^{-bd_p}$

with b = 5.43 mm-1 and dp in mm. Short circuit to floats can usually be neglected except for material smaller than 0.5 mm.

6.2.5 Separation efficiency

The efficiency of separation is specified in terms of the corrected imperfection defined by equation (6.48)

$$I_c = \frac{\rho_{25} - \rho_{75}}{2\rho_{50}} = \frac{EPM}{\rho_{50}} \tag{6.48}$$

$R_c(\rho_{25}) = 0.25$

$R_c(\rho_{75}) = 0.75$

The imperfection of the corrected partition curve is independent of the short circuit flows and it is better to base a predictive model on the corrected imperfection than on the imperfection of the actual partition curve. The imperfection increases as particle size decreases and the partition curves become steadily flatter as particle size decreases. a useful quantitative relationship for the imperfection of the corrected partition curve is determined through equation (6.49)

$$I_c - 0.013 = \frac{3.8}{d_p} \tag{6.49}$$

d_p in microns

6.2.6 The corrected partition function

A variety of empirical one-parameter expressions for the corrected partition curve has appeared in the literature. Once a particular function has been chosen to model the corrected partition curve, the actual partition curve can be constructed from the four parameters α, β, α, β, ρ_{50} and I_c.

It is then a simple matter to calculate the recovery of each particle type to floats and sinks in the separator. The Table shows some empirical equations for the corrected partition functions.

Table 6.1: Empirical equations for the corrected partition function for dense-medium separators, $x = \rho/\rho_{50}$

Type	Function	Relationship between Ic and λ
1	R(x)=G[λ(1-x)]	λIc=0.674
2	R(x)=1-G(λlnx)	$I_c = Sinh\left(\frac{0.674}{\lambda}\right)$
3	$R(x) = \frac{1}{1+\exp(\lambda(x-1))}$	λIc=1.099
4	$R(x) = \frac{1}{(1+x^{\lambda})}$	$I_c = Sinh\left(\frac{1.099}{\lambda}\right)$

In most large dense-medium vessels handling coarse material, I_c is usually assumed to be independent of particle size. Although similar to each other, these functions in table do exhibit some differences in shape so that one of the functions can fit a particular set of measured experimental data better than the others.

When choosing a suitable function to model a particular dense-medium separator the available measured data should be tested against all the functions and the one with the best fit can be chosen.

A probability scale is used for the ordinate to emphasize the differences in shape among the different functions. In this coordinate system the type 1 function will plot as a straight line and this is often considered to represent good normal operating behaviour. Downward curvature below this straight line is taken to indicate less than optimal operation of the dense-medium separator. The different separator types and cut point are presented in Table 6.2

Table 6.2: Separator types and cut point

Separator type	Cut point	Cutpoint shift	SG differential	Imperfection	Particle size
Chance cone	1.54 1.37 1.37	0.033		0.021 0.01 0.03 0.015	+ 50 mm 12.5x6.5 mm
Dense medium vesel	1.41 1.35			0.02 0.018 0.033	50x25mm 12.5x6.3mm
Dense medium cyclone	1.49 1.50 1.51 1.53 1.57			0.019 0.017 0.021 0.025 0.051	

6.2.7 Quantitative Model for Stratification

The stratification resulting from the change of position between two particles of different density in a settled bed is governed by potential energy variation. Any particle (density ρ) changing position (Figure. 6.5) in a bed of particles (density $\overline{\rho}$) causes a change of potential energy (ΔE) given by equation (6.50) and (6.51)

$$\Delta E = E(\text{particle at } H + \Delta H) - E(\text{particle at } H) \quad (6.50)$$

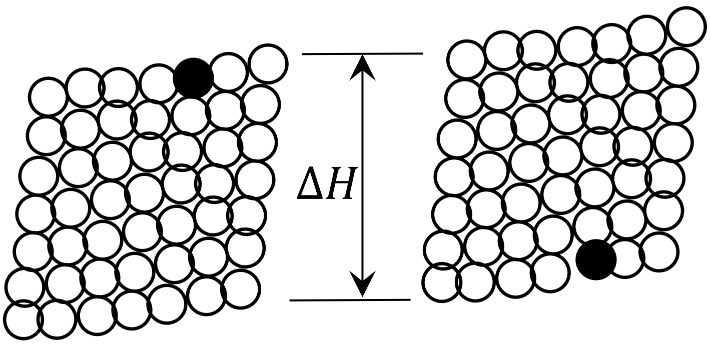

Figure 6.5: Change of potential energy when heavy particle change position in a bed of particles

$$\Delta E = v_p\rho(H+\Delta H)g + v_p\overline{\rho}Hg - v_p\overline{\rho}(H+\Delta H)g - v_g\rho Hg \quad (6.51)$$

$$\Delta E = v_p g(\rho - \overline{\rho})$$

v_p: volume of the particle

This potential energy changes at a rate that is determined through equation (6. 52) :

$$\frac{dE}{dH} = v_p g(\rho - \overline{\rho}) \quad (6.52)$$

The particle migrate upward if $\rho < \overline{\rho}$ or downward if $\rho > \overline{\rho}$ and the migration velocity is given by $\mu\frac{dE}{dH}$.

μ is the specific mobility of the particle, it is defined as the velocity at which a particle penetrates the bed under a unit potential energy gradient. μ is dependent of the particle size, shape and the bed expansion mechanism, but it is independent of the particle density.

The stratification flux of particles (density ρ) in a bed (average density $\overline{\rho}$) caused by the potential energy gradient is given by equation (6.53)

$$n_s = -C_p\mu\frac{dE}{dH} \quad m^3/m^2S \quad (6.53)$$

Where C_p is the volume concentration of particles of density ρ in the bed; n_s : Stratification flux. The negative sign means that particles tend to move down where potential energy gradient is minimal.

Combination of Equations 6.52 and 6.53 leads to equation (2.54)

$$n_s = -C_p u v_p g(\rho - \overline{\rho}) \quad (6.54)$$

The stratification flux is opposed to diffusive flux resulting from the random particle–particle and particle–fluid interactions and given by equation (6.55)

$$n_D = -D\frac{dC_p}{dH} \quad (6.55)$$

Where n_D is the diffusive flux; D: Diffusion coefficient *(*dependent on the particle size, shape, and bed expansion mechanism).

A dynamic equilibrium is established when the action due to potential energy gradient equals that of diffusion due to concentration gradient. Meaning

$n_D = -n_s$, (6.56)

Combining equations (6.55) and (6.56) yields equation (6.57)

$$\frac{dC_p}{dH} = -\frac{ugv_pC_p}{D}(\rho - \overline{\rho}) \quad (6.57)$$

Considering that the relative height is represented as in equation (6.58) and the expression $\frac{ugv_pH_b}{D}$ called specific stratification constant (α) presented by equation (6.59) is independent of particle density but depends on particle size and bed expansion mechanism , equation can be converted into equation (6.60)

$$h = \left(\frac{H}{H_b}\right) \quad (6.58)$$

H_b: is the total bed depth.

$$\alpha = \frac{ugv_pH_b}{D} \quad m^3/kg \quad (6.59)$$

$$\frac{dC_p}{dH} = -\alpha C_p(\rho - \overline{\rho}(h)) \quad (6.60)$$

Equation 6.60 shows that the average bed density $\overline{\rho}$ is function of h and can be represented by equation (6.61)

$$\overline{\rho}(h) = \int_0^\infty \rho C_p(h) d\rho \quad (6.61)$$

Solution of Equation 6.60 gives the vertical concentration profile of particles of density ρ. It does not have boundary conditions because the concentration of any particle cannot be determined at the top or bottom of the bed, the solution should satisfy the conditions of equation (6.62) and (6.63)

$$\int_0^1 C_p dh = C_p{}^f \text{ for all } \rho \quad (6.62)$$

$C_p{}^f$: the concentration of particles of density ρ in the feed to the bed and

$$\int_0^\infty C_p d\rho = 1 \text{ for } 0 \leq h \leq 1 \quad (6.63)$$

Practically, the particle population is split into n grade classes, each with its own density. To reflect this Equations 6.60‑7.63 are written in the Form of equation (6.64)

$$\frac{dC_i(h)}{dh} = -\alpha C_i(h)\left(\rho_i - \overline{\rho}(h)\right) \text{ for i=1,2,…n} \quad (6.64)$$

With

$$\overline{\rho}(h) = \sum_{i=1}^{n} C_i(h)\rho_i \quad (6.65)$$

Where

$$\sum_{i=1}^{n} C_i(h) = 1 \text{ for all h} \quad (6.66)$$

$$C_i{}^f = \int_0^1 C_i(dh) \text{for all i} \quad (6.67)$$

6.2.8 Stratification of a Two-Component System

The set of differential Equations 6.64 can be solved easily in closed form when the bed consists of only two components. Equation 6.64 integral gives

$$C_i(h) = C_i(0) exp\left[-\alpha\rho_i h + \alpha \int_0^h \overline{\rho}(y) dy\right] \text{ for i=1 and 2} \quad (6.28)$$

At height h, the average density of the two components system is given by equation (6.69)

$$\overline{\rho} = \rho_1 C_1(h) + \rho_2 C_2(h) \quad (6.69)$$

The initial condition $C_i(0)$ represents the concentration of particles i at the bottom of the bed. This is an unknown and must be calculated for each component, but the solution must satisfy Equations 6.66 and 6.67. Equation 7.66 requires that equation (6.70) is satisfied at every level in the bed.

$$C_1(h) + C_2(h) = 1 \quad (6.70)$$

The vertical profile of $\overline{\rho}(h)$ is also unknown, therefore equation 6.68 alone cannot help to determine the vertical concentration profile $(C_i(h))$ of the different particle types. However, the ratio of the concentrations of the two species in a two-component system is independent of $\overline{\rho}(h)$, and is represented by equation (6.71)

$$\frac{C_1(h)}{C_2(h)} = \frac{C_1(h)}{1-C_1(h)} = \frac{C_1(0)}{C_2(0)} \exp[-\alpha(\rho_1 - \rho_2)h] \quad (6.71)$$

From which equation (6.72) is deduced

$$C_1(h) = \frac{\frac{C_1(0)}{C_2(0)}\exp[-\alpha(\rho_1-\rho_2)h]}{1+\frac{C_1(0)}{C_2(0)}\exp[-\alpha(\rho_1-\rho_2)h]} \quad (6.72)$$

Equation (6.72) gives the vertical concentration profile of species 1 as a function of the ratio $\frac{C_1(0)}{C_2(0)}$ at the bottom of the bed. This ratio is fixed by the composition of the jig bed feed and can be determined from equation 6.67.

$$C_i^{\,f} = \int_0^1 C_i(h) f dh \quad (6.73)$$

Integration of Equation 6.73 using equation 6.72 and solution for $\frac{C_1(0)}{C_2(0)}$ gives equation (6.74)

$$\frac{C_1(0)}{C_2(0)} = \frac{1-\exp\left[-\alpha(\rho_1-\rho_2)C_1^{\,f}\right]}{\exp\left[-\alpha(\rho_1-\rho_2)C_2^{\,f}\right]-1} \exp[\alpha(\rho_1 - \rho_2)] \quad (6.74)$$

which is easy to determine when the composition of the feed is known. Substitution of this ratio into equation 6.72 gives the vertical concentration profile. Typical concentration profiles are shown in figure 6.6.

The grade and recovery in the two product streams can be calculated after the equilibrium stratification profiles has been calculated. The yield of total solids to the heavier fraction can be obtained by integrating the concentration profile. Equipment that is designed separate parte particles based on stratification always has a mechanism that enables the stratified bed to be split at some horizontal position. The top layers of the bed contain the lighter particles and the lower layers will include the heavier particles.

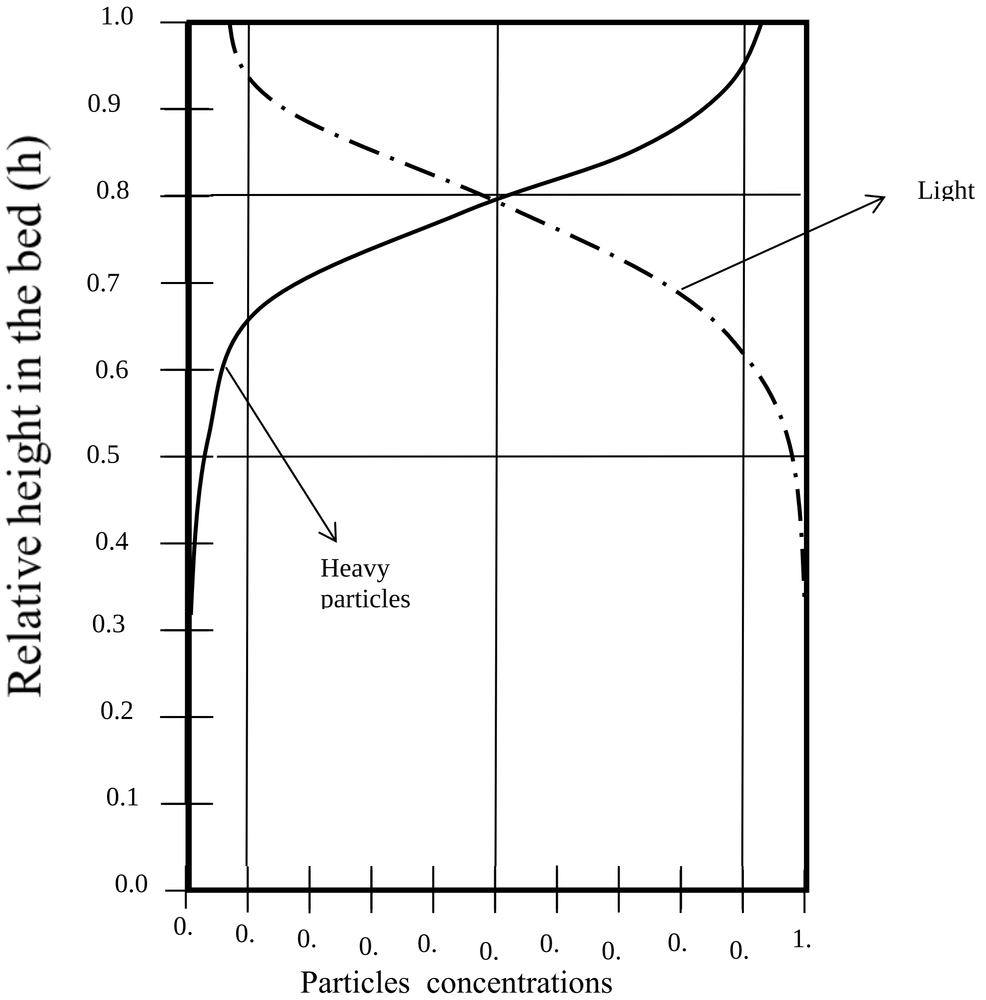

Figure 6.6: Typical concentration profiles

Figure 6.6 shows the calculated equilibrium stratification profiles for a binary mixture having components with densities 2670 and 3300 kg/m3 and initial concentration 0.2 of the lighter component. The specific stratification constant is 0.02. The mass yield of solids in the lighter product obtained by slicing the bed at a relative height h_s is given by equation (6.75

$$Y(h_s) = \frac{\int_{h_s}^{1} \bar{\rho}(h)dh}{\int_{o}^{1} \bar{\rho}(h)dh} \tag{6.75}$$

The recovery of the ith density component to the lighter product at a height h_s is given by equation 6.76 while the concentration of component i in the lighter product is given by equation (6.77)

$$R_i(h_s) = \frac{\int_{h_s}^{1} C_i(h)dh}{\int_{0}^{1} C_i(h)dh} = \frac{\int_{h_s}^{1} C_i(h)dh}{C_i^f} \tag{6.76}$$

$$C_i^p = \frac{C_i^f R_i(h_s)}{\sum_i C_i^f R_i(h_s)} \tag{6.77}$$

Equations 6.75, 6.76, and 6.77 can be used to generate grade–recovery and recovery–yield curves using the relative splitting height h_s as the operating variable.

6.2.9 Stratification in Multicomponent Beds

When the material to be processed contains more than two particle types, the convenient analytical solution given in the previous section is no longer available, and a numerical technique must be used to solve the system of differential Equations 6.64 subject to the conditions in equations 6.65 to 6.67.

6.3 Flotation

6.3.1 A Kinetic Approach to Flotation Modelling.

The model can be formulated in terms of a rate of flotation which can be quantified. It is based on an analysis of the individual sub processes that affect an individual particle in the flotation environment.

For a particle to be recovered in the froth, it must:

1. achieve a level of hydrophobicity that will permit it to attach to a rising bubble.
2. be suspended in the pulp phase of the cell.
3. collide with a rising bubble.
4. adhere to the bubble.
5. not detach from the bubble during passage through the pulp phase.
6. not detach from the bubble as the bubble leaves the pulp phase and enters the froth phase.
7. not detach and drain from the froth during the passage of the froth to the weir.

Lets us consider the pulp phase and the froth phase separately as the kinetic differ in each. The particles are considered to be in one of four possible states in the flotation cell:

- suspension in the pulp phase,
- attached to the bubble phase,
- attached to the air-water interface in the froth phase
- suspended in the Plateau borders of the froth phase.

6.3.2 The pulp phase

It consists of suspended and moving particles in water.

At any point in the pulp the bubbles are moving upward relative to the
pulp at their local rise velocity and the particles are moving downward at their local settling velocity.

this relative velocity between particles and bubbles is responsible for collisions between particles and bubbles.

Particles leave the pulp phase through:

- collision with and attachment to a bubble
- go to the froth phase by entrainment at the pulp-froth interface. These two phenomena govern the kinetic behaviour of the particles in a flotation cell.

Particles can re-enter the pulp phase by detachment from a bubble or by draining from the Plateau borders in the froth.

6.3.3 The bubble phase

The bubble phase consists of of bubbles that rise through the pulp phase. A particle moves from the pulp phase to the bubble phase by a process called **bubble-particle collision and particle attachment.**

Once a particle is attached to a bubble will either go with it until the froth phase or be detached.

6.3.4 Froth phase

The froth phase consists of the bubbles and particles that manage to cross pulp-froth interface. The bubbles do not burst when they cross the interface and each one carries a skin of water into the froth phase. The bubbles move close together with a single film which is curved in case the bubbles are small. When the liquid drains from the film, it break causing adjacent bubbles to coalesce and the bubbles growing into polyhedral shape. The junction of the polyhedral edges makes the **Plateau borders** through which the liquid moves downward..
Particles can become detached from the liquid film and move through the plateau border to the pulp phase.

6.3.5 Entrained phase

Particles are entrained in the Plateau borders and tend to settle down toward the pulp-froth interface by gravity. Water drains as well from the film to the interface through plateau and reenters the pulp phase. Particles enter the entrained phase by detachment from the air-water surfaces in the froth and also by direct entrainment from the pulp phase immediately below the pulp-froth interface on the top of the pulp

6.3.6 A Kinetic Model for Flotation

The kinetic model is based on the principle: a single bubble rising upward through the pulp phase will collide with suspended particles and some of these particles will attach to the bubble surface and will travel upward with it.

The rate at which bubbles collide with particles depends on: the size of the bubbles and the size of the particles, their relative velocities, and the concentration of particles in the pulp.

The number of particles that can collide with the bubble can be calculated in the following way. The volume of pulp that is swept by a bubble per second is determined through equation (6.78)

$$v_p = \frac{\pi}{4} D_{bh}{}^2 U_b \tag{6.78}$$

Where Ub the local rise velocity of the bubble; D_{bh} the bubble diameter projected on to the horizontal plane.

The population of particles in the cell can be divided into classes according to the population balance approach so that particles any class can be similar in size and composition. The number of potential collisions with the particles of type ij is proportional to the concentration c_{ij} of these particles in the pulp phase

The diameter of the swept volume from which a particle of size

d_{pi} may be captured is $D_{bh} + d_{pi}$

The number of potential collisions with particles of size dpi is given by equation (6.79)

Number of potential collisions with particles of type ij = $\frac{\pi}{4}\left(D_{bh} + d_{pi}\right)^2\left(U_b + v_{Tij}\right)C_{ij}$ (6.79)

Where v_{Tij} the free fall velocity of the particle, They are considered as terminal velocities

The rate of transfer of particles from the pulp phase to the bubble phase is given by equation (6.80):

$$\text{Ideal rate transfer} = \frac{\pi}{4}\left(D_{bh} + d_{pi}\right)^2\left(U_b + v_{Tij}\right)C_{ij} x \frac{G_v \tau_b}{\frac{\pi}{6} D_{be}{}^3} \text{ in } {}^{kg}/_{m^3} \text{ of cell volume} \tag{6.80}$$

Where $G_v$the specific aeration rate in m3 air/s m3 cell volume; $\tau_b$the average bubble residence time in the cell; $D_{be}$the effective spherical diameter of the bubble.

This is just ideal because all potential collisions do not happen, it modified to equation (6.81):

$$\text{Rate of transfer} = \frac{\pi}{4}\left(D_{bh} + d_{pi}\right)^2\left(U_b + v_{Tij}\right)C_{ij} x \frac{G_v \tau_b}{\frac{\pi}{6} D_{be}{}^3} E_{Cij} E_{Aij}\left(1 - E_{Dij}\right) \ {}^{kg}/_{m^3} \text{ of cell volume} \tag{6.81}$$

Where $E_{Cij}$the fraction of particles that are in the path of the bubble which actually collide with it; $E_{Aij}$is the fraction of bubble-particle collisions that lead to successful attachment; $E_{Dij}$the fraction of particles of type ij that are detached from the bubble during the time that it takes the bubble to rise through the pulp phase

6.3.7 Particle-bubble collisions

All particles in the path of the bubble do not necessary collide with it. as the bubble advances it moves away water which carries the particles out of the path. There are two different flow regimes around the bubble:

Streamlines for water around a rigid spherical bubble calculated assuming potential flow (left-hand side) and Stokes flow (right-hand side). Stokes flow which applies when the bubble Reynolds number is very much less than unity and potential flow which applies when the bubble Reynolds number is very much larger than unity. Particle on this path will collide with the bubble only if it is on a streamline that has it closest approach to the bubble less than or equal to the radius of the particle.

On the other hand a neutrally buoyant particle of the same size would touch the bubble surface if it were as far out as 56% of the bubble radius under potential flow conditions. Potential flow leads to much higher collision efficiencies than Stokes flow.

The streamlines are governed by equation (6.82) and (6.83)

$$\psi = \frac{\psi}{U_b {R_b}^2} = \mathrm{Sin}^2\theta\left[\frac{1}{2}\left(\frac{r}{R_b}\right)^2 - \frac{3r}{4R_b} + \frac{R_b}{4r}\right] = \mathrm{Sin}^2\theta £_{St}(r) \text{ for stokes flow} \quad (6.82)$$

$$\psi = \frac{\psi}{U_b {R_b}^2} = \mathrm{Sin}^2\theta\left[\frac{1}{2}\left(\frac{r}{R_b}\right)^2 - \frac{R_b}{2r}\right] = \mathrm{Sin}^2\theta £_{Pot}(r) \text{ for potential flow} \quad (6.83)$$

Where r and θ are respectively spherical spatial coordinates with the bubble center as origin; R_b the radius of the bubble; U_b the velocity of rise of the bubble

These streams line are ideal

In practice, at Reynold number 0-100, it was established through equation (6.84) and (6.85)

$$\psi = \mathrm{Sin}^2\theta(\alpha £_{St}(r) + (1-\alpha)£_{Pot}(r)) = \mathrm{Sin}^2\theta £(r) \quad (6.84)$$

$$£(r) = \frac{1}{2}\left(\frac{r}{R_b}\right)^2 - \frac{3\alpha r}{4R_b} + \left(\frac{3}{4}\alpha - \frac{1}{2}\right)\frac{R_b}{r} \quad (6.85)$$

α dimensionless parameter that depends on the bubble Reynolds number and is determined through equation (6.86) and (6.87)

$$\alpha = \exp\frac{4{Re_b}^{0.72}}{45}\frac{{r_p}'}{1+{r_p}'} \quad (6.86)$$

$$r_p' = \frac{R_p}{R_b} \tag{6.87}$$

Where R_p is the radius of the particle

6.3.8 Model for Collision efficiency

The collision efficiency is calculated as the fraction of the particles which are in the path of the bubble that actually collide with the bubble. Particles deviate from the fluid streamlines because they fall relative to the fluid as a result of their greater density and because inertia prevents the particle from accelerating at the same rate as the fluid when the fluid deviates from a straight line path as it approaches a bubble. The radial and azimuthal components of the fluid velocity in from of the bubble are given by equation (6.88) and (6.89)

$$u_r = -\frac{1}{r^2 \sin\theta}\frac{\partial\psi}{\partial\theta} = -2\frac{U_b {R_b}^2}{r^2}\cos\theta £(r) \tag{6.88}$$

$$u_\theta = -\frac{1}{r\sin\theta}\frac{\partial\psi}{\partial\theta} = \frac{U_b {R_b}^2}{r}\cos\theta £(r) \tag{6.89}$$

If the inertia of the particles is neglected, the particles move relative to the fluid at their terminal settling velocities, vT. Terminal settling velocities can be calculated. And the components of the particle velocity vector are given by equations (6.90) and (6.91)

$$v_r = u_r - v_T \mathrm{Sin}\theta \tag{6.90}$$

$$v_\theta = u_\theta - v_T \mathrm{Sin}\theta \tag{6.91}$$

The stream function for the particle motion is therefore deduced through equation (6.92)

$$\boldsymbol{\psi_p} = \mathbf{U_b}\mathbf{R_b}^2 \mathrm{Sin}^2\theta\left(£(r) + \frac{1}{2}\frac{v_T}{U_b}\left(\frac{r}{R_b}\right)^2\right) \tag{6.92}$$

The collision efficiency for particles of type ij is calculated as the flux of particles crossing an imaginary hemisphere of radius Rb + Rp that shrouds the front hemisphere of the bubble divided by the flux of particles that cross a horizontal plane of area . $(R_b + R_p)^2$.

Therefore the collision efficiency for particles of type ij is determined using equation (6.93)

$$\mathbf{E_{Cij}} = \frac{-2\pi\int_0^{\frac{\pi}{2}} \mathbf{v_{r\backslash r=R_b+R_p}}(\mathbf{R_b}+\mathbf{R_p})\mathbf{sin\theta}(\mathbf{R_b}+\mathbf{R_p})\mathbf{d\theta}}{\boldsymbol{\pi}(\mathbf{R_b}+\mathbf{R_p})^2(\mathbf{U_b}+\mathbf{v_{Tij}})} \tag{6.93}$$

The latitude angle at which the particle on streamline $\boldsymbol{\theta}$ strikes the bubble can be calculated using equation (6.94)

$$\boldsymbol{\theta_c} = \mathbf{arcsin}\left(\left(\frac{\boldsymbol{\psi_0}}{£(R_b+R_p)+\frac{1}{2}\frac{v_T}{U_b}\left(\frac{R_b+R_p}{R_b}\right)^2}\right)^{\frac{1}{2}}\right) \tag{6.94}$$

6.3.9 Rise times of loaded bubbles.

The diameter of the horizontal projection of the bubble can be calculated from the effective volume diameter using the empirical relationship presented in equation (6.95), (6.96), (6.97) and (6.98)

$$\frac{D_{be}}{D_{bh}} = \frac{1+0.6Ta^3}{1+Ta^3} \tag{6.95}$$

$$Ta = Re_{be}Mo^{0.23} \tag{6.96}$$

$$Re_{be} = \frac{D_{be}U_b\rho}{\mu} \tag{6.97}$$

$$D_{be} = \left(\frac{6V_b}{\pi}\right)^{\frac{1}{3}} \tag{6.98}$$

Where V_b is the bubble volume; Mo is the Morton number and

$$Mo = \frac{g\mu^4}{\rho\sigma^3} \tag{6.99}$$

Where σ the surface tension of the solution at the bubble surface

The terminal rise velocity of a partly loaded bubble can be calculated from equation (6.100)

$$U_b = \frac{D_{be}}{D_{bh}}\left(\frac{4(\rho_w - LL_{max})gD_{be}}{3C_D\rho_w}\right)^{\frac{1}{2}} \tag{6.100}$$

Where LLmax is the specific load carried by the bubble is expressed as the weight of particles carried per cubic meter of bubble; C_D the drag coefficient of the rising bubble resulting from equations (6.101) and (6.102)

$$C_D = 0.28\left(1 - \frac{9.0.6}{{Re_{bh}}^{1/2}}\right)^2 \text{ for } Re_{bh} \leq 108 \tag{6.101}$$

$$C_D = 0.98\ for Re_{bh} \geq 108 \tag{6.102}$$

Example 6.2

Calculate the terminal rising velocity of the following bubbles in a dilute solution of butanol having surface tension 0.052 N/m. The density of the water is 999.1 kg/m3, and its viscosity 0.001 kg/ms.

a) Small bubble of volume effective diameter =0.5 mm

b) Intermediate bubble of effective volume diameter = 2mm

c) Large bubble having volume effective diameter =12 mm

Solution

a) Small bubble of volume effective diameter = 0.5 mm

The Drag coefficient of rising bubble can be determined graphically or mathematically knowing.

$$\emptyset = C_D Re_{bh}{}^2 = \frac{4\rho_W{}^2 g D_{be}{}^3}{3\mu^2}$$

$$\emptyset = \frac{4999.1^2 9.81x(0.5x0.001)^3}{30.001^2} = 1.63x10^3$$

The value of CD can now be evaluated equation:

Knowing $C_D = 0.28\left\{\frac{\left[1+0.0921x(\emptyset)^{1/2}\right]^{1/2}+1}{\left[1+0.0921x(\emptyset)^{1/2}\right]^{1/2}-1}\right\}^2$ for $\emptyset < 1.14x10^4$

$$C_D = 0.28\left(\frac{\left(1+0.0921x\left((1.63x10^3)^{1/2}\right)^{1/2}+1\right.}{\left(1+0.0921x\left((1.63x10^3)^{1/2}\right)^{1/2}-1\right.}\right)^2 = 2.05$$

Bubbles of this small size will remain spherical shape while rising in water , thus we $^{D_{be}}/_{D_{bh}}$ as a first estimate

$$U_b = \frac{D_{be}}{D_{bh}}\left(\frac{4(\rho_w - LL_{max})gD_{be}}{3C_D\rho_w}\right)^{\frac{1}{2}},\ U_b = \left(\frac{4x9.81x0.5x10^{-3}}{3x2.05}\right)^{1/2} = 0.056$$

Check the value of $^{D_{be}}/_{D_{bh}}$

$$Mo = \frac{g\mu^4}{\rho\sigma^3}$$

$$M_O = \frac{9.81x(0.001)^4}{999.1x(0.052)^3} = 6.98x10^{-11}$$

$$Re_{be} = \frac{D_{be}xU_bx\rho_w}{\mu}$$

$$Re_{be} = \frac{0.5x10^{-3}x0.056x999.1}{0.001} = 28.0$$

$$Ta = Re_{be}Mo^{0.23}$$

$$T_a = 28.0x(6.98x10^{-11})^{0.23} = 0.129$$

$$\frac{D_{be}}{D_{bh}} = \frac{1+0.6Ta^3}{1+Ta^3}$$

$^{D_{be}}/_{D_{bh}} = \frac{1+0.6x0.129^3}{1+0.129^3} = 0.999$ which confirms the estimate

The calculated value can be compared to 0.042 m/s measured by Allen for a 0.48 mm diameter bubbles in water

b) Intermediate bubble of effective volume diameter = 2mm

$$\emptyset = C_D Re_{bh}{}^2 = \frac{4x999.1^2 9.81x(2x0.001)^3}{3x0.001^2} = 1.044x10^5$$

Re_{bh} Bubble Renold number

Since $\emptyset > 1.14\ x10^4, C_D = 0.98$

A bubble of 2 mm diameter in water is elliptic in shape , and the value of the ratio $\frac{D_{be}}{D_{bh}}$ must be calculated. This requires some iterative calculation. Start the calculation at intermediate value of $\frac{D_{be}}{D_{bh}} = 0.8$

$U_{10} = \frac{D_{be}}{D_{bh}} \left(\frac{4x9.81x2x10^{-3}}{3x0.98}\right)^{1/2} = 0.8x0.163\frac{m}{s} = 0.13$

The diameter ratio must be refined

$Re_{be} = \frac{2x10^{-3}x0.8x0.163x999.1}{0.001} = 261$

$\mathrm{Ta} = \mathrm{Re_{be}Mo^{0.23}}$, $T_a = 261x(6.98x10^{-11})^{0.23} = 1.204$

$\frac{D_{be}}{D_{bh}} = \frac{1+0.6x1.204^3}{1+1.204^3} = 0.746$

Refining the value of U_b using this value for the diameter ratio gives

$\frac{D_{be}}{D_{bh}} = 0.76$ and $U_b = 0.76x0.163 = 0.122m/s$

This answer can be compared to the value of 0.136 m/s measured by Furstenau and Wayman (1958) for a 1.97 mm bubbles in water

c) Large bubble having volume effective diameter =12 mm

Bubbles as large as this will have a spherical cap shape, and therefore $\mathrm{C_D}$ =0.98 and the diameter ratio has the limting value 0.6

$\mathrm{U_b} = 0.6\left(\frac{\mathrm{4x9.81x12x10^{-3}}}{\mathrm{3x0.98}}\right)^{1/2} = 0.24\ \mathrm{m/s}$

This can be compared with value 0.236 m/s measured by Fuerstennau and Wayman for a bubble having a volume effective diameter of 12.2 mm

Example 6.3

Calculate the terminal rise velocity of a 0.5 mm diameter air bubble (spherical) that is carrying 5 galena particles that may be taken as cubes of side 100 microns. The density of galena is 7500 kg/m3. The specific load carried by the bubble is expressed as the galena load per cubic meter of bubble:

$\frac{\mathrm{5x(100x10^{-6})^3x7500}}{\frac{\pi}{6}\mathrm{(0.5x10^{-3})^3}} = 573.0\,\mathrm{kg/m^3}$

$\emptyset = \mathrm{C_D Re_{bh}}^2 = \frac{\mathrm{4x(999.-573.0)999.1x9.81x(0.5x0.001)^3}}{\mathrm{3x0.001^2}} = 696$

$$C_D = 0.28\left(\frac{\left(1+0.0921x\left(696^{1/2}\right)^{1/2}+1\right.}{\left(1+0.0921x\left(696^{1/2}\right)^{1/2}-1\right.}\right) = 11.21$$

$$U_b = \left(\frac{4x(999.1-573.0)x9.81x0.5x10^{-3}}{3x11.21x999.1}\right)^{1/2} = 0.016\ \mathrm{m/s}$$

Which is about 1/3 of the rise velocity of an unloaded bubble. Bubbles of this small size will remain a spherical shape while rising in water , thus we try

Example 6.4

Workout the terminal rise velocity of a 0.5 mm diameter air bubble (spherical) that is carrying through water (ρ = 1000 kg/m3) 4 galena particles that may be taken as cubes of side 45 microns. The density of galena is 7500 kg/m3. The viscosity of water is 0.001 N/mS.

The specific load S_l carried by the bubble is expressed as the galena load per cubic meter of bubble:

$$S_l = \frac{4x\frac{\pi(d_p)^3}{6}x7500}{\frac{\pi(d_b)^3}{6}} = \frac{4x7500x(d_p)^3}{(d_b)^3} = \frac{4x7500x\left(45x10^{-6}\right)^3}{(0.5x10^{-3})^3} = 546.75\ \mathrm{kg/m^3}$$

$$\emptyset = C_D {Re_{bh}}^2 = \frac{4x(1000-546.75)1000x9.81x(0.5x0.001)^3}{3x0.001^2} = 29.64255$$

$$\emptyset < 1.14x10^4$$

$$C_D = 0.28\left\{\frac{\left[1+0.0921x(29.64)^{1/2}\right]^{1/2}+1}{\left[1+0.0921x(29.64)^{1/2}\right]^{1/2}-1}\right\}^2 = 27.31$$

$$U_b = \left(\frac{4x(1000-546.75)x9.81x0.5x10^{-3}}{3x27.31x1000}\right)^{1/2} = 0.01\ \mathrm{m/s}$$

6.4 Thickening

Thickening is used for the partial dewatering of relatively dense slurries. The particles settling rate depends on their nature. The settling flux, is the mass of solid crossing a horizontal plane in the slurry per unit time and specified per unit area of the plane. According to Kynch, settling velocity is a function only of the local concentration of solids in the slurry. The flux is related to the settling velocity by equation (6.103)

$$\emptyset = CV(C)\ \mathrm{m^3/m^2S} \qquad (6.103)$$

Cs represents the concentration of an ideal fully settled incompressible sediment. In practice sediments are rarely incompressible. Consequently it is not possible to determine Cs but can be assumed.

6.4.1 Continuous cylindrical thickener

The figure below shows A steady state Kynch . Once introduced the slurry is assumed to spread instantly across the cross-section of the thickener and to dilute to concentration CL. Lower down in the thickener, a layer of concentration CM develops and at the bottom the slurry is discharged through the discharge pipe at concentration CD. This is just ideal for modelling.

The operation of the thickener is governed by the behaviour of these layers as show figure 6.7.

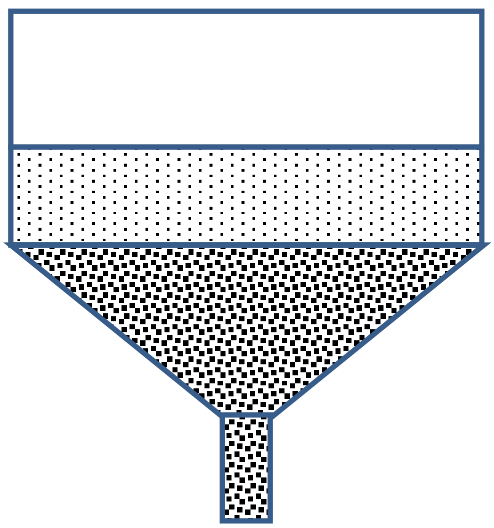

Figure 6.7: Different layers in the thickener

The total settling flux at any level where the concentration is C must include the effect of the pulp discharge at the bottom and the settling flux of the solid relative to the slurry itself. If the total flux is represented by f(c) and the volumetric flux of slurry below the feed by q then equation (6.104) is used to determine it.

$$f(C) = qC + \delta(C) \tag{6.104}$$

In batch settling q = 0 so that f (C) and **δ** (C) are identical, where q is the underflow volumetric flow. At any discontinuity across the thickener, the Flux of solid into the discontinuity from above will be determined using by equation (6.105) and equation (6.106) which are generalized in equation (6.107)

$$f(C^{+}) = C^{+}q + C^{+}V(C^{+}) \tag{6.105}$$

Flux of solid leaving from below:

$$f(C^{-}) = C^{-}q + C^{-}V(C^{-}) \tag{6.106}$$

$$f(C^+) = f(C^-) \tag{6.107}$$

If solid accumulates at the discontinuity, then the accumulation is positive if

$f(C^+) > f(C^-)$ and negative if $f(C^+) < f(C^-)$

If the accumulation is positive the discontinuity moves upward a distance Δx during a time interval Δt and the two are related throrugh equation (6.109) which is the rate of movement of the discontinuity.

$$A\Delta x(C^- - C^+) = [f(C^+) - f(C^-)]A\Delta t \tag{6.109}$$

Equation (6.109) will apply as well to continuous thickener as indicated in equation (6.110)

$$\delta(C^+, C^-) = \lim_{\Delta t\to 0}\frac{\Delta x}{\Delta t} = -\frac{f(C^+) - f(C^-)}{C^+ - C^-}\ \text{m/s} \tag{6.110}$$

In steady state $\delta\ C^+, C^-$ must be zero across every discontinuity. The concentrations in the layers on each side of a discontinuity make up a conjugate pair. These conjugate concentrations must be stable and fixed. There is stability only if the total settling flux has a local minimum. Thus as soon as the underflow volumetric flux q is fixed the conjugate concentrations can be determined by drawing the horizontal tangent to the total flux such as line A–B. If the minimum does not occur at a concentration less than C_s, the conjugate concentrations are found by drawing the horizontal line from the point G as shown by line G–F . A model for continuous thickening can be developed based on the steady state where all the solid must pass through every horizontal plane in the thickener. Meaning all solid will be discharged at the underflow. The flux through any horizontal plane in a steady state thickener must equal the feed flux as show equation (6.111) and the underflow as show equation (6.112)

$$f_F = \frac{Q_F C_F}{A} \tag{6.111}$$

$$f_D = \frac{Q_D C_D}{A} = qC_D \tag{6.112}$$

where $q = \frac{Q_D}{A}$ is the total downward volumetric flux at any horizontal layer below the feed well. Thus

$$f_F = qC + \psi(C) \tag{6.113}$$

where C is the concentration at any level in the thickener.

Equation (6.113) can be plotted on the $\psi(C)$ vs C axes as a straight line of slope q as shows Figure 6.8. Re-arranging equation (6.113) give equation (6.114) which shows that the line intersects the $\psi(C)$ axis at $\psi = f_F$

$$\psi(C) = f_F - qC \tag{6.114}$$

Since, $f_D = qC_D = f_F$, the line intersects the C axis at C = CD.

The quantity $\psi(C) = f_F - qC$ is called demand flux because this flux must be transmitted through every horizontal level in the thickener otherwise the thickness could not operate at steady state.

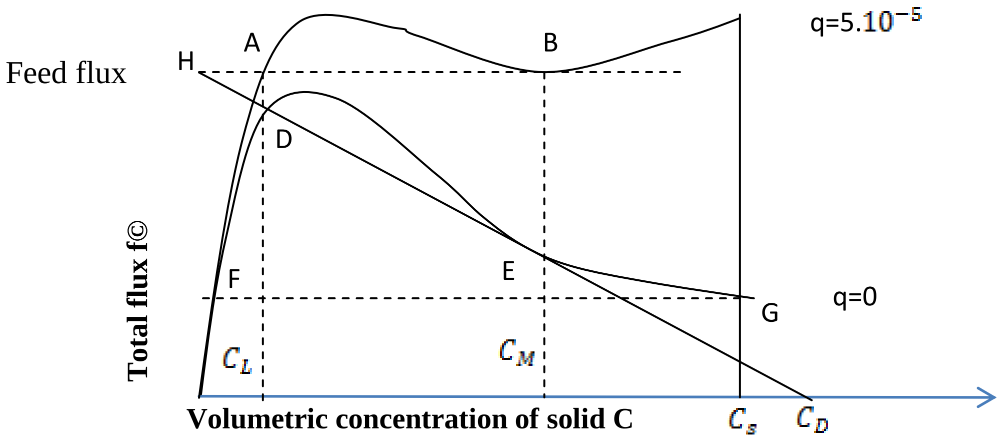

Figure: 6.8: Total flux as function of volumetric concentration of solid

The straight line representing Equation 6.11 is tangential to the (C) function at point E, which has the same abscissa value C_M as the conjugate operating point B. The point E is directly below B. Likewise the intersection D between the straight line and the (C) curve has the same concentration as the lower conjugate point A.

Point A is defined by $f_F = qC_A + C_A$

and the point D is defined by $f_F - qC_D = C_D$

These two equations are true simultaneously only if CD = CA = CL.

6.4.1.1 |Long tube Methods for estimating thickener dimensions

This method is used to size Sizing a thickener for pulps that do not have clear demarcation line. The test takes place in 3-4m high and 0.075m diameter tube.

6.4.2 Dewatering screens

The feed to the screens is a slury. The solid material is retained on the screen retains the solids while the water drains through the screen. The movement of the bed of solids through the screen surface is induced by vibration. The model represented in figure 6.9 outlines an approach to describe the screen operation

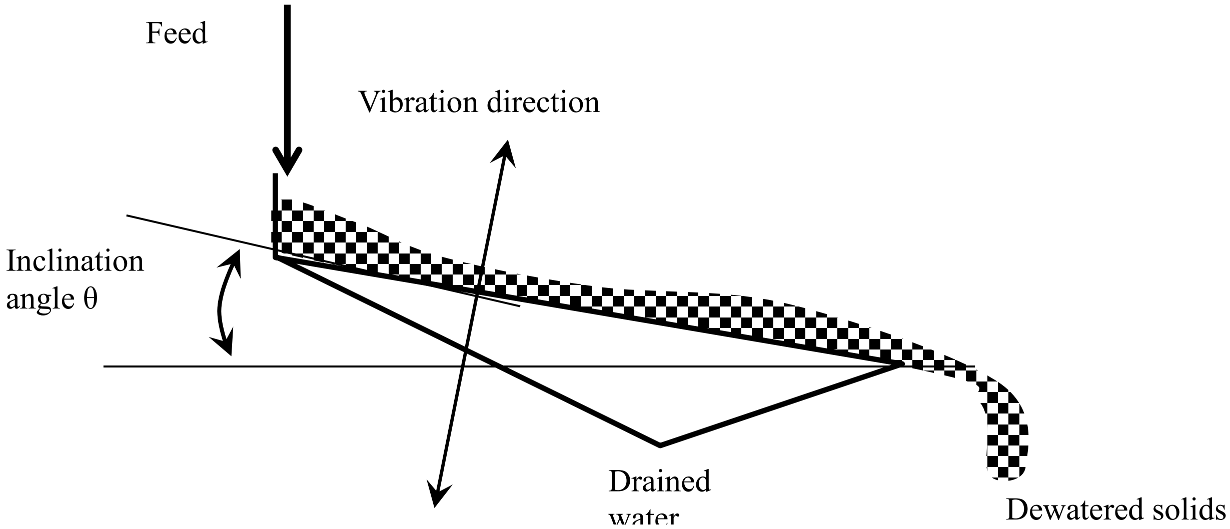

Figure 6.9: Schematic of a dewatering screen

The bed transport mechanism and the dewatering mechanism are modelled separately.
The bed movement rate is determined through gravitational parameter as represented in equation (6.115)

$$G_y = \frac{g\cos\theta}{\omega^2 A_y} \tag{6.115}$$

The transport velocity is a dimensionless parameter given by equation (6.116)

$$X = \frac{u}{\omega A_x} \tag{6.116}$$

Where θ is angle of inclination of the screen; ω the angular speed of vibration in radians/s; Ay the amplitude of vibration in the direction normal to the screen surface; u: velocity of travel along the screen; Ax: amplitude of the vibration in the direction parallel to the screen Surface

For mineral slury, commonly used model is represented by equation (6117)

$$X = aexp\left(-bG_y\right) \tag{6.117}$$

Where

b = 1 .44 − 2 .32 θ

The extent of dewatering is characterised by equation (6.118)

$$t = \frac{L}{u} \tag{6.118}$$

Where t is the time the slurry spends on the screen; u the velocity of bed travel and the length

L: length of the screen; a parameter specific to the material

The dewatering process is governed by:

- the inertial effects from the rapid acceleration and deceleration of the material on the screen
- water should leave the bottom of the screen by drip dislodgement.

Since the complete dewatering is not possible there is a minimum achievable moisture called **saturation moisture content,** which is function of physical properties of the bed and the vibration mechanism.

The rate of dewatering can be described by equation (6.119), for which the integration is presented i9n equation (6.120)

$$\frac{dS}{dt} = -\alpha(S - S_\infty)^\beta \qquad (6.119)$$

$$S - S_\infty = t^{-q} \qquad (6.120)$$

with $q = \frac{1}{\beta - 1}$ and $\left(\alpha(\beta - 1)\right)^{-q}$

Combining Equations 6.118 and 6.120 gives the water content of the discharged slurry as presented in equation (6.121)

$$S = S_\infty + p\left(\frac{L}{u}\right)^{-q} \qquad (6.121)$$

Where $S\infty$: represents the saturation moisture content; S: saturation; t screening time

Other research shows that :

q = 0.33+0.081 (h-1) (6.122)

The carrying capacity of the dewatering screen can be calculated approximately from equation (6.123), (6.124) and (6.125)

$$W = \frac{W_\infty}{b}(1 - e^{-4h}) \qquad (6.123)$$

Where $\frac{W_\infty}{b}$ is the capacity per unit width of screen at large mesh size; h is the screen mesh size in millimetres

$$\frac{W_\infty}{b} = 20 + 2.5{d_{50}}^F \text{ tonne/hr m for } {d_{50}}^F < 12\ mm \qquad (6.124)$$

$$\frac{W_\infty}{b} = 50 + 0.3{d_{50}}^F \text{ tonne/hr m for } {d_{50}}^F > 12\ mm \qquad (6.125)$$

Example 6.5

Calculate the water content of a coal slurry after dewatering on a 0.6-mm mesh screen, 3.66 m long by 0.914 m wide, with angle of inclination of 15°. The Vibration mode has amplitude 2 cm at a frequency of 300 rpm and is inclined at 45°

to the surface of the screen. The saturation water content of the coal is 7.35%.

$\omega = \frac{300}{60} \text{ x } 2\pi = 31.42 \text{ rad/s}$

$G_y = \frac{9.81 \text{ x} \cos 15^o}{31.42^2 \text{ x } 0.02 \text{ x} \sin 45^o} = 0.679$

b = 1.44 – 2.52 x 0.262 = 0.780

$\dot{X} = 1.87 \exp(-0.780 \text{ x } 0.679) = 1.101$

$A_x = 0.02 \text{ x} \cos 45^o = 0.014 \text{ m}$

$u = 1.101 \text{ x } 31.42 \text{ x } 0.014 = 0.489 \text{ m/s}$

$t = \frac{3.66}{0.489} = 7.485$

$p = 0.234; q = 0.33 + 0.081(0.5 - 1) = 0.298$

The water content of over flow stream is:

$S = 0.0735 + 0.234 \text{ x } (7.485)^{-0.298} = 0.202 \text{ kg water/kg slurry}$

6.5 Metallurgical Accounting

Metallurgical accounting can be defined as the monitoring of the valuable metals from the time the ore is broken at the primary crusher until the time that saleable products and residues are obtained.

The overall purpose of metallurgical accounting is to provide management with up-to-date information that can be used to control mining and metallurgical operations. The decisions that are taken on the basis of the information that the metallurgical accounting system provides should result in improved control and, ultimately, increased revenue.

6.5.1 Metallurgical Test work

Mineral processing projects start life is based on metallurgical test work conducted during a Feasibility Study. It is common for test work samples to be representative of the actual plant feed. Test work results are regularly misinterpreted. Operating efficiencies have a negative impact on the accounting and poor plant design can limit test work results being achieved.

Usually there is a learning curve, particularly for base metals flotation plants. Quite often the metallurgical accounting is blamed, or at least not believed, because of performance results being different to the original test work.

6.5.2 The Metallurgical Balance

A metal balance in a processing plant equates the material going into the plant with the products leaving the plant. In a gold plant, there are usually two final products, gold bullion and tailings. For a base metals concentrator, it is a concentrate for shipment to a smelter and tailings which are stored on site.

6.5.3 Examples of gold accounting

This method applies equally well to base metals concentrators, mineral sands plants, acid leach plants etc. The basic flows and analyses are determined by measuring:

- The weight of the ore for a given period (as measured by a weightometer)
- The percentage moisture content of the plant feed
- Representative samples of solids and liquids from the plant feed and tailings
- The pulp density of the feed to the process circuit
- Assay values of the solids and liquids

The contained metal in the ore should be calculated from the plant feed or, preferably, cyclone overflow, because of the fineness of the solid fraction. Sufficient sample can be collected to obtain a representative sample of the feed. At coarser sizes, the sample size must satisfy statistical requirements at a size of $P_{80} = 75$ microns, two kilograms is an acceptable minimum for ease of drying and preparation.

6.5.4 Plant Losses

Plant losses are normally measured in the tailings stream. However there are also other causes for losses that need to be considered and can influence the metallurgical balance in a negative way such as:

Stream losses**,** Theft, Preg robbing, Disposal of gold smeared steel from gravity concentrators, Gold on old smelting pots, Lock up of gold on mill liners, sumps, gold traps. Gold lost in slag**,** Re-precipitation**,** Gold lost on fine carbon**,** Mill upsets and coarse grinds, Gold settling in tanks, gold room sumps or locked up in roasters etc**.**

6.5.5 Dry" Feed Rate Determination

All the methods for mass measurement determine the total mass of "wet" ore into the plant. These measurements are usually made by a weightometer on the feed belt and correction is required for moisture content to obtain the "dry" mass flow for reporting and calculations.

The standard convention is always to use dry tonnes of ore milled.

All weightometers have a limit of accuracy depending on the make, installation and attention given to calibration. Modern electronic weightometers should achieve an error within plus or minus half a percent if properly maintained.

Different methods are used to determine the moisture E.g Microwave technology.

A more common practise at mine sites is to take samples from the mill feed belt every two hours and to determine the moisture content by calculating the weight lost in drying.

For slurry density measurement, usually as percent solids, the most accurate method is, again, wet and dry weights. Indirect measurements, such as Marcy densities, are not considered accurate enough for inventories even though it is acceptable for daily mill control.

6.5.6 Other Measurements

The installation of automatic control systems, which improvements in the instrumentation available. In general terms, automatic control in a concentrator is aimed at one or more of the following:

- Increased throughput
- Improved recovery of the valuable minerals
- Improved concentrate grade (resulting in cost savings in subsequent processing)
- Reduced operating costs (e.g., by savings in reagents, more productive use of mill personnel)

The following instruments have allowed real time data collection:

- Density gauges
- Weightometers
- Tank level gauges
- Mass flow meters
- Feed, concentrate and tailings grade analysers

6.5.7 Sampling

Sampling is a necessary adjunct to metallurgical accounting to assure correctly evaluated results. Great responsibility rests on a very small sample; therefore it is essential that samples are truly representative of the bulk of the material. Proper collection of a representative sample requires an understanding of the physical characteristics and mineralogy of the material to be sampled as well as determination of the minimum number and size of increments to be taken.

6.5.8 Gold Plant Case Study

The sampling was excellent where ore was to be milled on a blended basis. This system consisted of a PLC controlled, primary cross cut sampler into a Wescone crusher and then a rotary Vezin sampler to split out two samples into duplicate

6.5.9 Sample Preparation

The sample collected was further processed to produce samples for assay and composite leach tests.

6.5.10 Recovery Determination

A composite was prepared and two leach tests conducted on both the Cornishman ore and the combined mill feed. Recovery was then assigned to the Cornishman ore in the blend based on the results.

The recovery was factored to:

R = R(test) * Rplant(actual)

This adjustment takes into account a plant recovery, which could be higher or lower than the laboratory test recovery. Tests were carried out at a fixed residence time, fixed grind size and fixed reagent conditions.

6.5.11 Assaying

Accurate analyses of routine plant samples and end of month inventory stocks are two of the most important aspects of metallurgical accounting. In terms of cost, the aqua regia digestion method is cheaper than fire assay but, generally, the results are not as accurate because a well performed fire assay determination provides total gold. It is common for grade control assays to be carried out by PAL (pulverise and cyanide leach) or aqua regia while plant samples are processed by aqua regia or fire assay methods.

The PAL technique is particularly beneficial where the “nugget” effect is a serious problem.

PAL (pulverised and leach)advantages:

- High gold recovery (95-97%)
- Simple recovery testing (Fire Analysis "tails")
- Suitable for oxide or fresh material

- Large sample charge size (up to 1 kg)
- Ability to enlarge machine for 3 or 5 kg assay charges
- Excellent repeatability of assay results, as shown in Figure 3
- Excellent grind (95% passing 75µ)
- Good accuracy compared to standards
- Time (Standard <21 hours turnaround, minimum 3 hours)
- Partial batches possible (run pots with water and grinding medium)
- Good mechanical reliability (robust)

6.5.12 Inventory Measurement

The gold inventory is identification of the gold present in the plant at any instant in time. It will vary due to factors such as feed grade, equipment availability, feed rate etc. Inventory sampling is extremely important because metallurgical accounting is based on the fundamental premise of measuring real, physical quantities and the differences in them is over the reporting period which is usually monthly. The inventory sampling must include all sources of gold (or other valuable metal) within the plant.

The parameters to be inventoried are: Solids, Solutions, Carbon, From leach tanks, Thickeners, Gravity Concentrates, Mattes, Flotation Concentrates

The three product formulae give equations that are normally used to determine recoveries and yielded masses as show equation s (6.126) and (6.127), particularly based on sulphur and gold assays. This depends on the accurate weight of the ore milled during the period and reasonably accurate assays of the feed, concentrate and tailings. In the case of pyrite gold, the concentrate may be assayed for sulphur and gold in order to average the weight of concentrate derived.

$$R = \frac{100xc(f-t)}{f(c-t)} \tag{6.126}$$

$$C = \frac{Fx(f-t)}{c-t)} \tag{6.127}$$

Where F, C, T are the tonnages of feed, concentrate and tailings; f, c, t are the respective assays; R is the metal recovery.

The fact that errors in assaying of this magnitude are usually compensating, makes the net error for a shift or a day quite small. The gold content of any process stream is the tonnes times the assay.

6.5.13 Relative Accuracy

It helps to place the relative accuracy of measurements in some order which can come from

Weightometers	0.5
Stockpile surveys	5
Moisture measurement	0.5
Inventory reproducibility	5-10
Carbon determination inventory	5
Assays Au	10
Cu, Pb, Zn	3-5
Iron ores	1-2
Mineral sands	2-5
Calculated vs. Assay Head (not coarse gold)	3
Flow meters	3
Density gauges	1
Weighbridges	0.1

6.5.14 Calculated Versus Assay Head

The mill calculated grade is the official mill grade because it is based on physical gold poured and the result of physical inventories. The calculated assay in grams per tonne should be ±0.1 Au g/t to conform to acceptable industry standards, based on a 3 Au g/t mill feed grade.

6.5.15 Mine vs. Mill

It is very easy to prove using Pierre Gy theory that the mine grade can never be as accurate as the mill calculated grade

References

[1] O. Adeleke et. al, Mineralogical and Geochemical Characterization of Gold Bearing Quartz Veins and Soils in Parts of Maru Schist Belt Area, Journal of Geological Research, Nigeria, July 2014

[2] Metso Expert results, Basics in Mineral Processing, 2015

[3] King R.P., Mineral liberation, technical notes 10, 2000.

[4] N. C. Eduardo, Development of a Method to Measure Charges in Tumbling Mills, Mining and Petroleum Engineering Department, EM: R. Esc. Minas, Ouro Preto, 67(3), 311-316, jul. sep. | 2014

[5] P. P. King, Particle populations and distribution functions., Technical notes 2, 2000

[6] A.Gupta and D.S.Yan, Introduction to Mineral Processing Design and Operation, 2006

[7] Nagaraj., CYTEC industries, Mineral recovery and processing , 2005

[8] King R.P., Modeling and Simulation of Mineral Processing Systems, Department of Metallurgical Engineering University of Utah,2001, USA,

[9] W. L. Luyben, Process Modelling , Simulation, and control for chemical engineers,McGraw- Hill, New York 1990.

[10] R. Sinnott and C. Towler, Eds, Chemical enginnering design, Elsevier, USA, 2009.

[11] S. M. Peters, K. D. Timmerhaus, and R. E. West, Plant design and economics for chemical engineers, Eds, Mc Graw-Hill, New York, 2004.

[12] H. A. Jakobsen, Chemical reactor modelling, springer, Verlag Berlin Heidelberg, 2008.

[13] B. V. Babu, Process plant simulation, Oxford University press, India, 2005.

Appendix A1